EFFECTS OF METAL IONS RELEASED FROM IMPLANTS ON ENERGY METABOLISM IN MACROPHAGES

ZEINA SALLOUM

Thesis submitted to the University of Ottawa
in partial Fulfillment of the requirements for the
Doctorate in Philosophy degree in Biochemistry

Department of Biochemistry, Microbiology and Immunology
Biochemistry Graduate Program
Faculty of Medicine, University of Ottawa

To my parents

ACKNOWLEDGEMENTS

I would like to express my sincerest gratitude to my thesis supervisor, Dr. Isabelle Catelas, for her expertise, support and patience throughout the completion of this thesis project. I appreciate the trust she has given me to advise undergraduate and graduate students. I am also extremely grateful that I developed my leadership skills with her guidance. These experiences have contributed greatly to my professional development.

I would like to thank the thesis examiners committee members, Dr. Céline Aguer, Dr. Mary-Ellen Harper, Dr. Katey Rayner, and the external examiner Dr. Carey Lumeng, for dedicating their time and efforts in reviewing my thesis.

I would like to thank my thesis advisory committee (TAC) members, Dr. Mary-Ellen Harper, Dr. Rosalind Labow, Dr. Ilona Skerjanc, and Dr. Paul White for dedicating their time and efforts in attending the meetings and advising me on my research throughout the past years up till completing my Ph.D.

Many thanks go to the members of the Orthopaedic Bioengineering Laboratory (OBL; Dr. Catelas' lab), especially Dr. Eric A. Lehoux, Research Associate in the lab. I thank him for contributing to my work, and for sharing his expertise and knowledge during this pursuit. I thank him for teaching me to go that "extra mile" in my search, and then again in my research.

Special thanks go to Dr. Mary-Ellen Harper for having her door open for my questions, her insights about my project and her encouragement. Also, I would like to thank her lab members for their continuous enthusiasm and tireless willing to help.

My sincere thanks go to my fellow lab mates and colleagues throughout the years, for their support and positivity. I am humbled that the youngest members have taught me lessons that I will carry on for life.

I would like to thank every person who, knowingly or unknowingly, made this work possible. I am thankful for my friends who have kept in touch in spite of the distance separating us. I am most thankful for my siblings Michel, Sawsan, Abir and Maher. Without their help and support all along the past few years, this work truly wouldn't have been possible.

My heartfelt appreciation goes to my parents who never fail to inspire and understand me throughout the years. Mom and Dad, I am eternally grateful for your unconditional support and for the lessons of resilience you have taught me. I am dedicating this work to you.

Je dirais à la fin, cette expérience fut une lumière.

ABSTRACT

Cobalt-chromium-molybdenum (CoCrMo) alloys are used extensively in orthopaedic applications. However, they can undergo wear and corrosion *in vivo*, leading to the release of Co and Cr ions that can limit implant functionality and survivorship because of their biological effects. Indeed, previous studies have shown that, Co^{2+} and Cr^{3+} can stimulate the production of bone-resorbing cytokines through the activation of redox-dependent mechanisms and induce an inflammatory response in macrophages. However, the effects of Co^{2+} and Cr^{3+} on the energy metabolism of macrophages remain largely unknown. The objectives of this thesis were to determine, in macrophages: 1. the effects of Co^{2+} and Cr^{3+} on oxidative stress and mitochondrial function; 2. the effects of Co^{2+} and Cr^{3+} on glycolytic flux and the stabilization of HIF-1α. RAW 264.7 murine macrophages were exposed to different Co^{2+} or Cr^{3+} concentrations for up to 48h. Biochemical, and immunoblotting assays as well as extracellular flux analyses were performed to analyze reactive oxygen species (ROS) production, oxidative damage, mitochondrial function, glycolytic activity, as well as stabilization of HIF-1α after macrophage exposure to the metal ions. Mitochondrial function and glycolytic activity were assessed by measuring oxygen consumption rates (OCR) and extracellular acidification rates (ECAR). Overall, results showed that Co^{2+} but not Cr^{3+} induced oxidative stress as well as a decrease in oxidative phosphorylation (OXPHOS). Both Co^{2+} and Cr^{3+} induced an increase in glycolytic flux, albeit to a lower level with Cr^{3+}. Moreover, Co^{2+} but not Cr^{3+} induced the stabilization of HIF-1α, likely contributing to the Co^{2+}-induced increase in glycolytic flux. Altogether, results suggest that Co^{2+} can induce a metabolic shift from OXPHOS towards aerobic glycolysis similar to that observed in macrophages upon polarization towards a pro-inflammatory phenotype. Further elucidation of the molecular

mechanisms activated by Co^{2+} and Cr^{3+} may facilitate the development of therapeutic approaches to modulate the inflammatory response to metal wear and corrosion products and re-establish immune homeostasis in periprosthetic tissues in order to increase implant longevity.

TABLE OF CONTENTS

LIST OF FIGURES

LIST OF ABBREVIATIONS

Abbreviation	Term
α-KGDH	Alpha-ketoglutarate dehydrogenase
Al_2O_3	Aluminum oxide
ALVAL	Aseptic lymphocyte-dominated vasculitis-associated lesion
AMPK	AMP-activated protein kinase
ANOVA	Analysis of variance
ATCC	American Type Culture Collection
ATP	Adenosine triphosphate
BCA	Bicinchoninic acid
BF	Buffering factor
BMDM	Bone marrow-derived macrophages
BNIP3	Bcl 2-interacting protein 3
BSA	Bovine serum albumin
CA	Carbonic anhydrase
CAT	Catalase
CC	Ceramic-on-ceramic
CCF	CO_2 contribution factor
CI	Confidence interval
CJRR	Canadian joint replacement registry
CO_2	Carbone dioxide
$CoCl_2.6H_2O$	Cobalt(II) chloride hexahydrate
CoCrMo	Cobalt-chromium-molybdenum

COX4	Cytochrome c oxidase 4
CPE	Ceramic-on-polyethylene
$CrCl_3.6H_2O$	Chromium(III) chloride hexahydrate
DAMP	Danger-associated molecular pattern
DCF	2′,7′-Dichlorofluorescein
$DCFH_2$	2′,7′- Dichlorofluorescin
DCFH-DA	2′,7′-Dichlorodihydrofluorescein diacetate
DMEM	Dulbecco's modified Eagle medium
DNA	Deoxyribonucleotide
DNP	2,4-Dinitrophenyl
DNPH	Dinitrophenylhydrazine
ECAR	Extracellular acidification rate
EDTA	Ethylenediaminetetraacetic acid
ETC	Electron transport chain
FBS	Fetal bovine serum
$FeCl_3$	Ferric chloride
Fe-S	Iron-sulfur
G6P	Glucose 6-phosphate
G6PD	Glucose 6-phosphate dehydrogenase
GAPDH	Glyceraldehyde 3-phosphate dehydrogenase
GPx	Glutathione peroxidase
Grx	Glutathione reductase
GSH	Glutathione
GSSG	Oxidized glutathione
H_2O_2	Hydrogen peroxide

HBSS	Hank's balanced salt solution
HCO_3^-	Bicarbonate
HIF-1	Hypoxia-inducible factor-1
HIF-1ß	Hypoxia-inducible factor-1 beta
HIF-1α	Hypoxia-inducible factor-1 alpha
$HO^{\bullet}$	Hydroxyl radical
HO-1	Heme oxygenase
$HOO^{\bullet}$	Hydroperoxide radical
HPLC	High-performance liquid chromatography
HR	Hip resurfacing
HRP	Horseradish peroxidase
HXLPE	Highly crosslinked UHMWPE
IDH	Isocitrate dehydrogenase
IFN-γ	Interferon-gamma
IL-10	Interleukin-10
IL-13	Interleukin-13
IL-1ß	Interleukin-1beta
IL-1α	Interleukin-1alpha
IL-4	Interleukin-4
IL-6	Interleukin-6
IL-8	Interleukin-8
iNOS	Inducible nitric oxide synthase
IRDye	Infrared dye
LC-MS	Liquid chromatography- mass spectrometry
LPS	Lipopolysaccharide

Lymphocyte Tc	Lymphocyte T cytotoxic
Lymphocyte Th	Lymphocyte T helper
M-CSF	Macrophage-colony stimulating factor
MDA	Malondialdehyde
MHC	Major histocompatibility complex
MHRA	Medicines and Healthcare products Regulatory Agency
MIP-1α	Macrophage inflammatory protein-1 alpha
MM	Metal-on-metal
MPE	Metal-on-polyethylene
mRNA	Messenger RNA
NADH	Nicotinamide adenine dinucleotide, reduced form
$NADP^+$	Nicotinamide adenine dinucleotide phosphate
NADPH	Nicotinamide adenine dinucleotide phosphate, reduced form
$NaHCO_3$	Sodium bicarbonate
NED	N-(1-naphtyl) ethylenediamine
NF-κB	Nuclear factor kappa B
NLR	NOD-like receptor
NLRP3	NLR Pyrin domain-containing 3
NO	Nitric oxide
NO_2^-	Nitrite
NO_3^-	Nitrate
NOD	Nucleotide-binding oligomerization domain
NOX	NADPH oxidase
NRF-2	Nuclear receptor factor-2
OCR	Oxygen consumption rate

OPG	Osteoprotegrin
OXPHOS	Oxidative phosphorylation
PAGE	Polyacrylamide gel electrophoresis
PBMC	Peripheral blood monocytes
PBS	Phosphate buffered saline
PDH	Pyruvate dehydrogenase
PDK-1	Pyruvate dehydrogenase kinase 1
PER	Proton efflux rate
PFK-1	Phosphofructokinase-1
PGDH	6-Phosphogluconate dehydrogenase
PKM2	Pyruvate kinase M2
PMA	Phorbol 12-myristate 13-acetate
ppb	Parts per billion
ppm	Parts per million
PPP	Pentose phosphate pathway
PRR	Pattern-recognition receptor
Prx	Peroxiredoxin
PVDF	Polyvinylidene fluoride
RANK	Receptor activator of nuclear factor kappa B
RANKL	Receptor activator of nuclear factor kappa B ligand
RNS	Reactive nitrogen species
ROS	Reactive oxidative species
SDS	Sodium dodecyl sulfate
SOD	Superoxide dismutase

TBA	Thiobarbituric acid
TBARS	Thiobarbituric acid-reactive substances
TCA	Tricarboxylic acid
TCR	T-cell receptor
THR	Total hip replacement
TLR4	Toll-like receptor 4
TNFR	TNF-α receptor
TNF-α	Tumor necrosis factor-alpha
TRAF6	TNF receptor associated factor 6
TRAP	Tartrate-resistant acid phosphatase
Trx	Thioredoxin
TXNIP	Thioredoxin interacting protein
UHMWPE	Ultra-high molecular weight polyethylene
ZrO_2	Zirconium oxide

CONTRIBUTION OF CO-AUTHORS

This thesis includes two manuscripts. The first manuscript (Chapter 3) is published in the Journal of Orthopaedic Research (J Orthop Res, 2018; 36(12): 3178-3187; DOI 10.1002/jor.24130). The second manuscript (Chapter 4) is currently under review for publication in the same journal.

All authors contributed to the design of the experiments of Manuscript 1. All data were collected by myself, with the assistance of Dr. Lehoux (Research Associate in Dr. Catelas' lab) who also performed parts of the protein oxidation experiments. The extracellular flux analysis experiments were performed in Dr. Harper's laboratory. All data were analyzed by myself with the assistance of Corey DeVlugt (a former student of Dr. Harper) for the Seahorse experiments. The first draft of the manuscript was written by myself and reviewed by Dr. Catelas (my supervisor), Dr. Lehoux (Research Associate), and Dr. Harper (co-author on the manuscript).

All authors contributed to the design of the experiments of Manuscript 2 (Chapter 4). All data were collected by myself. The extracellular flux experiments were performed in Dr. Harper's laboratory. All data were analyzed by myself. The first draft of the manuscript was written by myself and reviewed by Dr. Catelas (my supervisor), Dr. Lehoux (Research Associate), and Dr. Harper (co-author on the manuscript).

1. LITERATURE REVIEW

1.1 Joint replacements

Arthroplasty is an effective and safe method for treating severe degenerative, post-traumatic and other injuries/diseases of the joint. It is a surgical procedure during which all or part of the joint is replaced with an artificial device in order to restore joint functionality after injury or disease. An implant is used to replace the damaged cartilage within the joint. Among all arthroplasties, hip and knee arthroplasties are being performed worldwide with promising results.[1,2]

A hip arthroplasty, which has been labelled as the operation of the century,[3] can be performed with two types of implant devices: stem-type devices and hip resurfacing (HR). Stem-type devices will be referred to as total hip replacements (THR) in this thesis, to differentiate them from the HR. With a THR, both the femur head and neck are surgically excised and a synthetic socket is implanted into the pelvis replacing the acetabulum after the damaged cartilage and subchondral bone have been removed. The natural femur head is replaced by an artificial ball attached to a metal stem fitted into the femur bone. On the other hand, with a HR, the natural femoral head is resurfaced by a metal component in the absence of a stem component. Although less commonly used, HR have the advantage of preserving the femoral bone stock and have been used mostly in younger patients.

A knee arthroplasty is the surgery to replace a painful damaged or diseased knee joint with an implant. The patella is moved out of the way to expose the joint underneath. The ends of the femur and tibia are cut to fit the implant. Similarly, the under-surface of the patella cap is often cut to allow for placement of an artificial component.

While a primary surgery is the first replacement procedure, where the natural bone is replaced with an artificial joint implant, revisions are replacements of an existing artificial hip or knee joint implant. A revision procedure may be necessary when an existing worn-out hip or knee component needs to be removed and replaced with a new implant. This may include removing one or more components of the implant, as necessary.[4]

Extending the longevity of the implants has been a major focus of medical research and industry. Hip implants can reliably relieve pain and improve joint function in the majority of patients for a period of 15 to 20 years or more postoperatively.[5] On this basis, the expected implant survival time is insufficient for the younger and generally more active population.

As the population ages, the number of primary joint replacement procedures performed each year is rising in conjunction with an increasing revision burden. According to the Canadian Joint Replacement Registry (CJRR), in 2016–2017, 55,981 hip replacements and 67,169 knee replacements were performed in Canada.[4] This represents increases of 17.8% and 15.5%, respectively, compared with 5 years earlier. The main reason for having a primary hip replacement remains degenerative arthritis, while the main reason for hip revision is aseptic loosening. Moreover, the number of hip replacement procedures is increasing in the younger and more active population. About 26.8% of the patients undergoing a primary hip replacement were between 55 and 64 years old, while 12.1% of the patients were under 55 years old.[4] Close to 8.3% of the reported cases were revision surgeries for the hip artificial joint, respectively. While revisions may represent a relatively small proportion of all joint replacements, these types of surgeries are more complex than primary surgeries and have difficult implications, such as reduced patient mobility, longer patient recovery time and higher health care costs.[4] Therefore, examining risk factors for

early revision can inform clinicians for better practices and decisions regarding joint replacement patients, and can provide information on the medical costs for the health care system.[4]

1.2 Evolution of implant surface selection in joint replacements

The materials used to manufacture hip replacement bearing surfaces enable the joint to move with low friction.[6] The material choice for different components of hip implants, mainly the bearing surfaces, constitutes a critical factor determining the success of any hip replacement surgery. Many bearing combinations are available, each associated with different advantages and disadvantages. The most common hip implants have been made of a metal (cobalt-chromium-molybdenum [CoCrMo] or titanium alloy) femoral head, articulating against a polyethylene acetabular component. These implants are referred to as metal-on-polyethylene (MPE) implants. However, large volumes of the original ultra-high molecular weight polyethylene (UHMWPE) wear particles detected at the implant-bone interface were shown to be the major cause of a significant inflammatory response leading to periprosthetic osteolysis and aseptic implant loosening.[7,8] This problem urged for implant revision after only about 10 years in some cases.[9,10] Therefore, other more wear-resistant bearing surfaces than conventional MPE, including metal-on-metal (MM) and ceramic-on-ceramic (CC) have been developed based on the concept that the use of harder materials than polyethylene could improve wear resistance and decrease volumetric wear. During the last two decades, highly crosslinked UHMWPE (HXLPE) was also introduced to improve the wear properties of the MPE bearings.[11,12] *In vitro* studies have shown 40% to 95% reductions in wear rate compared with conventional UHMWPE.[13-15] However, the more brittle nature of the HXLPE[16] and the generation of predominantly submicron-sized particles[17,18] have raised concerns regarding the long-term clinical performance of HXLPE.[19,20]

CoCrMo alloys have become increasingly important as the number of various implanted devices, e.g., orthopedic, cardiovascular, and dental implants, is increasing.[21] These alloys are used in orthopaedic applications, because of their strength, durability, and corrosion resistance.[21,22] The CoCrMo alloys consist usually of 62-67% cobalt (Co) and 27-30% chromium (Cr), but also include 7% molybdenum (Mo) and less than 1% of manganese (Mn), iron (Fe), nickel (Ni).[10] They are used for hip and knee implant bearing surfaces specifically owing to their properties of excellent wear and corrosion resistance.[22] MM hip implants consist of a CoCrMo ball replacing the femur head and a CoCrMo socket replacing the acetabulum. The first generation of MM implants in 1950s/1960s showed a volumetric wear up to 100 times lower than that of conventional MPE bearings.[23] Although some continued to function well into the second and third decade, the first MM implants were used with only limited success.[9] Following the problem of osteolysis observed with conventional MPE implants, a second generation of MM hip implants was introduced in the 1980's.[9,23,24] with a volumetric wear rate of one to two orders of magnitude lower than the clinical wear rates reported with the first-generation MM hip implants.[25]

MM hip implants were reintroduced as a low-wear, high-performance alternative to MPE, especially in younger, more active patients. There were several advantages noted with the MM implants. For example, compared to conventional MPE implants, the lower volumetric wear rates of large head metal articulation were shown to be significantly decreased.[26] However, CoCrMo-based implants can still undergo wear/corrosion and nanometer size wear particles, along with the release of metal ions was shown to cause adverse events leading to high revision rates. For instance, starting in 2010, national registries data began to reveal significantly higher revision rates (2–3X) in MM implants in comparison with other hip implants.[27,28]

1.3 Implant wear and corrosion products: wear particles and metal ions

Wear products from hip implants, including particles and ions, have been found to accumulate in periprosthetic tissues.

The composition, morphology and size of the wear particles generated by the implants have been shown to influence cell response.[19,29,30] Indeed, the evidence of periprosthetic osteolysis has been first described in response to UHMWPE particles generated from conventional MPE implants. These particles were found in the periprosthetic tissues in different morphologies.[31] Particles with a roughened surface and a fibular shape appeared to induce a greater level of inflammatory cytokine production than particles with a smooth surface and a globular shape in an *in vivo* murine inflammation model.[31,32] Moreover, human monocyte-like cells are most responsive to UHMWPE particles in the size range of 0.21-7.2μm.[30]

Wear particles from MM implants have been reported to be primarily round to oval nanometer-size chromium oxide particles (~50 nm average), with some more elongated CoCrMo microparticles (1-10 μm).[33,34]

Ceramics are used in CC hip implants or ceramic-on-polyethylene (CPE) hip or knee implants. Alumina (Al_2O_3) and zirconia (ZrO_2) particles generated from CC implants have overlapping submicron-size distributions (0.44 ± 0.25 μm for Al_2O_3 and 0.28 ± 0.08 μm for ZrO_2 particles).[35] Others studies revealed the presence of a bimodal size distribution of ceramic particles with nanometer-size particles ranging from 1-35 nm and larger micrometer-size particles ranging from 0.021 to 10 μm.[36,37]

Metal ions can arise from wear (mainly from the bearing surfaces), but also from macrophage-mediated degradation of wear particles and corrosion of implant surface.[38] Implants not subjected to any mechanical stress can still release metal ions through metal corrosion.[39] Cobalt

and chromium are the major elements of the CoCrMo alloy. Co exists in two common oxidation states (+2 and +3). However, Co^{3+} are rapidly reduced to Co^{2+} in aqueous environments[40] Similarly, Cr exists in two or more oxidation states, most commonly +3 and +6, but Cr^{6+} are rapidly reduced to Cr^{3+} under physiological conditions.[40]

Based on its role in activating the erythropoietin protein production and increasing blood flow, Co^{2+} has been used in the treatment of anaemia, as well as in sports as an attractive alternative to traditional blood doping.[41] In addition, Co^{2+} is a necessary component of vitamin B_{12} which plays a very important role in the proper functioning of the human organism.[41] However, while Co^{2+} is necessary as a trace element for normal biological function, high concentrations of this ion are toxic and have been shown to interfere with several biological processes. The extent of the effects directly depends on the ion concentrations and length of exposure. High concentrations of Co^{2+} released from the implant have been linked to inflammatory reactions[42,43] and alterations in bone modelling that lead to aseptic loosening and implant failure.[22,44,45] Co^{2+} has been shown to bind toll-like receptors 4 (TLR4) in human macrophages and to activate downstream mechanisms leading to inflammatory cytokine release.[46,47] Also, Co^{2+} can enter cells through calcium channels and act as a blocker, thereby inhibiting biological processes activated by calcium signaling.[48] These biological processes include the activity of mitochondrial enzymes such as pyruvate dehydrogenase (PDH), alpha ketoglutarate dehydrogenase (α-KGDH) and isocitrate dehydrogenase (IDH).[49] These enzymes are part of the tricarboxylic acid (TCA) cycle and thereby participate in mitochondrial adenosine triphosphate (ATP) production.

On the other hand, the toxicity and essentiality of chromium ions depend on their oxidation state *in vivo*. While Cr^{6+} can readily cross the cellular membrane and be reduced inside the cell through the antioxidant system, free ionic Cr^{3+} cannot cross the plasma membrane barrier unless

it is complexed to other organic or inorganic molecules. Cr^{3+}, likely complexed with phosphates or phosphoproteins, will be taken up by the cells through pinocytosis or endocytosis depending on the size of the complexes formed.[50,51] Interestingly, Cr^{3+} supplementation has been described to have pharmacological benefits in treating patients with diabetes since it has been shown to potentiate insulin activity.[52] However, Cr^{3+} and its complexes have also been shown to induce DNA damage, oxidative damage as well as Cr–DNA adducts formation, and very high chromium (Cr^{3+} and Cr^{6+}) concentrations or long exposure can result in genotoxic effects.[53]

Measuring metal ion concentrations in biological fluids is a well-established clinical tool used to monitor the patients that have undergone hip replacement surgery. For instance, blood metal ion levels can be a reliable proxy for hip wear rate[54] and to effectively identify patients at low risk of adverse reactions after metal on metal hip replacement.[55] Serum cobalt levels of 0.13-0.80 ppb and serum chromium levels of 0.19-0.87 ppb have been reported in healthy control subjects, while postoperative concentrations in serum ranged from 0.61-115.8 ppb for cobalt and 0.12-127.8 for chromium.[56] However, postoperative metal ions levels have yet to be in agreement between different laboratories or studies likely because of the difference in samples processing and there is currently no consensus on threshold values above which frequent monitoring should be performed or revision surgery is required. In 2012, the Mayo clinic proposed a serum threshold of 10 ppb for cobalt and 15 ppb for chromium, above which postoperative metal ions levels should be closely monitored.[57] Also starting in 2012, the Medicines and Healthcare products Regulatory Agency (MHRA) medical alerts recommended a threshold of 7 ppb for whole blood samples above which frequent testing should be performed.[58] A recent study by Hartmann et al.[59] relying on epidemiological studies revealed that median metal ion concentrations were persistently elevated in all investigated media (whole blood, serum, plasma, erythrocytes, urine) post-implantation of

MM-bearings, irrespective of patient characteristics and study characteristics. It is noteworthy that metal ions levels in the body fluids depends on the renal function and excretion efficiency in urine.[59] Moreover, metal ion levels in the synovial fluid are expected to be higher than in whole blood and serum[60] since they reflect the local concentration of metal ions and particles in the periprosthetic region.[54] Notwithstanding, the levels of metal ions in whole blood and in the synovial fluid are correlated with each other, and they are higher post-implantation than pre-implantation.[59,60] However, interestingly, increased metal ion and wear levels do not always correlate with the level of tissue destruction.[61]

1.4 Implant failure mechanisms in joint replacements

As mentioned earlier, joint replacement is an effective surgery to restore joint functionality. However, implant failures remain a cause for concern, with implant loosening being the main contributor. Implant loosening is defined as a mechanical instability at the interface between the implant and bone,[62] due to periprosthetic osteolysis (bone loss around the implant).

The concept of aseptic loosening as a result of periprosthetic tissue reaction was first introduced in 1977 by Willert and Semlitsch.[63] It is generally associated with pain and loss of function although it may also occur asymptomatically. In order to prevent implant failure, there is a need to investigate the mechanisms that cause instability at the implant and bone interface. The current concepts suggest that aseptic implant loosening is the result of a combination of mechanical and biological events at the implant and bone interface.[62] These events are also tightly linked to a variety of factors such as the host response (including genetic predisposition), the implant design as well as the surgery's success, which have been identified as contributing factors to development of aseptic loosening and osteolysis.[64] Wear particles and metal ions have been reported to be the main culprit in the inflammatory response leading to periprosthetic osteolysis, leading to implant

failures.[8,65-67] The distribution of wear and corrosion products across the joint is facilitated by the joint fluid that is synthesized by synovial-like macrophages and fibroblasts.[68] This increased distribution further leads to tissue damage, in addition to the activation of resting tissue macrophage towards pro-inflammatory macrophages around the implant, thereby expanding the inflammatory reaction.[62] In addition to the fact that metallic products directly impact the local response and the implant survivorship, their biological effects are not limited to the local tissue response since metal ions in particular have been found disseminated into other tissues distant from the implant region.[72]

Therefore, understanding the underlying molecular mechanisms involved in the biological response to metal wear and corrosion products is critical to possibly modulate their effects and increase implant longevity.

1.4.1 Innate immune response to wear and corrosion products

The initial biological reaction to metallic products can be a non-specific response, i.e. an innate immune reaction.[69] This reaction involves pattern-recognition receptors (PRRs), for example toll-like receptors (TLRs) and nucleotide-binding oligomerization domain (NOD)-like receptors (NLRs) that recognize danger-associated molecular patterns (DAMPs), triggering rapid and robust signal transduction leading to an inflammatory response.[70] The role of the inflammatory response, in the general case, is to eliminate foreign bodies with limited damage of the inflamed tissue, followed by a tissue repair back to the pre-inflammation state. The resolution of inflammation is an essential part of the host response in order to avoid unnecessary tissue damage, reduce the energy demand associated with inflammation, in addition to pain relief, tissue remodelling, regeneration, and restoration of function. An inflammatory reaction that fails to

resolve (e.g., with wear and corrosion products) leads to a persistent reaction, otherwise called chronic inflammation.[71]

Aseptic loosening due to osteolysis has been associated with a chronic inflammatory reaction.[62] In general, bone loss occurs because of an increased bone resorption and/or reduced bone formation. Histological analysis of periprosthetic tissues taken from osteolytic lesions from both loose and well-fixed implants shows the presence of many types of cells including macrophages, fibroblasts, osteoclasts, as well as bioactive molecules such as chemokines, cytokines and degrading enzymes (collagenases, gelatinases, cathepsin).[72-74] During an inflammatory reaction, cytokine release from various cells including macrophages, fibroblasts and osteoblasts, was shown to promote macrophage differentiation into osteoclasts and decrease osteoblast proliferation.[22,75] Prolonged survival of the osteoclasts and inhibition of osteoblast proliferation lead to an increased bone resorption.

Wear and corrosion product-induced periprosthetic osteolysis is mainly driven by osteolytic cytokines,[8,65,73,76] including receptor activator of nuclear factor kappa B ligand (RANKL) which fundamentally controls osteoclast differentiation.[77,78] Osteolytic cytokines also includes TNF-α, which is considered as a key mediator of the inflammatory process.[79] TNF-α induces osteoclast precursor differentiation into mature osteoclasts and acts synergistically with other cytokines such as RANKL[80] and interleukin-1 alpha (IL-1α)[81] to stimulate bone resorption. Also, TNF-α regulates osteoblast proliferation and osteoclast survival rate.[82,83] The role of RANKL in osteoclast differentiation is however, countered by osteoprotegrin (OPG) produced mostly by osteoblasts, which when dimerized, has a high affinity for RANKL, therefore blocks the RANKL/RANK axis and thereby osteoclast differentiation.[84] These results indicate that inflammatory cytokines act through distinct cellular receptors and are operating in parallel to the

RANKL/RANK/OPG signaling pathway to induce osteoclast differentiation in the periprosthetic tissues.[77] Among other cell types involved, macrophages play a major role in periprosthetic osteolysis. They are osteoclast precursors that have been shown to differentiate into functional osteoclasts in response to wear particles *in vivo*.[85] They are listed as the predominant immune cells at the bone-implant interface as evidence of inflammation.[86,87] Finally, macrophages are essential phagocytes that are involved in inducing an innate immune reaction as well as initiating adaptive immunity.

1.4.2 Adaptive immune response in implant failure

Interestingly, Willert et al.[88] reported the presence of diffuse and perivascular infiltrates of T and B lymphocytes as well as plasma cells in MM periprosthetic tissues. The authors described this reaction histologically as aseptic lymphocyte-dominated vasculitis-associated lesion (ALVAL), suggesting the presence of a hypersensitivity reaction.[88] This tissue reaction pattern seems to be more prominent around loose MM implants. In general, professional cells such as macrophages and dendritic cells capture and process antigens to present them as major histocompatibility complexes (MHC) II-bound antigenic epitopes to the T-cell receptors (TCRs) of naïve CD_4^+ T-helper (Th) cells. The extent of T and B lymphocytes as well as plasma cells diffusion and infiltration at the periprosthetic tissues in response to metallic wear and corrosion products has been adopted as a criteria to rate ALVAL.[89] The identification of Th1 cells, a specific subset of T lymphocytes, observed in response to specific metal ions suggests the presence of a type-IV hypersensitivity reaction in response to metallic wear and corrosion products.[88,90] Implant-associated hypersensitivity reactions may occur after activation of T lymphocytes that have been exposed to organometallic complexes (haptens) recognized as a non-self-protein.[70,88,90,91] For example, Hallab et al.[96] reported a lymphocytic response to serum proteins complexed with metal

ions from implant alloy degradation. These lymphocytes release various cytokines resulting in further macrophage activation and monocyte recruitment. While this type IV lymphocyte-driven hypersensitivity reaction has been documented in a small percentage of cases with predominantly MM bearing surfaces,[66] it has also been described with other types of implants that typically contain at least one component made of a metal alloy such as CoCrMo.[92]

Another subset of T lymphocytes, CD_8^+ T cells, named cytotoxic lymphocytes, are specific for the class I MHC molecules binding modified proteins such as serum proteins modified by metal ions. The role of these lymphocytes in the periprosthetic region is still unclear. In studies where peripheral blood was taken from patients undergoing revision surgeries for their loose cobalt-alloy hip implant, Th cells (CD_4^+) and T cytotoxic (Tc, CD_8^+) lymphocytes were decreased, suggesting a generalized immunosuppressive effect of wear and corrosion products released from the prosthesis or sequestration of lymphocytes away from the systemic circulation.[93,94] Patients with MM or MPE implants showed a significant decrease in the number of circulating T lymphocytes and a significant increase in the serum level of chromium and cobalt after total hip arthroplasty,[92,94] suggesting a correlation between increased metal ion release and lymphocyte migration from the bloodstream towards to implant site.

Moreover, histological examination of periprosthetic tissues from patients with MM hip implants[89,95,96] as well as with MPE implants[97-100] has revealed the presence of periprosthetic soft tissue masses in some cases.[7,98] The number of reports depicting the presence of such "soft tissue mass", also called "enlarged bursa" or "cyst" and referred to as pseudotumor, has been increasing over the last decade. These soft tissue masses show histological features consistent with an inflammatory reaction in response to metal wear (with particle-loaded macrophages), but also features suggesting a hypersensitivity reaction (lymphocytic infiltrations and aggregates).[89,95]

Depending on the patient, these reactions may be symptomatic or asymptomatic and can lead to early implant failure.[94] Because of bone and soft tissue destruction, the revision procedures are often associated with a high risk of reoperation.[99] Pseudotumor occurrence, therefore, remain a cause for concern and their exact mechanisms remain unclear. In recent histopathological studies, evidence was presented that increased adverse tissue reactions correlated with elevated levels of implant wear.[99,100] However, pseudotumors have also been described in the presence of low wear and a hypersensitivity reaction.[89] Therefore, the extent of wear alone is not enough to explain the presence of pseudotumors, indicating that one or more other factors such as patient history/information, implant design and surgical techniques, may be contributing to this type of reaction.

1.5 Macrophage response to metal ions

1.5.1 Macrophage phenotypes

Macrophages are potent phagocytes acting as *surveillance* agents of the immune system. They are distributed in tissues throughout the body and contribute to both homeostasis and disease. They can be either tissue resident macrophages or macrophages derived from the differentiation of monocytes that migrate from the blood stream to the tissues under chemotaxis effect at a moment of injury.[101] Tissue-specific resident macrophages are monocytes that, after maturation in bone marrow, are released into the circulation, enter the tissues and differentiate into resting tissue macrophages that can survive for several months. There, they can be activated by pro-inflammatory (microbial/non-microbial) stimuli into pro-inflammatory [M1] macrophages, by anti-inflammatory cytokines such as interleukin-4 (IL-4), interleukin-13 (IL-13) into tissue remodelling, wound healing [M2] macrophages, or by other signals such as interleukin-10 (IL-10), immune complexes, or glucocorticoids into anti-inflammatory immunoregulatory [M2-like]

macrophages.[102] In this context, macrophages are polarized towards a specific phenotype depending on environmental conditions, therefore determining their function based on molecular determinants that have been used to identify them, whether *in vitro* or *in vivo*.[103] These markers include cell surface markers as well as intracellular and secreted signaling molecules (e.g., specific chemokines and cytokines).[103] In general, the pro-inflammatory macrophages are characterized by the expression of high levels of proinflammatory cytokines, high production of reactive nitrogen and oxygen intermediates, promotion of Th1 response, and strong antimicrobial and antitumor activity. In contrast, the anti-inflammatory macrophages are involved in tissue remodeling and tumor progression and have immunoregulatory functions. They are characterized by efficient phagocytic activity, the expression of mannose receptors (CD206), a high expression of IL-10, and low expression of interleukin-12 (IL-12) cytokines. However, in response to signals including IL-10, glucocorticoid hormones, apoptotic cells, and immune complexes, a subpopulation of the M2 macrophages share selected properties with anti-inflammatory macrophages (e.g., high mannose and scavenger receptors expression), but are distinct from them, for instance, in terms of the chemokine profile and IL-10 expression and release. These cells are referred to as immunoregulatory (M2-like) macrophages.[102,103] Interestingly, *in vivo* studies have shown that macrophage phenotype can change over time.[104] Therefore, although macrophage polarization towards a specific phenotype has been described in the literature, the functional characterization of macrophages subpopulations is still not fully apprehended because of macrophage plasticity.[102] Identifying macrophage phenotype using a single marker remains problematic since more than one marker can be shared by different subpopulations.[102] Therefore, there is a need for additional strategies in order to identify macrophage phenotype in response to exogenous or endogenous stimuli. Recently, the macrophage energy metabolism and metabolic pathways have been explored

as another determining factor in macrophage phenotype, energy metabolism being a driving force in determining macrophage phenotype.[105]

1.5.2 Metal ions and macrophage inflammatory response

Macrophages are concentrated at the bone-implant interface and are therefore considered as the most important immunological player in aseptic loosening of orthopedic implants.[106,107] There has been a growing interest in studying the effects of wear and corrosion products released from metal implants on macrophage polarization in periprosthetic tissues.[108,109] In this context, gene expression studies have shown that commonly known and other cytokines involved in macrophage polarization, such as interferon-gamma (IFN-γ) and IL-4 are low in peri-implant tissues compared to control osteoarthritic synovial membrane.[113] In contrast, there is a significant upregulation of pro-inflammatory chemokines, macrophage-colony stimulating factor (M-CSF), interleukin-8 (IL-8), IL-10, as well as markers of increased bone resorption such as tartrate-resistant acid phosphatase (TRAP), cathepsin K, and downregulation of OPG, while interleukin-1beta (IL-1ß), TNF-α, and CD206 were unchanged.[113] These findings suggest that monocyte recruitment and osteoclast formation are activated, involving factors other than pro-inflammatory cytokines in aseptic implant failure.[110]

In vitro studies addressing the effect of metal ions in a variety of cell lines showed the potent bioactivity of Co^{2+} and Cr^{3+} to induce cytotoxicity and a pro-inflammatory response.[42,43,111-113] For example, studies have shown that increasing concentrations of Co^{2+} and Cr^{3+} released from CoCrMo-based implants induce a decrease in macrophage viability, with Co^{2+} being more toxic than Cr^{3+}.[43,114] Apoptosis was predominant with both Co^{2+} and Cr^{3+} at low concentrations, whereas high concentrations induced mainly necrosis after extended exposure. Overall, the type and concentration of metal ions as well as the duration of macrophage exposure to metal ions determine

macrophage response to metal ions.[43,114] Other studies showed caspase pathway activation in macrophages stimulated with Co^{2+} and Cr^{3+} leading to cell death by apoptosis.[112,115] In addition, Co^{2+} and Cr^{3+} ions have been shown to induce TNF-α gene expression[116] and release[43] in macrophages. In synoviocytes and bone marrow macrophages, metal ions were able to induce the redox-dependent pathways which activated bone-resorbing cytokine production such as IL-1ß and interleukin-6 (IL-6).[117] Moreover, Co^{2+} and Cr^{3+} ions have been shown to induce chemokine secretion, especially macrophage inflammatory protein-1alpha (MIP-1α).[40,42,118] Finally, recent studies showed that Co^{2+}, but not Cr^{3+}, inhibit macrophage migration through ROS production.[119] Altogether, these studies demonstrate that metal ions can affect multiple biological processes including the inflammatory response, in macrophages as well as other cell types.

Interestingly, macrophages have been shown to engulf metallic wear particles leading to intracellular particle degradation through mechanisms involving lysosomes, leading to metal ion release in the extracellular matrix, and thereby propagation of the metal ion-induced inflammatory reaction.[44,120]

1.6 Oxidative stress and macrophage metabolic reprogramming

Recently, the energy metabolism has been tightly linked to the macrophage immune response under inflammatory conditions.[105,121,122] However, the pathways regulating the energy metabolism in macrophages exposed to wear and corrosion products still remain largely unknown.

One of the characteristics of the pro-inflammatory macrophages is the high production of reactive nitrogen and oxygen species (RNS and ROS, respectively).[103] Some beneficial effects of ROS (e.g., superoxide radical) and RNS (e.g., nitric oxide) occur at low/moderate concentrations and involve physiological roles, for example in the function of a number of cellular signaling pathways and in the defence against infectious agents.[123] However, excessive production of ROS

from mitochondrial electron transport chain (ETC) complexes and other mitochondrial enzymes such as PDH, or excessive stimulation of nicotinamide adenine dinucleotide phosphate (NADPH) oxidase (NOX) enzymes results in oxidative stress damage to cell structures, including lipids and membranes, proteins, and nucleic acids.[124] Oxidative stress is in fact defined as "an imbalance between oxidants and antioxidants in favor of the oxidants, leading to a disruption of redox [reduction-oxidation] signaling and control and/or molecular damage".[125] Moreover, this imbalance in the redox state has been linked to various disease states such as cancer, cardiovascular, and neurodegenerative diseases.[126] A significant number of physiological functions are regulated by redox-dependent signaling pathways, including the redox regulation of immune responses.[127,128] Interestingly, metal ions are key elements that usually act as cofactors of various cellular processes. Their homeostasis is regulated through controlled steps of uptake, storage and secretion. The breakdown of metal ions homeostasis, for example caused by metal ions overload, can lead to an uncontrolled and unbalanced ROS production, and thereby to cellular and further tissue damage.[126]

Several *in vitro* studies proposed that both Co^{2+} and Cr^{3+} ions induce oxidative stress in human monocytes as demonstrated by protein oxidation.[147] They can also increase production of ROS, which are involved in tissue damage and apoptosis.[44,112] Moreover, *in vitro* studies have shown that both Co^{2+} and Cr^{3+} can activate the production of bone-resorbing cytokines through the activation of redox-dependent mechanisms.[117]

1.6.1 Possible metal ion-induced mechanisms leading to oxidative stress

ROS are produced as part of normal cellular function. ROS production sites include enzymatic systems such as the NADPH oxidase (which produces superoxide anions), and organelles such as mitochondria, the endoplasmic reticulum (under stress), and peroxisomes.[129]

Importantly, Co^{2+}, Cu^{2+} as well as Ni^{2+} rank higher than Fe^{2+} on the Irving–Williams Series. Therefore, they can form more stable complexes than with Fe^{2+}.[130] Since Fe^{2+} plays an essential role in the regulation of fundamental biological processes (specifically protein complexes with both mitochondrial and non-mitochondrial functions),[126,131] it is possible that heme and non-heme enzymes regulated by Fe^{2+} would be affected by the presence of other metal ions including Co^{2+} and Cr^{6+}. Possible metal ion-regulated mechanisms leading to oxidative stress are discussed below.

1.6.1.1 Fenton/Haber-Weiss reactions

The Fenton reaction is a catalytic process that converts hydrogen peroxide into a highly toxic hydroxyl free radical ($HO^{\bullet}$), using ferrous ions (Fe^{2+}) as catalyst (equation 1).[132] The Fenton reaction is the first step of a two-step reaction named the Haber–Weiss cycle (equation 3). The second step is the ferric ion reduction to ferrous ion via reaction with superoxide (equation 2). Both reactions are associated with iron and generate highly toxic hydroxyl radicals.

$$Fe^{2+} + H_2O_2 \rightarrow Fe^{3+} + HO^- + HO^{\bullet} \text{ (equation 1)}$$

$$O_2^{\bullet-} + Fe^{3+} \rightarrow Fe^{2+} + O_2 \text{ (equation 2)}$$

$$O_2^{\bullet-} + H_2O_2 \rightarrow HO^- + HO^{\bullet} + O_2 \text{ (Haber-Weiss reaction; equation 3)}$$

These reactions give rise not only to hydroxyl radicals but also to several other intermediates including hydro peroxides (HOO•), superoxide ($O_2^{\bullet-}$) during various redox-cycling and propagation reactions.[132] $HO^{\bullet}$ can act as the chain carrier with the ability to react with Fe^{2+}, H_2O_2, or any organic species to propagate the redox reaction.[132] The existence and propagation of any of these reactions highly depends on the density of Fe and its required oxidation state (Fe^{2+} and Fe^{3+}) as well as the release rate. The Fenton reaction is known to occur *in vitro*, even though the available free catalytic iron is negligible due to its effective sequestration by the various metal-

binding proteins.[133] *In vivo* production of hydroxyl radical occurs according to the Fenton reaction when the redox-active metal ions is iron, copper, chromium, or cobalt (under different oxidation states).[134] Co^{2+} (as well as Cu^{2+} and Ni^{2+}) rank higher than Fe^{2+} on the Irving–Williams Series and can form more stable molecular complexes than Fe^{2+}.[130] Therefore, a source of increased ROS production in presence of Co^{2+} may be the redox-cycling reactions catalyzed by the increased free pool of redox metal ions such as Fe^{2+} displaced by the high concentration of Co^{2+} that become strong competitors to iron binding sites. Moreover, it has been shown that intracellularly-generated hydrogen peroxide may react with Co^{2+} to produce highly reactive hydroxyl radicals, which may contribute to Co^{2+}-induced cell injury.[44]

With regards to chromium ions, the redox active Cr^{6+} are readily reduced *in vivo* and in the intracellular milieu consuming the pool of antioxidants, thereby increasing the prevalence of oxidative stress and downstream activated pathways.[134] In contrast, Cr^{3+} represents the lowest most stable oxidation state for chromium under physiological conditions. Although it is unlikely that Cr^{3+} can be further reduced, previous studies have shown the induction of oxidative stress and oxidative damage in response to Cr^{3+} in various cell types.[44,112,135]

1.6.1.2 NADPH oxidase (NOX) enzymes

NADPH oxidase protein complexes, located in the cell plasma membrane, are particularly important for ROS production in certain phagocytic and non-phagocytic cell types, including macrophages.[129] NADPH oxidases are a family of enzymes that transfer electrons from NADPH and/or NADH to molecular oxygen via flavins within their structure to generate $O_2^{\bullet -}$. As Fe-containing enzymes, some of the NADPH oxidase enzymes (NOX) can be inactivated by either Fe^{2+} chelation or displacement of the Fe^{2+} from its active site by the less reactive Co^{2+}, which may

lead to a decrease in NOX activity.[131] However, the displacement of the active Fe^{2+} to the cytoplasm may lead to redox-cycling reactions and ROS production propagation.[131]

In vitro studies have shown that exposure of fibroblasts to CoCrMo nanoparticles triggered rapid generation of ROS that could be eliminated by inhibition of NOX activity, suggesting that NOX activation was mediated by phagocytosis of the particles.[136] Moreover, short-term exposure of human bronchial epithelial cell line, Beas-2B cells, to high doses of Cr^{6+} resulted in an increase in NOX activity and subunits expression, and therefore a rapid ROS generation.[137] Chronic exposure (up to 3 months) to low doses of Cr^{6+} also induced the expression of NOX subunits and resulted in the transformation of these cells, underlining Cr^{6+} carcinogenic potential.[137]

1.6.1.3 Mitochondrial ROS

Mitochondria are thought to be the major ROS-producing organelles in most cell types because a high number of redox reactions occur therein.[138] The mitochondrial ETC is the main source of ATP in mammalian cells. During electron transfer, a small number of electrons exit the ETC (i.e., leak) prior to the reduction of oxygen to water. The reaction of these electrons with oxygen forms superoxide,[139] which has been implicated in the pathophysiology of a variety of diseases.[140] Superoxide is produced mostly at complexes I (NADH-ubiquinone oxidoreductase) and III (cytochrome c reductase) of the ETC.[141] In its anionic form, superoxide cannot cross the inner mitochondrial membrane. It is produced either into the matrix through complex I, or into the matrix as well as the intermembrane space through complex III. In the matrix of the mitochondria or the intermembrane space, the dismutation of the peroxide is catalyzed into hydrogen peroxide and oxygen by the antioxidant activity of the superoxide dismutase 1 (SOD1; Cu/ZnSOD; mitochondrial intermembrane space) and superoxide dismutase 2 (SOD2; MnSOD; mitochondrial matrix).[142]

Mitochondrial ROS has been associated with cell signaling activation in the immune system and could be a result of activated signaling pathways. For example, West et al.[143] reported that upon TLR4 activation, TNF receptor-associated factor 6 (TRAF6) is recruited to the mitochondria, resulting in an increase in mitochondrial and cellular ROS generation. Moreover, other receptors such as the TNF-α receptor (TNFR) can mediate an inflammatory response through mitochondrial ROS production.[144,145] Finally, RANKL/RANK signaling was shown to mediate osteoclast differentiation also through mitochondrial ROS.[146]

Increased mitochondrial ROS production can also originate from different sources inside the mitochondria such as a deficiency or mutation in mitochondrial antioxidant enzymes,[147] mitochondrial DNA damage,[148] as well as deactivation of the ETC.[149] In this context, mitochondrial ROS production caused by the inhibition of complexes I and III in the mitochondria has been shown to activate the NLRP3 inflammasome pathway indicating that mitochondrial ROS can trigger an inflammatory response.[150] Interestingly, transition metal ions such as Cd^{2+} and Ni^{2+} have also been shown to inhibit the activity of mitochondrial enzymes in the ETC[149,151] and induce mitochondrial ROS production.[149,152] Moreover, it has been shown that Co^{2+} and Cu^{2+} can compete with Fe^{2+} for Fe binding sites in iron-sulfur (Fe-S) clusters such as those constituting the main subunits of the protein complexes in the ETC.[153] The resulting mismetallation can deactivate the mitochondrial complexes at the inner mitochondrial membrane, thereby inhibiting the electron transfer, leading to increased mitochondrial ROS production. With regards to chromium ions, the redox active Cr^{6+} can induce perturbations of mitochondrial bioenergetics.[154] Moreover, *in vitro* studies have shown the presence of carbonylated proteins in mitochondria-enriched cell extracts in macrophages exposed to Cr^{3+} ions.[44] Mitochondrial complexes deactivation by carbonylation could be another cause for ETC deactivation,[155] therefore source for mitochondrial ROS

production. In fact, ROS-induced protein carbonylation has been shown to increase ROS production implying a feed-forward control loop amplifying small changes in ROS production and consequently, protein carbonylation.[155]

1.6.2 Antioxidant system

It is now accepted that the redox environment determines cellular fate.[125] The antioxidant system is the cell tool to maintain a physiological equilibrium during ROS production. Therefore, the antioxidant system helps with the prevention and interception of oxidative stress. It includes the enzymatic and non-enzymatic antioxidants.

1.6.2.1 The enzymatic antioxidants

The enzymatic antioxidant system includes, in addition to the family of SOD enzymes (equation 4), the glutathione peroxidase (GPx; equation 5), glutathione reductase (GRx; equation 6), thioredoxin reductase (Trx reductase), catalase (CAT; equation 7). In addition, some enzymes such as the heme oxygenase (HO-1) and the enzymes involved in glutathione (GSH) synthesis, the glutamate cysteine ligase and the glutathione synthetase, can be indirectly associated with the antioxidant system.[140]

$$O_2^{\bullet-} + O_2^{\bullet-} \xrightarrow{\text{SOD}} H_2O_2 + O_2 \text{ (equation 4)}$$

$$H_2O_2 + 2\ GSH \xrightarrow{\text{GPx}} 2H_2O + GSSG \text{ (equation 5)}$$

$$GSSG \xrightarrow{\text{GRx}} GSH + GSH \text{ (equation 6)}$$

$$H_2O_2 + H_2O_2 \xrightarrow{\text{CAT}} 2H_2O + O_2 \text{ (equation 7)}$$

Interestingly, in Co^{2+}-treated mice, the activity of SOD, CAT and GPx measured in liver were inhibited whereas the activity of HO-1 was increased.[156] CAT activity was also inhibited by Cr^{3+} in a cell-free system.[44] Interestingly, *in vitro* studies showed that, in osteoblasts, HO-1 and

GPx protein expression increased in response to Co^{2+} as well as Cr^{3+}. However, Co^{2+} decreased CAT expression.[157] In macrophage-like cells U937, Co^{2+} induced the protein and mRNA expression of HO-1 only, whereas Cr^{3+} had no effect on the antioxidant enzymes studied.[158] On the other hand, Cr^{6+} induced the protein expression of several antioxidant enzymes but had no effect on their mRNA in the U937 cells, suggesting a Cr^{6+} effect at the post-transcriptional level.[158]

1.6.2.2 The non-enzymatic antioxidants

The non-enzymatic antioxidant system includes low-molecular-mass compounds such as GSH, Trx, peroxiredoxin (Prx; in endoplasmic reticulum mostly), as well as antioxidant dietary supplements such as ascorbic acid (vitamin C), alpha-tocopherol (vitamin E), and flavonoids.[125,140] Moreover, the nuclear receptor factor-2 (NRF-2) transcription factor has been shown to regulate the cellular response to oxidative stress response in rat liver cell lines.[159] More specifically, NRF-2 was activated in the presence of Co^{2+} and induced the expression of the detoxifying enzymes against oxidative stress.[159]

GSH may be the most important non-enzymatic antioxidant in the cell because of its multiple roles against oxidative stress. It is a tripeptide synthesized in the cytosol but it is abundant in the cytosol, nuclei, as well as the mitochondria. Namely, GSH acts as a direct scavenger of hydroxyl radicals and as an indirect reductant of hydrogen peroxide and lipid peroxides through the activity of GPx.[125] Moreover, GSH is able to regenerate important antioxidants such as vitamin C and E, into their active form. In addition to ROS and redox metal ions, non-redox metal ions such as arsenic (As^{3+}) and cadmium (Cd^{2+}) have been shown to contribute to oxidative stress by binding to critical thiols such as GSH and the sulfhydryl groups (-SH) of proteins, thereby decreasing the pool of antioxidants.[126] Interestingly, the effect of the strong oxidant Cr^{6+} are readily reduced by GSH resulting in Cr^{3+} and to the formation of mutagenic Cr(III)-DNA adducts.[160]

It is noteworthy to mention the role of Trx in sequestering thioredoxin interacting protein (TXNIP) in absence of oxidative stress conditions. In the presence of high ROS production, such as ROS originating from mitochondria, Trx is released and is involved in the antioxidant defense, while TXNIP can trigger inflammasome activation.[161] This mechanism has been suggested as one of the pathways leading to the inflammasome activation in macrophages under oxidative stress conditions, linking ROS production to inflammatory response.

1.6.3 Macrophage metabolic reprogramming

In addition to their primary role in regulating cellular energy metabolism, mitochondria have recently gained attention as critical regulators of the innate immune response.[128,162] In response to pro-inflammatory stimuli, either pathogenic or caused by a aseptic injury (such as in the case of metal ions), macrophages have exhibited a metabolic switch from oxidative phosphorylation (OXPHOS) caused by mitochondrial dysfunction towards glycolysis.[163]

1.6.3.1 Mitochondrial dysfunction

As an essential component of the eukaryotic cell, mitochondria exhibit numerous cellular functions including, most importantly, ATP production, which is used by cells to maintain signal transduction and function. In addition, mitochondria produce ROS under normal physiological conditions. However, various cellular stresses lead to an increase in ROS levels resulting in an imbalance between oxidant production and antioxidant activity, which can directly or indirectly target the mitochondria. Indeed, mitochondrial dysfunction, usually demonstrated by increased mitochondrial ROS production, can be triggered by multiple sources such as mitochondrial genetic diseases,[147] intracellular triggers such as NO-induced mitochondrial dysfunction,[148,164] or extracellular assailants such as metals, inhaled toxicants and pesticides that target directly the mitochondria.[162] Mitochondrial dysfunction has been linked to inflammatory responses.[165]

Accumulating evidence shows that increased mitochondrial dysfunction resulting in ROS production activates multiple pathways such as: NF-κB-regulated pathway,[166] hypoxia inducible factor- 1 (HIF-1)-regulated pathway,[167] as well as the inflammasome signaling,[150] all playing leading roles in the inflammatory response by mediating major pro-inflammatory cytokines release, mainly TNF-α, IL-1ß and IL-6. Finally, as a consequence of mitochondrial dysfunction, it is expected that energy-dependent processes will be compromised. For example, ATP-dependent processes such as apoptotic cell death, will be restricted, thereby favouring necrotic cell death.[168] These events, in turn, aggravate the cell response and overall the tissue damage.

Importantly, mitochondria have been shown to be involved in inflammation caused by aseptic injury.[169] However, the involvement of mitochondria in the immune cell response, specifically macrophages, following exposure to metal ions remain largely unknown. Since Co^{2+} can compete with Fe^{2+} for Fe binding sites in Fe-S clusters such as those constituting the main subunits of the protein complexes in the ETC, it is possible that a mismetallation inhibit the electron transfer, leading to increased mitochondrial ROS formation. Other transition metal ions such as Cd^{2+} and Ni^{2+} have been shown to inhibit the activity of mitochondrial enzymes in the ETC[149,151] and induce mitochondrial ROS production.[149,152] Interestingly, mitochondrial DNA has been shown to be more susceptible to oxidative damage than nuclear DNA, likely because of smaller genome size and higher localized ROS production.[170] Moreover, Co^{2+} has been shown to inhibit the activity of the SOD enzymes[156] likely because some of them are regulated by metal ions and are specific to the mitochondria. Finally, while cobalt chloride is used to quench calcein (used to detect intact mitochondria), Co^{2+} has been reported to inhibit ATP synthesis in isolated mitochondria by opening the mitochondria permeability transition pores.[171]

With regard to chromium ions, the redox active Cr^{6+} has been shown to induce perturbations of mitochondrial bioenergetics by targeting the mitochondrial complexes.[154] In the U937 cells, Cr^{6+} induced the protein expression of MnSOD and Cu/ZnSOD, but had no effect of their mRNA. However, Cr^{3+} had no effect on the antioxidant enzymes studied.[158] A recent *in vitro* study has shown that Cr^{3+} can decrease the mitochondrial membrane potential of hepatocytes or fibroblasts.[135] Mitochondrial complexes deactivation by carbonylation could be another cause for ETC deactivation, therefore mitochondrial dysfunction.[155]

Overall, both Co^{2+} and Cr^{3+} have been shown to be able to induce oxidative stress. However, the effects of Co^{2+} and Cr^{3+} on the energy metabolism of macrophages remain largely unknown. Determining the effects of Co^{2+} and Cr^{3+} on oxidative stress and mitochondrial function in macrophages constitute the first objective of this thesis.

1.6.3.2 Glycolytic flux activation

The glycolytic pathway is one of the central pathways in metabolism.[172] In the glycolytic pathway, the initial steps happen in the cytosol. After entering the cell through specific transporters, glucose is phosphorylated into glucose 6-phosphate (G6P) through the action of hexokinase, and therefore become trapped inside the cell. Several reactions then yield the production of pyruvate along with two ATP molecules. Pyruvate is the metabolic intermediate that bridges the initial glycolytic reactions happening in the cytosol and the OXPHOS through the TCA cycle happening in mitochondria.[173] Up until now, glycolysis has been considered an inefficient pathway for energy production.[173]

It is important to note that glycolysis branches into the pentose phosphate pathway (PPP) at the hexokinase step. The PPP is an essential source of NADPH that Trx and Grx use as a cofactor for the reductive regeneration of GSH from its oxidized form (GSSG), and it is also important for

the synthesis of biomolecules essential for cellular anabolic reactions. The PPP consists of two branches: the oxidative branch and the nonoxidative branch. In the oxidative branch, NADPH and phosphorylated sugars are generated. Phosphorylated sugars are interconverted through series of enzymatic reactions and become the building blocks (nucleotides, ribonucleotides and deoxyribonucleotides) for cellular macromolecules such as nucleic acids.[174] The nonoxidative branch provides sugar phosphate precursors for the synthesis of amino acids. NADPH is critically important since it provides the reducing power that fuels the protein-based antioxidant systems and recycles oxidized GSH. To preserve redox homeostasis under oxidative stress, ROS has been shown to inhibit multiple glycolytic enzymes, including glyceraldehyde 3-phosphate dehydrogenase (GAPDH), pyruvate kinase M2 (PKM2), and phosphofructokinase-1 (PFK-1).[175] Consequently, G6P will build up and will be rerouted into the oxidative branch of the PPP where a rising $NADP^+$/NADPH ratio further activates G6P dehydrogenase (G6PD).

Under specific disease conditions or in presence of pro-inflammatory stimuli, the glycolytic pathway has been shown to be upregulated,[176,177] resulting in an enhanced glycolytic flux leading to a rapid supply of energy through increased glycolytic ATP production. This increase in glycolytic ATP production can compensate for the shortage in mitochondrial ATP and help sustaining various cellular processes including an inflammatory response.[178] This mechanism simultaneously yields an increase in lactate production and release, along with an increase in extracellular acidification.[179]

Interestingly, Co^{2+} has been shown to induce glucose uptake and to increase lactate production through increased glycolytic enzymes activity, in liver cells, fibroblasts, and myoblasts.[180] Another transition metal ion, Ni^{2+}, has long been known to increase lactate production, likely by inhibiting PDH phosphatase.[181,182] This enzyme is responsible for PDH

activation through dephosphorylation. Consequently, pyruvate accumulates in the cytosol and is redirected into lactate production through the lactate dehydrogenase activity in order to maintain the glycolytic flux.[182] Cu^{2+} has also been shown to accelerate glycolytic flux in astrocytes, likely through increased glycolytic enzymes expression.[183] Moreover, Cr^{3+} has been shown to play a role in glucose metabolism by activating the translocation of glucose transporters to the plasma membrane in pre-adipocytes[52] and by enhancing glucose uptake in skeletal muscle cells.[184,185] Finally, another study showed that the expression of glycolytic enzymes such as triose phosphate isomerase and pyruvate kinase increased in fibroblasts after a prolonged exposure to CoCrMo microparticles.[186] The hypoxia inducible factor-1 alpha is tightly linked to macrophage metabolic reprogramming.[187] When activated (either by increased gene expression or by increased protein stability), the HIF-1α protein subunit, together with the HIF-1 beta (HIF-1ß) subunit, form the heterodimer HIF-1 complex that binds DNA and act as a transcription factor.[188] HIF-1α is expressed in several types of immune cells, including macrophages,[189] and is considered a master regulator of the cellular response to hypoxia[188,190,191] but also a key component during metabolic adaptation to a pro-inflammatory environment[192-194] and oxidative stress conditions.[195-197]

HIF-1α has been shown to induce the gene expression of several glycolytic enzymes and of other proteins involved in glucose metabolism such as glucose transporters.[198,199] Interestingly, it has been reported that metal ions such as Ni^{2+} and Cr^{6+}, but not Cr^{3+}, can stabilize HIF-1α protein expression in airway epithelial cells[200] and that Co^{2+} and Ni^{2+} can activate HIF-1 pathway and glycolytic enzymes expression in rat liver cell lines.[159,201] HIF-1α transcriptionally upregulates glycolysis and downregulates OXPHOS through multiple mechanisms, including: 1. HIF-1 induces the expression of pyruvate dehydrogenase kinase 1 (PDK-1), which phosphorylates PDH thereby inhibiting this enzyme and redirecting pyruvate away from mitochondria and towards

lactate dehydrogenase.[204] 2. HIF-1 induces the expression of Bcl-2 interacting protein 3 (BNIP3), which triggers the selective autophagy of mitochondria.[205] and 3. HIF-1 induces the expression of microRNA-210, which blocks the expression of iron-cluster assembly proteins ISCU1 and ISCU 2 that facilitate the assembly of iron-sulfur clusters, which are required for the function of the TCA cycle enzyme aconitase and ETC complex I.[206]

Importantly, HIF-1α has been shown to be essential for myeloid cell-mediated inflammation, as demonstrated by HIF-1α deletion studies,[192] and for the induction of proinflammatory cytokine gene expression, notably Il-1ß, in macrophages.[207] Furthermore, HIF-1α has been shown to be involved in the metabolic switch from aerobic respiration to aerobic glycolysis associated with macrophage polarization towards a pro-inflammatory phenotype.[208] Aerobic glycolysis is defined as glycolysis leading to OXPHOS as well as lactate production under normoxic conditions. The effects Co^{2+} and Cr^{3+} on glycolytic flux and the stabilization of HIF-1α in macrophages remain, however, largely unknown and constitute the second objective of this thesis.

2. THESIS OBJECTIVES AND HYPOTHESES

2.1 Objectives

The overall objective of this research was to identify molecular mechanisms involved in the inflammatory response of macrophages to metal ions (mainly Co and Cr ions) released from CoCrMo-based implants. The general hypothesis was that Co^{2+} and Cr^{3+} induce oxidative stress leading to changes in macrophage energy metabolism.

The specific objectives of this thesis were to:

1) Determine the effects of Co^{2+} and Cr^{3+} on oxidative stress and mitochondrial function in macrophages.
2) Determine the effects of Co^{2+} and Cr^{3+} on glycolytic flux and the stabilization of HIF-1α in macrophages.

Results from this work could unravel therapeutic strategies to target and control the inflammatory response to implant wear and corrosion products, and thereby increase implant longevity.

2.2 Hypotheses

The hypotheses of this thesis were:

1) Co^{2+} and Cr^{3+} induce oxidative stress as well as mitochondrial dysfunction in macrophages.
2) Co^{2+} and Cr^{3+} lead to an increase in glycolytic flux and the stabilization of HIF-1α in macrophages.

3. EFFECTS OF COBALT AND CHROMIUM IONS ON OXIDATIVE STRESS AND ENERGY METABOLISM IN MACROPHAGES IN VITRO

(MANUSCRIPT 1)

3.1 Foreword

As described in the literature review, wear and corrosion products have been associated with adverse local tissue reactions that can lead to implant failure. More specifically, metal ions have been shown to induce oxidative stress in macrophages but their effects on cell energy metabolism remain largely unknown. Therefore, the first objective of this thesis was to determine the effects of Co^{2+} and Cr^{3+}, released from CoCrMo implants, on oxidative stress and mitochondrial function in macrophages.

The results of this work are included in the manuscript entitled:

"Effects of cobalt and chromium ions on oxidative stress and energy metabolism in macrophages *in vitro*", by Zeina Salloum. Eric A. Lehoux, Mary-Ellen Harper, and Isabelle Catelas.

This manuscript was accepted for publication on July 21, 2018, in the Journal of Orthopaedic Research (J Orthop Res, 2018; 36(12): 3178-3187; DOI 10.1002/jor.24130).

3.2 Abstract

Cobalt and chromium ions released from cobalt-chromium-molybdenum (CoCrMo)-based implants are a potential health concern, especially since both ions have been shown to induce oxidative stress in macrophages, the predominant immune cells in periprosthetic tissues. Ions of other transition metal ions (Cd, Ni) have been reported to inhibit the activity of mitochondrial enzymes in the electron transport chain. However, the effects of Co and Cr ions on the energy metabolism of macrophages remain largely unknown. The objective of the present study was to analyze the effects of Co^{2+} and Cr^{3+} on oxidative stress and energy metabolism in macrophages *in vitro*. RAW 264.7 murine macrophages were exposed to 6-18 ppm Co^{2+} or 50-150 ppm Cr^{3+}. Results showed a significant increase in two markers of oxidative stress, reactive oxygen species level and protein carbonyl content, with increasing concentrations of Co^{2+}, but not with Cr^{3+}. In addition, oxygen consumption rates (OCR; measured using an extracellular flux analyzer) showed significant decreases in both mitochondrial respiration and non-mitochondrial oxygen consumption with increasing concentrations of Co^{2+}, but not Cr^{3+}. OCR results further showed that Co^{2+}, but not Cr^{3+}, induced mitochondrial dysfunction, including a decrease in oxidative phosphorylation capacity. Overall, this study suggests that mitochondrial dysfunction may contribute to Co^{2+}-induced oxidative stress in macrophages, and thereby to the inflammatory response observed in periprosthetic tissues.

Keywords: metal implants, metal ions, oxidative stress, energy metabolism, macrophages

3.3 Introduction

Cobalt-chromium-molybdenum (CoCrMo) alloys are used extensively in orthopaedic applications.[21] However, these alloys can undergo wear and corrosion *in vivo*, leading to the release of Co and Cr ions, which are a potential health concern.[32,209,210] Indeed, clinical studies have shown elevated concentrations of Co and Cr ions in the blood, serum, and synovial fluid of patients with a CoCrMo joint implant associated with adverse soft tissue reactions.[211-213] Nevertheless, the adverse effects of Co and Cr ions on cellular physiology remain largely unknown.

Both Co^{2+} and Cr^{3+} have been shown to induce adverse effects on cellular components including proteins, lipids, and nucleic acids.[124] For example, Petit et al.[214] reported that these metal ions induced an increase in protein carbonyl content (a measure of oxidative damage and a common marker for oxidative stress[215]) in U937 monocytes. In addition, Scharf et al.[44] reported a strong positive correlation between protein carbonyl content in periprosthetic tissues and the amount of Co and Cr present in these tissues. High levels of oxidative stress induced by Co^{2+} and Cr^{3+} may therefore contribute to adverse reactions in periprosthetic tissues, such as necrosis and soft tissue masses known as pseudotumors,[44] which often lead to implant failure.[22]

Oxidative stress (defined as "an imbalance between oxidants and antioxidants in favor of the oxidants, leading to a disruption of redox [reduction-oxidation] signaling and control and/or molecular damage"[216]) has been linked to various disease states.[125] Intracellular sources of reactive oxygen species (ROS) include enzymatic systems such as nicotinamide adenine dinucleotide phosphate (NADPH) oxidase (which produces superoxide anions) and organelles such as mitochondria, the endoplasmic reticulum (under stress), and peroxisomes.[129] NADPH oxidase protein complexes, located in the plasma membrane, are particularly important for ROS production in certain cell types, including macrophages.[129] Overall, in most cell types, mitochondria are

thought to be the major ROS-producing organelles because a high number of redox reactions occur therein. Major sites of mitochondrial ROS production include complexes I and III of the electron transport chain (ETC), and other redox enzymes such as pyruvate dehydrogenase.[217,218] The ETC, located in the mitochondrial inner membrane, is comprised of a series of four redox carrier complexes: nicotinamide adenine dinucleotide dehydrogenase, also known as NADH-ubiquinone oxidoreductase (complex I); succinate dehydrogenase (complex II); cytochrome c reductase (complex III); and cytochrome oxidase (complex IV). The ETC is coupled to oxidative phosphorylation through a proton gradient that is used by the F_0F_1 ATP synthase complex to produce ATP.

Redox-active metals play an essential role in the regulation of both mitochondrial and non-mitochondrial protein complexes.[126,131] Interestingly, it has been shown that Co^{2+} and Cu^{2+} can compete with Fe^{2+} for Fe binding sites in iron-sulfur clusters (which play a central role in the ETC), resulting in their mismetallation.[153] Since Co^{2+} and Cu^{2+} (as well as Ni^{2+}) rank higher than Fe^{2+} on the Irving-Williams Series, they can form more stable complexes than Fe^{2+}.[130] Furthermore, $Cd^{2+}$and Ni^{2+} have been shown to inhibit the activity of mitochondrial enzymes in the ETC[149,151] and induce mitochondrial ROS production.[149,152]

Finally, *in vitro* studies have shown that both Co^{2+} and Cr^{3+} can activate the production of bone-resorbing cytokines through the activation of redox-dependent mechanisms[117] and induce an inflammatory response in macrophages,[43,117] the predominant immune cells in periprosthetic tissues.[100,219] The bioenergetic demands of such an inflammatory response require a stepwise adaptation of cellular energy metabolism.[177] However, the effects of Co^{2+} and Cr^{3+} on the energy metabolism of macrophages remain largely unknown. Therefore, the objective of the present study

was to analyze the effects of Co^{2+} and Cr^{3+} on oxidative stress and energy metabolism in macrophages *in vitro*.

3.4 Materials and Methods

Unless otherwise specified, water was reagent grade (ASTM Type I).

3.4.1 Metal ions

Stock solutions of Co^{2+} and Cr^{3+} were prepared fresh, as previously described.[40] Briefly, $CoCl_2$•$6H_2O$ (99.5% purity; Fisher Scientific, Waltham, MA) and $CrCl_3$•$6H_2O$ (100.8% purity; Sigma, St Louis, MO) were dissolved in cell culture-grade water (Lonza, Walkersville, MD) and the solutions were sterilized by filtration through 0.2-μm pore size cellulose acetate syringe filters (VWR, Mississauga, ON). Sterilized solutions of Co^{2+} and Cr^{3+}contained ≤ 0.01 endotoxin unit (EU)/ml, as determined using a chromogenic *Limulus* amebocyte lysate assay (GenScript, Piscataway, NJ).

3.4.2 Cells

The RAW 264.7 murine macrophage cell line (American Type Collection Culture [ATCC[a]]; Manasas, VA) was maintained in 100-mm diameter tissue culture-treated polystyrene dishes (Greiner Bio-One; Monroe, NC) at 37ºC in a humidified atmosphere of 95% air and 5% CO_2. The cells were cultured in Dulbecco's modified Eagle medium (DMEM)-based growth medium (DMEM [Wisent; St. Bruno, QC] supplemented with 10% [v/v] qualified-grade heat-inactivated fetal bovine serum [FBS; Gibco, Carlsbad, CA]), and passaged ≤ 10 times from the working culture received from ATCC. For experiments (and routine subculture), cells were detached by pipetting using a Class A volumetric glass pipette (Sibata Scientific Technology,

[a]Erratum: correct expansion of ATCC acronym is American Type Culture Collection

Soka, Japan) and resuspended in the above growth medium to 0.5×10^6 cells/mL, unless otherwise specified.

3.4.3 Cell mortality

Tissue culture-treated polystyrene 6-well plates (Greiner Bio-One) were seeded with 2 ml of cell suspension (0.5×10^6 cells/ml) per well and incubated 2-3h under cell culture conditions to allow cell attachment. At the end of the incubation, the culture supernatants were replaced with 2 ml of growth medium containing Co^{2+} (6-24 ppm), Cr^{3+} (50-250 ppm), or cell culture-grade water (negative control), and the cells were incubated an additional 24h.

At the end of the incubation, cells were detached by gentle pipetting using a 1-ml manual single-channel pipette (Mettler Toledo, Oakland, CA) and the cell suspensions were transferred into 5-ml untreated polystyrene culture tubes (Corning, Corning, NY). Cell mortality was analyzed by dye-exclusion hemocytometry under phase contrast microscopy using trypan blue (0.04% [w/v] final concentration; Sigma-Aldrich) and an improved Neubauer hemocytometer (Hausser Scientific, Horsham, PA).

3.4.4 Cytosolic reactive oxidative species (ROS)

Tissue culture-treated black-wall polystyrene 96-well plates with a clear flat bottom (Greiner Bio-One) were seeded with 200 µl of cell suspension (0.5×10^6 cells/ml) per well and incubated 2-3h under cell culture conditions to allow cell attachment. At the end of the incubation, the culture supernatants were discarded and the cells in each well were washed twice with 100 µl of phenol red-free Hank's balanced salt solution (HBSS; Lonza) to remove traces of phenol red and FBS. Cytosolic ROS level was measured using a cell-based fluorescence assay (OxiSelect™ Intracellular ROS assay kit; Cell Biolabs, San Diego, CA) as per the manufacturer's instructions. Briefly, cells were incubated 1h at 37°C with 100 µM 2′,7′-dichlorodihydrofluorescein diacetate

(a cell-permeant fluorogenic probe) prepared in phenol red-free low glucose DMEM (Sigma-Aldrich) supplemented with 1.5 g/L of cell-culture grade $NaHCO_3$ (Sigma-Aldrich) and an additional 3.5 g/L of cell-culture grade D-glucose (Sigma-Aldrich) to replicate the formulation of the DMEM used to culture the cells. The cells were then washed two more times with phenol red-free HBSS and incubated 6h in 100 µl of phenol red-free DMEM (Sigma-Aldrich) supplemented with 10 % (v/v) heat-inactivated FBS, $NaHCO_3$ and D-glucose as above, and containing Co^{2+} (6-18 ppm), Cr^{3+} (50-150 ppm), H_2O_2 (100 µM; positive control; data not shown)[b] or cell culture-grade water (negative control). At the end of the incubation, dichlorofluorescein (DCF) fluorescence was measured with a hybrid microplate reader (Synergy™ 4; Biotek, Winooski, VT) using excitation and emission wavelengths of 480 and 530 nm, respectively.

3.4.5 Protein carbonylation

One hundred-mm diameter tissue culture-treated dishes (Greiner Bio-One) were seeded with 12 ml of cell suspension (0.5×10^6 cells/ml) per dish and incubated 2-3h under cell culture conditions to allow cell attachment. At the end of the incubation, the culture supernatants were replaced with 12 ml of growth medium containing Co^{2+} (6-18 ppm), Cr^{3+} (50-150 ppm), or cell culture-grade water (negative control), and the cells were incubated an additional 24h.

At the end of the incubation, the cells were washed twice with ice-cold Dulbecco's phosphate-buffered saline (DPBS) without Ca^{2+} and Mg^{2+} (Sigma-Aldrich) and detached carefully, using a 2-cm chiseled-edge polypropylene cell lifter (Fisher Scientific), in 1 ml (per dish) of ice-cold lysis buffer (50 mM tris [Sigma-Aldrich]; 150 mM NaCl [Fisher Scientific]; 1 mM ethylenediaminetetraacetic acid [EDTA; Fisher Scientific], pH 7.4) supplemented with an EDTA-free protease inhibitor cocktail (cOmplete™; Roche Diagnostics; Indianapolis, IN) as per the

[b]See Figure A1 in Appendix

manufacturer's instructions. The detached cells (in ca. 1-ml aliquots) were lysed by nitrogen cavitation (see Discussion section) following a 5-min exposure to a pressure of 1,250 psi inside a 45-ml capacity cell-disruption vessel (model number 4639; Parr Instrument, Moline, IL). Insoluble cellular material was removed from the lysates by centrifugation (21,000 × *g* for 30 min at 4°C). Supernatants were concentrated by centrifugal filtration (3,500 × *g* for 30 min at 4°C) using 4-ml capacity 10-kDa molecular weight cut-off low-binding regenerated cellulose filters (Millipore, Billerica, MA). Aliquots of the concentrated samples, in argon-filled 0.5-ml polypropylene cryovials (Simport; Beloeil, QC), were frozen and stored in liquid nitrogen for future protein carbonyl content analysis.

Protein determination was performed using the bicinchoninic acid colorimetric assay with bovine serum albumin (BSA) as the protein standard (Thermo Scientific, Rockford, IL). Absorbance was measured at a wavelength of 562 nm using a hybrid microplate reader (Biotek). Protein carbonyl content was quantified by immunochemical detection after derivatization with 2,4-dinitrophenylhydrazine (DNPH) as described by Wehr et al.[220], with minor modifications. Cell lysate proteins oxidized by exposure to $FeCl_3$ and ascorbate[221] (which together act as a ROS-generating system[222]) were used as a positive control (data not shown). Briefly, samples (3 µg protein/µl) were mixed with one volume of 20% [w/v] sodium dodecyl sulfate (SDS; Fisher Scientific) and two volumes of 20 mM DNPH solution (Sigma-Aldrich) in 10% (v/v) trifluoroacetic acid (Sigma-Aldrich), then incubated 15 min at room temperature. The incubation was terminated by adding two volumes of neutralization solution (1.5 M tris, 22.5% [v/v] glycerol [Sigma-Aldrich]). Aliquots (3 µg proteins) of the derivatized samples were mixed with sample loading buffer (LI-COR, Lincoln, NE), as per the manufacturer's instructions (except that the final loading buffer concentration was 0.5X and, as recommended by Wang et al.,[223] the reducing agent

was omitted), and analyzed by SDS-polyacrylamide gel electrophoresis (PAGE) using precast mini-format Tris-glycine gradient (8-16%) gels (Bio-Rad; Hercules, CA). Pre-stained (visible and near-infrared) protein molecular weight standards (LI-COR) and 2,4-dinitrophenyl (DNP)-derivatized protein molecular weight standards (OxyBlot® Protein Oxidation Detection Kit; Millipore) were used (note: the molecular weights provided by the manufacturer for the DNP-derivatized standards are those of the underivatized proteins and are therefore likely underestimated). Two identical gels were run in parallel: one was used for western blotting (this gel was truncated above the 260 kDa molecular weight mark prior to electrotransfer to avoid gel compression artifacts), and the other was stained with Coomassie Brilliant Blue R-250 dye (Bio-Rad). For western blotting, proteins were electrotransferred onto a 0.45-µm pore size fluorescent-grade polyvinylidene fluoride (PVDF) membrane (Immobilon-FL; Millipore). The membrane was air-dried overnight, reversibly stained for total protein with acid blue (REVERT™ total protein stain; LI-COR) as per the manufacturer's instructions, and imaged at 700 nm using a near-infrared fluorescence/chemiluminescence imaging system (Odyssey® Fc; LI-COR). Immunodetection was performed using a rabbit anti-DNP antibody as the primary antibody and a goat anti-rabbit horseradish peroxidase (HRP)-conjugated antibody as the secondary antibody (OxyBlot® Protein Oxidation Detection Kit; Millipore), as per the manufacturer's instructions. DPBS containing 0.1% (v/v) polysorbate 20 (Fisher Scientific) and 1% (w/v) BSA (Sigma-Aldrich) was used as the blocking and antibody dilution buffer. Chemiluminescence detection was performed using chemiluminescent HRP substrate (Millipore) as per the manufacturer's instructions, and the blots were imaged using a near-infrared fluorescence/chemiluminescence imaging system (LI-COR). Chemiluminescence intensity was normalized to protein content determined by acid-blue staining. Both acid-blue staining and chemiluminescence were analyzed by densitometry using Image

Studio™ software v.2.0 (LI-COR). No chemiluminescence was detected when DPNH was omitted from the derivatization step, thereby confirming the specificity of the detection system for the DNP moiety of the derivatized proteins (data not shown).

3.4.6 Cellular oxygen consumption

Cellular oxygen consumption rates (OCR) were measured using an extracellular flux analyzer (Seahorse XF96e; Agilent Technologies, Santa Clara, CA). Briefly, the cartridge sensors were incubated overnight at 37°C in a hydration/calibration solution (XF Calibrant; Agilent Technologies). Specially designed polystyrene tissue culture-treated 96-well microplates with a clear flat bottom (Seahorse XF96 V3 PS Cell Culture Microplates; Agilent Technologies) were then seeded with 80 µl of cell suspension (1.0×10^6 cells/ml) per well and incubated 2-3h under cell culture conditions to allow cell attachment.

At the end of the incubation, the culture supernatants were replaced with growth medium containing Co^{2+} (6-18 ppm), Cr^{3+} (50-150 ppm), cell culture-grade water (negative control), or lipopolysaccharide (LPS) from *E. coli* O55:B05 (1 µg/ml; Sigma-Aldrich; positive control [data not shown])[c]. The cells were incubated 6h under cell culture conditions, then washed and incubated 45min at 37°C in base medium (phenol red-free low glucose DMEM [Sigma-Aldrich] supplemented with 3.5 g/l of cell-culture grade D-glucose [Sigma-Aldrich]). OCR were measured to assess resting respiration, then ATP production-dependent respiration, maximal respiration, and non-mitochondrial oxygen consumption, after sequential injections of oligomycin (an ATP synthase inhibitor) at 1 µM (final concentration), carbonyl cyanide *m*-chlorophenyl hydrazone (an ionophore acting as a proton uncoupler) at 2 µM, and rotenone and antimycin A (complex I and complex III inhibitors, respectively) at 0.5 µM. Spare respiratory capacity, a measure of the ability

[c]See Figure A2 in Appendix

of cells to respond to increased energy demand, was calculated by subtracting resting respiration from maximal respiration. ATP production-dependent respiration was calculated by subtracting the lowest OCR after oligomycin injection from resting OCR. Proton leak, represented by basal respiration (i.e., mitochondrial respiration that is not coupled to ATP production), was calculated by subtracting the OCR corresponding to non-mitochondrial oxygen consumption from the lowest OCR after oligomycin injection. Non-mitochondrial oxygen consumption was subtracted from the reported resting respiration, maximal respiration, spare respiratory capacity, and ATP production-dependent respiration. For each parameter, OCR measurements were performed three times at 6-min intervals. All OCR measurements were corrected for the OCR of cell-free wells containing only medium. Upon completion of the OCR measurements, the cells were washed once with PBS and lysed in 1M NaOH (40 µl/well). The lysates were kept at 4°C for up to 24h, and protein determination was performed using the Bradford colorimetric assay with BSA as the standard protein (Thermo Scientific). Absorbance was measured at a wavelength of 595 nm using a hybrid microplate reader (Biotek).

3.4.7 Statistical analysis

Statistical analysis was performed using IBM SPSS Statistics software for Windows, version 24.0 (IBM, Armonk, NY). The data were assumed to be normally distributed and Levene's test was used to determine if the assumption of homogeneity of variance was met. When met, a two-way analysis of variance (ANOVA) was used for group-wise comparisons followed by Tukey-Kramer post-hoc tests. When unmet, a Welch ANOVA was performed followed by Games-Howell post-hoc tests. $p<0.05$ was considered significant. Effect sizes are presented as Cohen's d with 95% confidence intervals (CI). Data are presented as means ± standard errors of the means (SEM).

3.5 Results

3.5.1 Effects of Co^{2+} and Cr^{3+} on macrophage mortality

Results revealed a Co^{2+} concentration-dependent increase in the percentage of dead macrophages of up to 33% with 24 ppm Co^{2+} (d=2.5, 95% CI [0.3, 4.6]; p<0.001, Fig. 3.1A), relative to the negative control (cells unexposed to Co^{2+} or Cr^{3+}). Cr^{3+} also induced a concentration-dependent increase in the percentage of dead cells of up to 27% with 250 ppm (d=5.2, 95% CI [1.9, 8.6]; p<0.001, Fig. 3.1B), relative to the negative control. It should be noted that since the percentage of dead cells is calculated based on the total number of cells (live + dead) present at the end of the 24-hour exposure, disintegrated cells are excluded from this percentage.

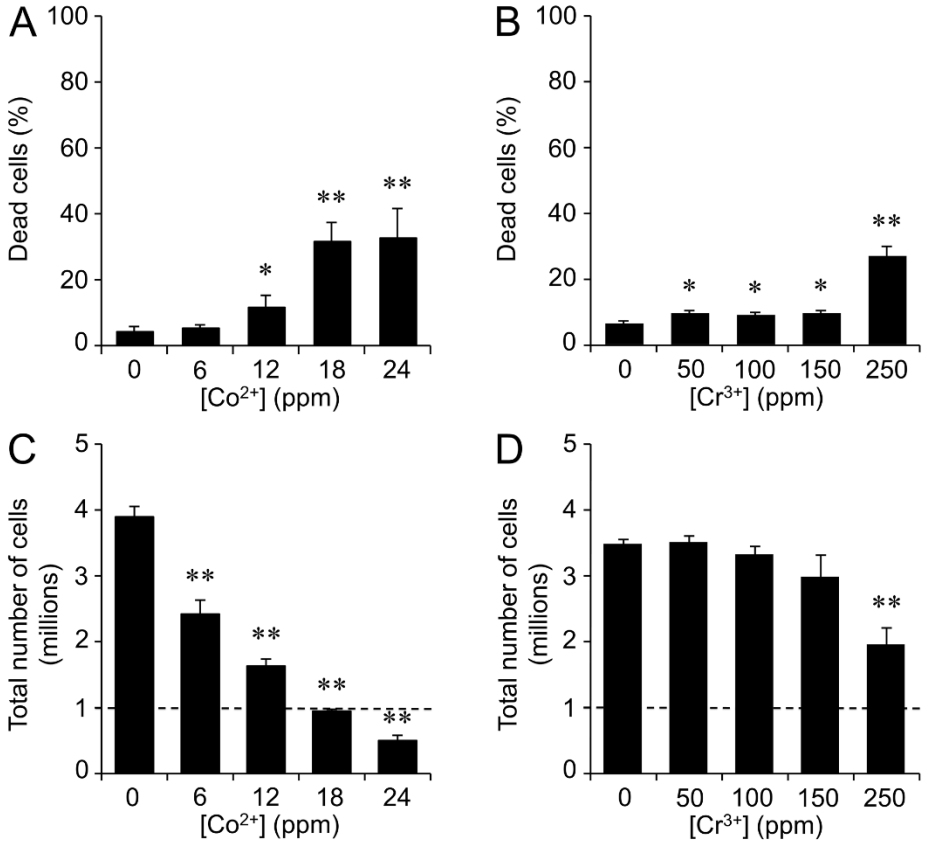

Figure 3.1: Mortality of RAW 264.7 macrophages after a 24-h exposure to Co^{2+} or Cr^{3+}. Percentage of the total number of cells (viable + dead) that were dead after exposure to (A) Co^{2+} or (B) Cr^{3+}. Total number of cells (viable + dead) after exposure to (C) Co^{2+} or (D) Cr^{3+}. Cells were incubated under cell culture conditions with the indicated concentrations of Co^{2+} or Cr^{3+}. At the end of the incubation, mortality was analyzed by dye-exclusion hemocytometry using trypan blue. The dashed line represents the number of cells 3h prior to the start of the 24-h exposure (see Materials and Methods section). Statistical analysis was performed using a Welch ANOVA followed by Games-Howell post-hoc tests since the homogeneity of variance assumption was unmet, as per Levene's test. An asterisk (*) and double-asterisk (**) indicate a significant difference between a given condition and the negative control (cells unexposed to Co^{2+} or Cr^{3+}), with $p<0.05$ and $p\leq0.001$, respectively. Data are presented as means ± SEM of three independent experiments, each performed with three replicate samples per condition.

The total number of macrophages (live + dead) exposed to Co^{2+} and Cr^{3+} increased due to proliferation, except with 18 and 24 ppm Co^{2+} where death resulting in cellular disintegration decreased the total number of cells below the initial 1×10^6. However, the total number of macrophages was lower after exposure to Co^{2+}, relative to the negative control, at all the

concentrations tested (up to 87% lower with 24 ppm Co^{2+}; d=15.1, 95% CI [6.4, 23.8]; p<0.001, Fig. 3.1C). In contrast, after exposure to Cr^{3+}, the total number of macrophages was lower, relative to the negative control, only at the highest concentration tested (44% lower with 250 ppm Cr^{3+}; d=5.2, 95% CI [1.8, 8.5]; p<0.001, Fig. 3.1D).

3.5.2 Effects of Co^{2+} and Cr^{3+} on oxidative stress in macrophages

Results revealed a Co^{2+} concentration-dependent increase in cytosolic ROS level of up to 520% with 18 ppm Co^{2+} (d=10.2, 95% CI [5.9, 14.4]; p<0.001; Fig. 3.2A), relative to the negative control, after a 6-hour exposure. In contrast, Cr^{3+} did not induce any significant changes in ROS level (Fig. 3.2B).

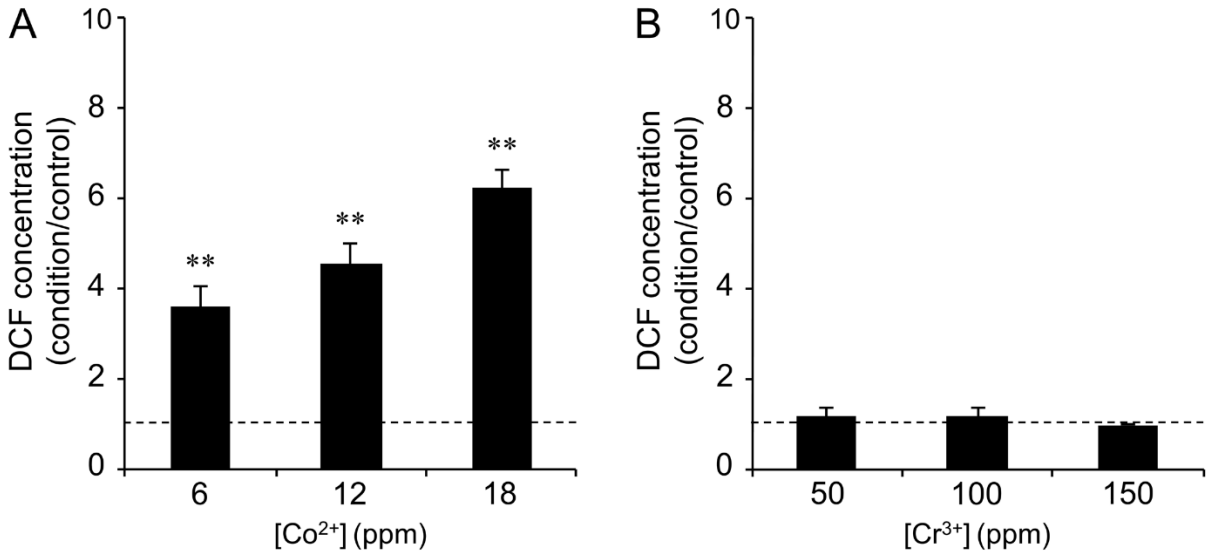

Figure 3.2: Cytosolic reactive oxygen species (ROS) levels in RAW 264.7 macrophages after a 6-h exposure to (A) Co^{2+} or (B) Cr^{3+}. ROS were assayed using the redox sensitive probe 2′,7′-dichlorodihydrofluorescein diacetate. 2′,7′-Dichlorofluorescein (DCF) concentration, expressed relative to the DCF concentration in the negative control (cells unexposed to Co^{2+} or Cr^{3+}; represented by a dashed line), is directly proportional to the level of cytosolic ROS. Data are presented as means ± SEM of three independent experiments, each performed with 5-6 replicate samples per condition. Statistics as in Figure 1.

Results also revealed a Co^{2+} concentration-dependent increase in protein carbonyl content of 31% and 86% with 12 ppm and 18 ppm Co^{2+}, respectively (d=8.7, 95% CI [3.5, 13.9] and d=3.8, 95% CI [1.1, 6.5], respectively; p<0.05; Fig. 3.3A), relative to the negative control, after a 24-hour exposure. In contrast, Cr^{3+} did not induce any significant changes in protein carbonyl content (Fig. 3.3B).

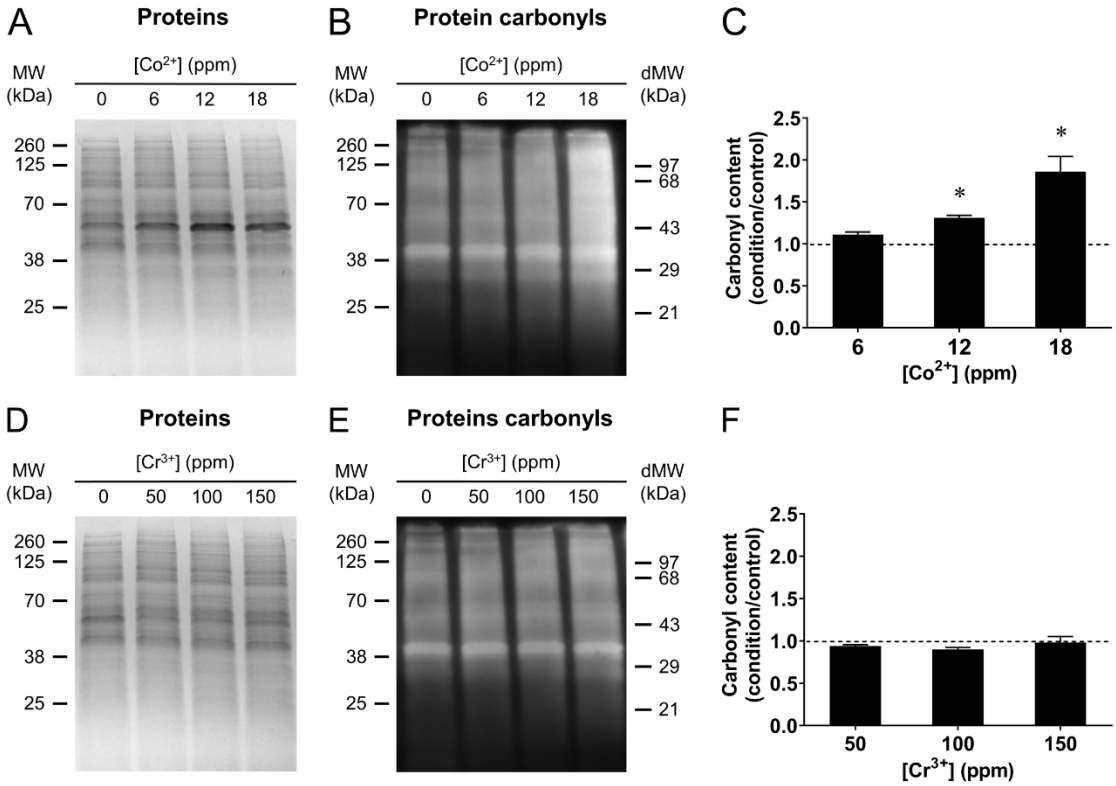

Figure 3.3: Protein carbonyl content in RAW 264.7 macrophages after a 24-h exposure to Co^{2+} (A-C) or Cr^{3+} (D-F). (A) and (D): Polyacrylamide gels of whole-cell extracts treated with 2,4-dinitrophenylhydrazine, analyzed by SDS-PAGE (3µg proteins per lane), and stained with the protein-binding dye Coomassie Brilliant Blue. (B) and (E): Western blots of protein carbonyls performed with gels ran in parallel to those shown in panels (A) and (D). (C) and (F): Protein carbonyl content (determined by densitometric analysis of the western blots) normalized to protein content (determined by acid-blue staining of the blots) and expressed relative to the negative control (cells unexposed to Co^{2+} or Cr^{3+}; represented by a dashed line). Representative gels and western blots are shown. Data in panels (C) and (F) are presented as means ± SEM of three independent experiments. MW: pre-stained protein molecular weight standards. dMW: 2,4-dinitrophenyl (DNP)-derivatized protein molecular weight standards – the indicated molecular weights are those of the corresponding underivatized proteins. Statistics as in Figure 1.

3.5.3 Effects of Co^{2+} and Cr^{3+} on macrophage oxygen consumption rates

Results revealed a Co^{2+} concentration-dependent decrease in resting respiration of up to 26% with 18 ppm Co^{2+} (d=3.8, 95% CI [2.8, 4.7]; p<0.001; Fig. 3.4A), relative to the negative control. Similarly, a decrease was observed in ATP production-dependent respiration (up to 24%; d=2.9, 95% CI [2.1, 3.8]), maximal respiration (up to 43%; d=4.4, 95% CI [3.3, 5.4]), and spare respiratory capacity (up to 60%; d=4.0, 95% CI [3.0, 5.0]) (p<0.001 in all cases; Fig. 3.4A).

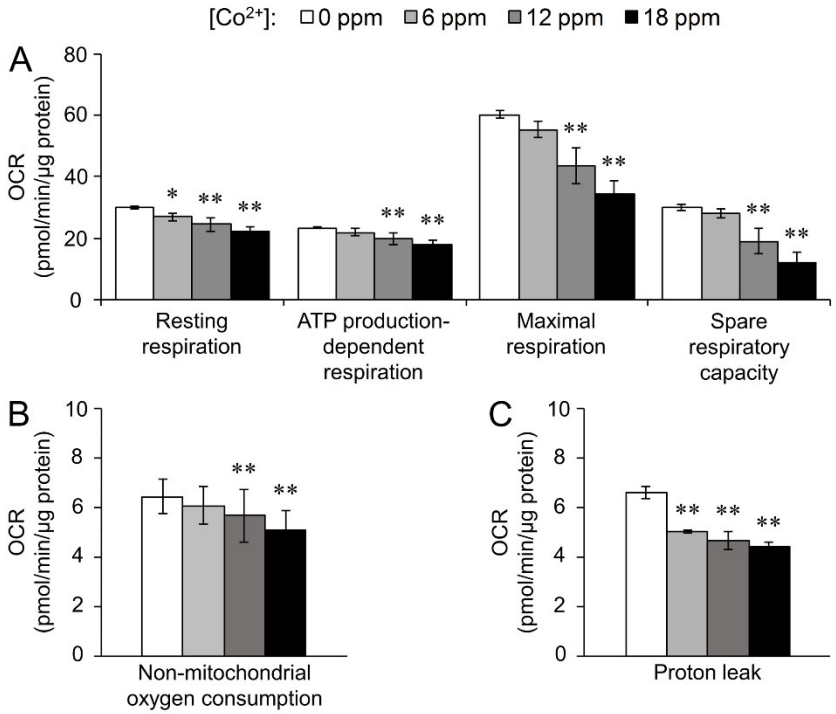

Figure 3.4: Cellular oxygen consumption rates (OCR) of RAW 264.7 macrophages following a 6-h exposure to Co^{2+}: (A) Mitochondrial respiration parameters; (B) Non-mitochondrial oxygen consumption; (C) Proton leak, represented by basal respiration (i.e., mitochondrial respiration that is not coupled to ATP production). OCR (measured using an extracellular flux analyzer) were normalized to protein content (determined using a colorimetric assay). Data are presented as means ± SEM of three independent experiments, each performed with 7-8 replicate samples per condition. Statistics as in Figure 1 except that, since the homogeneity of variance assumption was met for some parameters as per Levene's test, a two-way ANOVA and Tukey-Kramer post-hoc tests were used to analyze these parameters.

A decrease was also observed in non-mitochondrial oxygen consumption (up to 21%; d=1.1, 95% CI [0.4, 1.7]; p<0.001; Fig. 3.4B), and in proton leak with all Co^{2+} concentrations (up to 33%; d=5.3, 95% CI [4.1, 6.5]; p<0.001; Fig. 3.4C).

In contrast, Cr^{3+} did not induce any significant changes in OCR except for proton leak, which decreased only with 100 ppm Cr^{3+} (d=4.2, 95% CI [3.2, 5.2]; p<0.001; Fig. 3.5C), relative to the negative control.

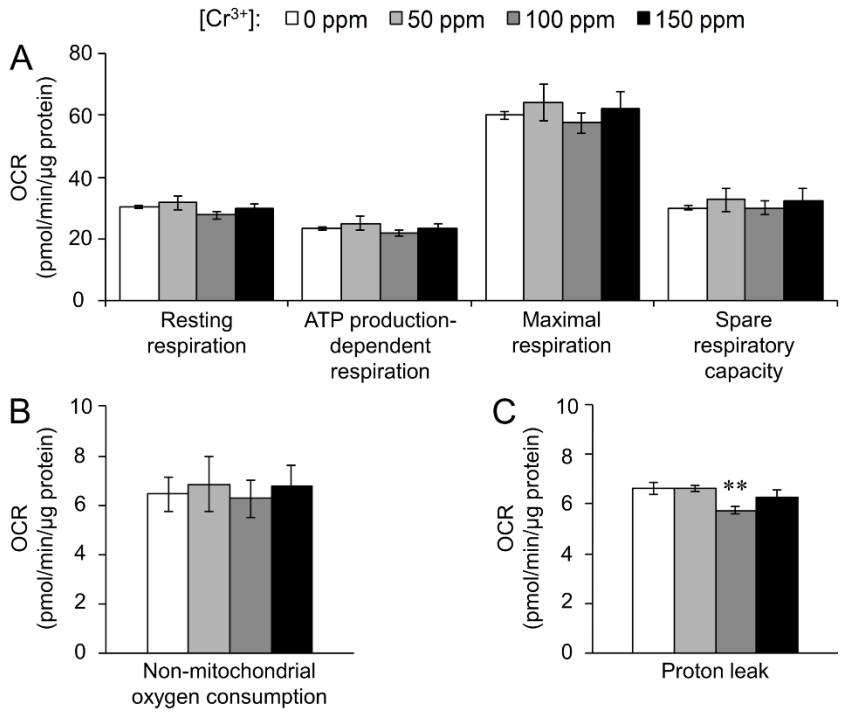

Figure 3.5: Cellular oxygen consumption rates (OCR) of RAW 264.7 macrophages following a 6-h exposure to Cr^{3+}: (A) Mitochondrial respiration parameters; (B) Non-mitochondrial oxygen consumption; (C) Proton leak, represented by basal respiration (i.e., mitochondrial respiration that is not coupled to ATP production). OCR (measured using an extracellular flux analyzer) were normalized to protein content (determined using a colorimetric assay). Data are presented as means ± SEM of three independent experiments, each performed with 7-8 replicate samples per condition). Statistics as in Figure 4.

3.6 Discussion

The present study analyzed the effects of Co^{2+} and Cr^{3+} on oxidative stress and energy metabolism in macrophages, the predominant immune cells in periprosthetic tissues.[100,219] To the

best of our knowledge, this is the first study to examine the effects of these metal ions on mitochondrial respiration parameters *in cellula* and on oxidative stress in the context of mitochondrial dysfunction. Results showed that Co^{2+}, but not Cr^{3+}, induced ROS production and protein carbonylation, suggesting that Co^{2+} may be inducing oxidative stress through ROS. Results also showed that Co^{2+}, but not Cr^{3+}, adversely affected mitochondrial function.

The effects of Co^{2+} and Cr^{3+} were studied because Co and Cr are the primary components of CoCrMo alloys that are used extensively in orthopaedic applications. Co exists in two common oxidation states (+2 and +3). However, Co^{2+} was used in the present study because Co^{3+} is rapidly reduced to Co^{2+} in aqueous environments.[40] Similarly, Cr exists in two common oxidation states (+3 and +6), but Cr^{3+} was used in the present study because Cr^{6+} is rapidly reduced to Cr^{3+} under physiological conditions.[40] The ranges of Co^{2+} and Cr^{3+} concentrations used in the present study were based on: (1) previous studies analyzing the effects of Co^{2+} and Cr^{3+} on oxidative stress and inflammatory cytokine release from macrophages *in vitro*[42,43,117,118,214]; (2) the assumption that the concentration of these ions is higher in periprosthetic tissues than in body fluids where their concentrations are in the ppb range; and (3) the consideration that macrophage stimulation probably requires higher concentrations of a stimulating agent *in vitro* than it does *in vivo,* where cells are exposed to multiple stimulating factors simultaneously.[43,118] The RAW 264.7 murine macrophage cell line was used because it is a common model for *in vitro* studies of molecular pathways activated by implant wear particles or metal ions,[114,224,225] and of oxidative stress and mitochondrial function.[226] Immortalized cells, as opposed to primary cells, were selected to avoid potential inter-donor variability. Limitations of the RAW 264.7 macrophage model include its murine origin,[227] as well as higher metabolic rates and OCR than primary murine macrophages.[228]

Mortality analysis showed a Co^{2+} concentration-dependent increase in the percentage of dead cells and lower total numbers of cells (live + dead) after a 24-hour exposure to Co^{2+}, relative to the negative control. The lower total numbers of cells were due to a concentration-dependent reduction in cell proliferation (as evidenced by a decrease in the proportion of actively dividing cells, as determined by fluorescence microscopy using Hoechst 33342 DNA staining; data not shown), as well as death resulting in cellular disintegration. In contrast to the results obtained with Co^{2+}, exposure to Cr^{3+} only increased the percentage of dead cells at the highest concentration analyzed and the total number of cells was lower only at that concentration. Overall, these results reflect the greater cytotoxicity of Co^{2+}, relative to Cr^{3+}, in agreement with previous macrophage studies.[229-231]

The effects of Co^{2+} and Cr^{3+} on oxidative stress were analyzed through measurements of cytosolic ROS level and total protein carbonyl content. In macrophages, elevated concentrations of ROS (which are by-products of oxidative metabolism) can induce an inflammatory response through redox signaling,[127,232] and possibly lead to oxidative damage of cellular components and consequent impairment of cellular functions.[232] Reversible and irreversible oxidative modifications of proteins by ROS occur during redox signaling and as a consequence of acute or chronic oxidative stress.[220] Since protein carbonylation occurs in many of these modifications, it is a standard marker for oxidative stress.[220] Overall, the results showed that Co^{2+}, but not Cr^{3+}, increased ROS levels by up to 520% and protein carbonyl content by up to 86%. By comparison, the exposure of RAW 264.7 macrophages to phorbol 12-myristate 13-acetate (PMA), a potent inducer of ROS production via NAPDH oxidase, has been reported to increase ROS production by up to ca. 1,200% at peak oxidative burst, and protein carbonyl content by up to ca. 30% approximately 25 min post-peak oxidative burst.[233] Nevertheless, the magnitude of changes in

ROS levels in the cells exposed to Co^{2+} should be interpreted cautiously given the technical challenges presented by the detection of intracellular ROS.[234] Notwithstanding, the results of the present study suggest that exposure to Co^{2+} can cause a substantial increase in oxidative stress in macrophages by inducing ROS production. The mechanisms by which Co^{2+} induce ROS production in macrophages remain unclear. One of the mechanisms may involve Fenton-like reactions where intracellularly generated hydrogen peroxide (normally decomposed by catalase into water and oxygen) reacts with Co^{2+} to produce highly reactive hydroxyl radicals.[44] Excessive production of these radicals can overwhelm cellular antioxidant systems thereby causing oxidative stress.[235] *In vivo* exposure to Co^{2+} for 24h has also been reported to decrease the activity of superoxide dismutase and catalase, two antioxidant enzymes playing a prominent role in the neutralization of ROS.[156] Other mechanisms by which Co^{2+} induce ROS production in macrophages may involve the ETC and NADPH oxidase. As previously mentioned, in the absence of exogenous metal ions, cellular ROS production originates primarily from mitochondria and the plasma membrane where NADPH oxidase complexes are located.

In the present study, the analysis of oxygen consumption showed significant decreases in mitochondrial respiration with increasing Co^{2+} concentrations, suggesting that Co^{2+} induces mitochondrial dysfunction and affect overall cellular energy metabolism. Specifically, results showed that Co^{2+}, but not Cr^{3+}, decreased resting respiration by up to 26%, ATP production-dependent respiration by up to 24%, and maximal respiration by up to 43%. By comparison, the polarization of naïve murine bone marrow-derived macrophages (BMDM) to the inflammatory (M1) phenotype by LPS and interferon-γ has been reported to decrease these respiration parameters by ca. 60%, 65%, and 85%, respectively.[236] The effects of Co^{2+} on the mitochondrial respiration parameters are therefore substantial and consistent with dysfunctional oxidative

phosphorylation. A Co^{2+}-induced decrease in the capacity of mitochondria to produce ATP may thus have a significant impact on overall cellular energy metabolism and, as discussed below, may lead to the activation of mechanisms that help maintain cellular energy homeostasis. The effects of Co^{2+} on mitochondrial respiration parameters may be due to interactions with pathways involved in the regulation of energy metabolism and/or mitochondrial components, including the ETC located in the mitochondrial inner membrane. ETC complexes I, II, and III contain iron-sulfur clusters and, as previously mentioned, Co^{2+} can cause mismetallation of these clusters by competing with Fe^{2+} for Fe binding sites.[153] This mismetallation may lead to ETC dysfunction and cause the release of Fe ions into the intracellular environment. The released Fe ions may produce ROS through the Fenton reaction and further contribute to oxidative stress by consuming cellular antioxidants through redox cycling between Fe^{2+} and Fe^{3+}.[237] Interestingly, divalent ions of cadmium (Cd^{2+}), a transition-metal ion, have also been shown to inhibit the complexes of the ETC (especially complexes II and III) and induce ROS production at the complex III site.[149] Therefore, Co^{2+} may similarly interfere with electron transfer in the ETC and induce ROS production. The decrease in proton leak observed in the presence of Co^{2+} is in agreement with this possibility since inhibition at any position in the ETC would decrease proton pumping activity, thereby decrease the proton-motive force and consequently proton leak.[139,238] In addition, carbonylation of mitochondrial complexes has been reported in heart tissue (complexes I, II, III and the F_0F_1 ATP synthase)[239] as well as in muscle and white adipose tissue (complex I).[155] Furthermore, ROS-induced carbonylation of complex I has been shown to increase ROS production implying a feed-forward control loop amplifying small changes in ROS production and consequent protein carbonylation.[155] Therefore, Co^{2+}-induced ROS production may result in the carbonylation of mitochondrial complexes leading to mitochondrial dysfunction and further ROS production.

Finally, results showed a Co^{2+}-induced decrease in non-mitochondrial oxygen consumption, suggesting that Co^{2+} may also affect NADPH oxidase reactions.[131,238,240]

Interestingly, while the present study showed that Co^{2+}, but not Cr^{3+}, induced oxidative stress, other studies have reported increased oxidative stress in macrophages exposed to Cr^{3+},[44,214,241] albeit to a lesser extent than in macrophages exposed to Co^{2+}.[9,11] This discrepancy in the effects of Cr^{3+} may be explained by differences in methodologies. For example, in the present study (unlike in previous studies[44,214]), nitrogen cavitation was used to lyse cells for the determination of protein carbonyl content because the cells exposed to Co^{2+} or Cr^{3+} exhibited an ion concentration-dependent resistance to lysis by non-ionic detergents (unpublished observation). Furthermore, in the present study the DNPH and neutralization solutions were prepared in-house because the solutions provided with the OxyBlot® Protein Oxidation Detection Kit (a kit used in previous studies[44,214]) generated overly acidic samples resulting in protein precipitation and SDS-PAGE artifacts (data not shown). Problems with reagents from the OxyBlot® Protein Oxidation Detection Kit have also been reported by others.[223] Notwithstanding, it should be emphasized that the results of the present study are consistent, i.e., Co^{2+}-induced ROS production is associated with an increase in protein carbonylation and mitochondrial dysfunction, whereas Cr^{3+} induced neither ROS production, protein carbonylation nor mitochondrial dysfunction. Finally, the use of different cell models (RAW 264.7 vs. U937, J774A.1, and murine BMDM) cannot presently be excluded as a potential cause of, or contributing factor to, the discrepancy in the effects of Cr^{3+} on oxidative stress.

The observed Co^{2+}-induced decrease in ATP production may lead to the activation of AMP-activated protein kinase (AMPK), resulting in the stimulation of catabolic pathways and inhibition of anabolic pathways to conserve energy.[163] Under these conditions, energy-dependent

cellular functions may be negatively affected, especially under scenarios of high energy demand such as those prevailing in macrophages actively involved in immune functions. For example, exposure of macrophages to particles of a Ni- and Cu-based material has been shown to impair phagocytic capacity and mitochondrial function, suggesting a possible causal relationship.[226] In the context of periprosthetic tissues, a Co^{2+}-induced decrease in ATP production could therefore decrease the capacity of macrophages to clear metal wear products. Co^{2+}-induced mitochondrial dysfunction may also prevent repolarization of macrophages from the inflammatory to the anti-inflammatory phenotype.[236] Furthermore, since the energy requirements of the pro- and anti-inflammatory responses of macrophages are primarily met by anaerobic glycolysis and aerobic respiration, respectively, a Co^{2+}-induced decrease in ATP production would be expected to primarily decrease the capacity of macrophages to mount an anti-inflammatory response.[242]

3.7 Conclusion

The present study showed that Co^{2+}, but not Cr^{3+}, induced ROS production and protein carbonylation, suggesting that Co^{2+} induces oxidative stress through an increase in ROS production and possibly through a weakening of antioxidant defenses. Results also showed that Co^{2+} caused mitochondrial dysfunction, including a decrease in oxidative phosphorylation capacity. Overall, these results suggest that mitochondrial dysfunction may contribute to Co^{2+}-induced oxidative stress in macrophages, and thereby to the inflammatory response observed in periprosthetic tissues.

3.8 Acknowledgements

The authors thank Dr. Rodney L. Levine and Nancy B. Wehr for expert advice on the protein carbonyl quantification assay, as well as Corey DeVlugt and Dr. David Patten for expert assistance with the cellular OCR analyses. This work was supported by the Canadian Institutes of Health Research (CIHR; operating grant MOP-133712) (IC), the Canada Research Chairs (CRC)

Program (IC), the Ontario Ministry of Research and Innovation (MRI; Early Researcher Award ER10-07-112) (IC), as well as by the Natural Sciences and Engineering Research Council of Canada (NSERC; Discovery Grant RGPIN 04973) (M-EH).

4. EFFECTS OF COBALT AND CHROMIUM IONS ON GLYCOLYTIC FLUX AND THE STABILIZATION OF HYPOXIA-INDUCIBLE FACTOR-1α IN MACROPHAGES IN VITRO

(MANUSCRIPT 2)

4.1 Foreword

As described in the first manuscript (Chapter 3), results on the effects of metal ions on energy metabolism in macrophages revealed that Co^{2+}, but not Cr^{3+} decreased OXPHOS. A central pathway of cellular energy metabolism is the glycolytic pathway. Interestingly, pro-inflammatory stimuli have been shown to cause macrophages to undergo a metabolic switch away from OXPHOS towards glycolysis. However, the effects of Co^{2+} and Cr^{3+} on glycolytic flux remain largely unknown. Therefore, the second objective of this thesis was to determine the effects of Co^{2+} and Cr^{3+} on glycolytic flux and the stabilization of HIF-1α in macrophages.

The results of this work are included in the manuscript entitled:

"Effects of cobalt and chromium ions on glycolytic flux and the stabilization of HIF-1α in macrophages *in vitro*", by Zeina Salloum, Eric A. Lehoux, Mary-Ellen Harper, and Isabelle Catelas.

This manuscript is currently under review for publication in the Journal of Orthopaedic Research (J Orthop Res). Minor revisions have been made since submission.

4.2 Abstract

Implant wear and corrosion products can lead to chronic inflammation and, consequently, periprosthetic osteolysis. Wear and corrosion products are therefore of great clinical concern. For example, Co^{2+} and Cr^{3+} released from cobalt-chromium-molybdenum (CoCrMo)-based implants, have been shown to induce a pro-inflammatory response in macrophages *in vitro*. Previous studies have also shown that macrophage activation by pro-inflammatory stimuli can cause a hypoxia-inducible factor-1α (HIF-1α)-dependent metabolic shift away from oxidative phosphorylation towards glycolysis. However, the effects of Co^{2+} and Cr^{3+} on energy metabolism in macrophages remain largely unknown. Therefore, the objective of this study was to analyze the effects of Co^{2+} and Cr^{3+} on glycolytic flux and the stabilization of HIF-1α in macrophages. RAW 264.7 murine macrophages were exposed to 6-24 ppm Co^{2+} or 50-250 ppm Cr^{3+}. Glycolytic flux was measured by extracellular flux analysis and lactate determinations. HIF-1α stabilization was analyzed by immunoblotting. Results showed that Co^{2+}, and to a lower extent Cr^{3+}, induced an increase in glycolytic flux. Finally, results showed that only Co^{2+} stabilized HIF-1α, suggesting that HIF-1α is involved in the Co^{2+}-induced increase in glycolytic flux in macrophages. Overall, these results, together with our previous results showing that Co^{2+} increases oxidative stress and decreases oxidative phosphorylation, suggest that Co^{2+} (but not Cr^{3+}) can induce a HIF-1α-dependent metabolic shift away from oxidative phosphorylation towards aerobic glycolysis in macrophages. This metabolic shift, similar to that associated with the metabolic reprogramming of macrophages towards a pro-inflammatory phenotype, may play a central role in the proinflammatory response induced by Co^{2+} in the periprosthetic environment.

Keywords: metal implants, metal ions, macrophages, glycolysis, lactate production, HIF-1α.

4.3 Introduction

Wear and corrosion at modular interfaces of joint implants have been associated with early adverse local tissue reactions (ALTR) leading to implant failure.[243] In addition, the long-term release of wear and corrosion products can lead to chronic inflammation and, consequently, periprosthetic osteolysis. Wear and corrosion products are therefore of great clinical concern. For example, Co and Cr ions, released from cobalt-chromium-molybdenum (CoCrMo)-based implants, can induce a pro-inflammatory response in macrophages *in vitro,*[43,117,118] the predominant immune cell type in periprosthetic tissues.[100,219] Furthermore, activation of macrophages by pro-inflammatory stimuli has been shown to cause a metabolic shift away from oxidative phosphorylation towards glycolysis.[163,244] Consequently, a better understanding of the effects of Co^{2+} and Cr^{3+} on the energy metabolism of macrophages could provide insights into the pathomechanisms of these metal ions in the periprosthetic environment. Our group recently showed that exposure to Co^{2+}, but not Cr^{3+}, induced oxidative stress and a decrease of oxidative phosphorylation in RAW 264.7 macrophages.[245] However, the effects of these metal ions on glycolytic flux in macrophages remain largely unknown.

Several metal ions have been shown to affect glucose catabolism in non-immune cells. For example, exposure to Co^{2+} has been shown to increase glucose uptake and lactate production in primary articular chondrocytes,[246] as well as in Clone 9 liver epithelial cells, 3T3-L1 preadipocytes, and C2C12 myoblasts.[180] Furthermore, in Clone 9 cells, these effects were associated with an increase in hexokinase and lactate dehydrogenase activity. Ni^{2+} and Cu^{2+} have been shown to increase glycolytic flux in human lung carcinoma cells[151] and primary astrocytes,[183] respectively. In contrast to these divalent metal cations, Cr^{3+} has been reported to have no effect on glucose uptake in murine 3T3-L1 cells[52] and rat L6 muscles cells,[247] although the concentration

of chromium picolinate supplement was very low (5.2 ppm). Finally, prolonged exposure to CoCrMo alloy particles (1-7 μm diameter) has been reported to increase the expression of two glycolytic enzymes: triosephosphate isomerase and pyruvate kinase, in fibroblasts.[186]

Co^{2+} and Ni^{2+}, but not Cu^{2+}, are thought to increase glycolytic flux by stabilizing hypoxia-inducible factor-1α (HIF-1α),[151,183,246] a subunit of the heterodimeric transcription factor HIF-1, which is known to transcriptionally upregulate glycolysis.[248] For example, both Co^{2+} and Ni^{2+} have been shown to stabilize HIF-1α and increase the expression of HIF-1-regulated genes, including genes encoding glycolytic enzymes, in H4-II-E-C3 rat hepatoma cells.[159,201] Ni^{2+} and Cr^{6+} have also been shown to stabilize HIF-1α and induce HIF-1-regulated gene expression in 1HAEo human airway epithelial cells.[200,249] Interestingly, Cr^{6+} has been shown to stabilize HIF-1α but only until it is reduced to Cr^{3+}.[249]

Many metal ions, including Co^{2+}, Ni^{2+}, and Cr^{6+} have been shown to stabilize HIF-1α by oxidizing intracellular ascorbate, either directly, catalytically, or indirectly through oxidative stress.[200,249,250] Ascorbate is a cofactor of the propyl hydroxylase domain (PHD) proteins that hydroxylate HIF-1α, leading to its proteasomal degradation.[248] Interestingly, Co^{2+} has also been reported to stabilize HIF-1α by binding directly to the transactivation domain of the protein.[251]

The essential role of HIF-1α in myeloid cell-mediated inflammation was highlighted by a study showing that, in the absence of functional HIF-1α, the ATP pool in isolated peritoneal macrophages was drastically reduced and their capacity for homotypic adhesion, motility, invasiveness, and bacterial killing were greatly inhibited.[192] This study further showed that macrophages with inactivated von Hippel-Lindau factor (pVHL), and thereby inhibited degradation of HIF-1α, presented evidence of a hyperinflammatory response and displayed a high level of glycolytic activity.[192] It has since been established that stabilization and transactivation of

HIF-1α transcriptionally upregulates glycolysis and downregulates oxidative phosphorylation through multiple mechanisms, including the induction of glycolytic enzymes and pyruvate dehydrogenase kinase 1.[204] This kinase phosphorylates pyruvate dehydrogenase, thereby inhibiting this enzyme, which leads to the redirection of pyruvate away from the mitochondria towards glycolysis.[248] This HIF-1α-dependent metabolic shift from oxidative phosphorylation to aerobic glycolysis has been shown to play a central role in the polarization of macrophages towards a pro-inflammatory phenotype.[252] Moreover, recent findings suggest that a metabolic shift towards glycolysis (such as that induced by the overexpression of glucose transporter 1 [GLUT1]), by itself, may be sufficient to impart a M1-like (i.e., proinflammatory) phenotype in macrophages.[253,254]

Given the central and potentially determinant role of energy metabolism in macrophage effector function, analyzing the effects of metal ions released from metal implants on glycolysis and oxidative phosphorylation is critical to understand the pathomechanisms of the immune response in the periprosthetic environment. As previously mentioned, we recently demonstrated that Co^{2+}, but not Cr^{3+}, can increase oxidative stress and decrease oxidative phosphorylation in RAW264.7 macrophages.[245] In the present study we analyzed the effects of Co^{2+} and Cr^{3+} on glycolytic flux and HIF-1α stabilization in the same model system.

4.4 Materials and Methods

4.4.1 Metal ions

Sterile solutions of Co^{2+} and Cr^{3+} in cell culture grade water were prepared fresh, as previously described.[40]

4.4.2 Cells

The RAW 264.7 murine macrophage cell line (American Type Collection Culture;

Manasas, VA) was maintained as previously described.[245] For experiments, cells were detached by pipetting using a Class A volumetric glass pipette (Sibata Scientific Technology, Soka, Japan), and resuspended in growth medium (Dulbecco's modified Eagle medium [DMEM; Wisent; catalog number 319-007-CL) supplemented with 10% [v/v] qualified-grade heat-inactivated fetal bovine serum [Gibco, Carlsbad, CA]).

4.4.3 Extracellular acidification rates (ECAR)

ECAR were measured using an extracellular flux analyzer (Seahorse XFe96; Agilent Technologies, Santa Clara, CA). Briefly, the cartridge sensors were hydrated overnight at 37°C, as per the manufacturer's instructions, in a commercial calibration solution (XF Calibrant; Agilent Technologies). Specially designed tissue culture-treated polystyrene 96-well microplates with a clear flat bottom (Seahorse XFe96 V3 PS Cell Culture Microplates; Agilent Technologies) were seeded with 80 µL of cell suspension (0.5×10^6 cells/mL) per well and incubated 2–3h under cell culture conditions (37ºC, humidified atmosphere of 95% air and 5% CO_2) to allow cell recovery. At the end of the incubation, the culture supernatants were replaced with pre-warmed (37°C) growth medium containing Co^{2+} (6–24 ppm), Cr^{3+} (50–250 ppm), cell culture-grade water (negative control; Lonza, Walkersville, MD), or lipopolysaccharide (LPS) from *E. coli* O55:B05 (1 µg/mL; Sigma-Aldrich, St Louis, MO; positive control [data not shown])[d]. The cells were incubated 6h under cell culture conditions, then washed and incubated 1h at 37°C in extracellular flux analysis medium (sodium bicarbonate-, glucose-, phenol red-, pyruvic acid-, and glutamine-free modified DMEM [Sigma-Aldrich, catalog no. D5030] freshly supplemented with cell culture-grade L-glutamine [4 mM; Wisent], and 4-(2-hydroxyethyl)-1-piperazineethanesulfonic acid [HEPES; 4.5 mM; Sigma-Aldrich], pH adjusted to 7.35-7.40 at room temperature) supplemented

[d]See Figure A3 (for ECAR) and Figure A4 (for PER) in Appendix

with carbonic anhydrase (Sigma-Aldrich). Carbonic anhydrase, reconstituted in cell culture-grade water (500 U/mL final concentration in the medium) and sterilized by filtration through 0.2-µm pore size cellulose acetate syringe filters (VWR, Mississauga, ON) before medium supplementation, was used to ensure quantitative conversion of CO_2 to HCO_3^- and H^+.[255] ECAR were measured to assess basal acidification (i.e., acidification in the absence of exogenous glucose) followed by glycolysis, glycolytic capacity and maximal glycolytic capacity after sequential injections of D-glucose (10 mM final concentration in the microplate; Sigma-Aldrich), rotenone and antimycin A (0.5 µM each), and monensin (20 µM; Sigma-Aldrich; ionophore used to increase the rate of ATP hydrolysis by the Na^+/K^+-ATPase) together with carbonyl cyanide *m*-chlorophenyl hydrazone (2 µM; Sigma-Aldrich; a protonophore acting as an oxidative phosphorylation uncoupler). 2-Deoxy-D-glucose (2-DG; 50 mM; Sigma-Aldrich; an analog of D-glucose that inhibits glycolysis primarily through competitive inhibition of phosphoglucoisomerase) was injected last as a control to confirm that the measured ECAR is specific to glycolysis (data not shown). Each condition was prepared in octuplicates. ECAR measurements were performed 3 times for basal acidification and glycolytic capacity, and 4 times for glycolysis and maximal glycolytic capacity, at 6-min intervals using the flux analyzer. All 3 or 4 ECAR measurements were averaged for each glycolytic parameter except glycolysis where only the 4^{th} measurement was used. All ECAR measurements were corrected for the ECAR of cell-free wells containing only supplemented medium.

Upon completion of the ECAR measurements, the cells were gently washed with pre-warmed (37°C) phosphate-buffered saline without Ca^{2+} and Mg^{2+} (PBS; Wisent) and lysed in cold (4°C) 1M NaOH (Fisher Scientific; 40 µL/well). The lysates were kept at 4°C for ≤ 24h, and protein determination was performed using the Bradford colorimetric assay with BSA as the

standard protein (Thermo Fisher Scientific). Correction for potential interference by NaOH introduced by the lysate samples was performed by including exogenous NaOH (50 mM, final concentration in assay mixture) in the BSA standard curve. Absorbance was measured at a wavelength of 595 nm using a hybrid microplate reader (Synergy^{TM} 4; Biotek, Winooski, VT).

4.4.4 Proton efflux rates (PER)

Proton efflux rates (PER) were calculated as described in a white paper by Romero et al.[256] The buffering factor (2.4 ± 0.1 mmol H^+/L/pH unit) and the CO_2 contribution factor (CCF; 0.4 ± 0.1 [n=55]) used in the PER calculations were determined experimentally as described by Romero et al.[256] Note that the CCF of all experimental conditions was averaged because the CCF was independent of experimental conditions (data not shown).

4.4.5 L-Lactate production

Tissue culture-treated polystyrene 48-well microplates (Greiner Bio-One) were seeded with 800 µL of cell suspension (0.5×10^6 cells/mL) per well and incubated 2–3 h under cell culture conditions to allow cell attachment. At the end of the incubation, the culture supernatants were replaced with pre-warmed (37°C) growth medium containing Co^{2+} (6–24 ppm), Cr^{3+} (50–250 ppm), cell culture-grade water (negative control), or LPS (1 µg/mL; positive control [data not shown])[e]. The cells were incubated an additional 6h under cell culture conditions, then washed in pre-warmed (37°C) extracellular flux analysis medium and incubated 1h in the same medium. At the end of the 1-h incubation, the medium was replaced with the above pre-warmed (37°C) medium further supplemented with D-glucose solution (10 mM, final concentration). All washes and media exchanges were performed on a 37°C-warming plate (Bel-Art Products, Wayne, NJ) to

[e]See Figure A5 in Appendix

minimize temperature perturbations. Enzymatic reactions were stopped, either immediately upon glucose addition or 30 min post-addition, by adding perchloric acid (20% [w/v]; Fisher Scientific) to a final concentration of 7.5% (w/v). Cells were scraped from the wells using 0.5-mm wide chiseled-edge polypropylene mini-cell lifters (Biotium, Fremont, CA). The cell extracts were collected in 1.5-mL polypropylene microcentrifuge tubes (Corning, Corning, NY), incubated 20 min on ice and centrifuged (16,000g for 15 min at 4°C). Protein pellets were frozen and stored at -80°C for future protein determination. The supernatants were collected and stored at 4°C for up to 24h, pH-neutralized using K_2CO_3 (5M; Sigma-Aldrich), and centrifuged (16,000g for 5 min at 4°C). The supernatants were then collected and frozen/stored at -80°C for future lactate determination.

The L-lactate content of thawed pH-neutralized extracts was determined enzymatically as described by Noll[257] with the following modifications. The assay concentrations of glutamate pyruvate transaminase (Sigma-Aldrich) and lactate dehydrogenase (Sigma-Aldrich) were increased to 2.3 U/mL and 65 U/mL, respectively. A commercial standard L-lactate solution (Sigma–Aldrich, catalog no. 07096) was used to generate a standard curve. Fluorescence was measured at an emission wavelength of 460 nm upon excitation at 340 nm[258] in tissue culture-treated black-wall polystyrene 96-well microplates with a clear flat bottom (Greiner Bio-One), using a hybrid microplate reader (Synergy™ 4). All lactate measurements were corrected for the presence of lactate (ca. 12 μM) in the cell-free supplemented media incubated under identical conditions. The corrected lactate content was normalized to protein content determined using the bicinchoninic acid colorimetric assay with BSA as the protein standard (Thermo Fisher Scientific, Rockford, IL). Normalized lactate production was determined by subtracting the normalized lactate content present at the start of the experiment (i.e., upon glucose addition) from the

normalized lactate content present 30 min post-glucose addition, and is expressed in pmol/min/µg protein. Co^{2+} or Cr^{3+} did not interfere with the enzymatic lactate assay, as determined by performing a lactate standard curve in the absence and presence of 0.1 ppm Co^{2+} or 1 ppm Cr^{3+}, i.e., approximately 5 times the concentration of these ions in pH-neutralized perchloric acid extracts of macrophages incubated with the highest concentrations of Co^{2+} (24 ppm) or Cr^{3+} (250 ppm), as determined by inductively coupled plasma-mass spectrometry (0.02 ± 0.01 ppm Co^{2+} [n=3] and 0.19 ± 0.05 ppm Cr^{3+} [n=3]; London Laboratory Services Group, London Health Sciences Centre, London, ON, Canada).

4.4.6 Cellular HIF-1α accumulation

Six-well tissue culture-treated polystyrene microplates (Greiner Bio-One) were seeded with 5 mL of cell suspension (0.4×10^6 cells/mL) per well and incubated 2–3h under cell culture conditions to allow cell attachment. At the end of the incubation, the culture supernatants were replaced with 5 mL of pre-warmed (37°C) growth medium containing Co^{2+} (6–24 ppm), Cr^{3+} (50–250 ppm), or cell culture-grade water (negative control), and the cells were incubated an additional 6h. At the end of the incubation, the microplates were placed on ice and the cells were washed twice with ice-cold Dulbecco's PBS (DPBS) without Ca^{2+} and Mg^{2+} (Sigma–Aldrich). The cells were immediately lysed in 250 µL/well of ice-cold lysis buffer (125 mM Tris-HCl, pH 6.8 [Fisher Scientific]; 2% (w/v) SDS [Fisher Scientific]; 10% (v/v) glycerol [Sigma-Aldrich]; 175 mM DL-1,4-dithiothreitol (DTT; [Amresco, Solon, OH]) with the aid of a 2-cm chiseled-edge polypropylene cell lifter (Fisher Scientific). Whole-cell lysates, transferred into low retention 1.5 mL polypropylene microcentrifuge tubes (Corning, Corning, NY) pre-cooled in ice, were sonicated on ice for 15s using an ultrasonic processor (Model 120 Sonic Dismembrator; Fisher Scientific) set at 20% amplitude and connected to a 1/8-inch probe microtip (model CL-18; Fisher

Scientific). The sonicated samples were incubated 5 min in boiling water, aliquoted, snap-frozen in liquid nitrogen, and stored at -80ºC.

Substances that may interfere with colorimetric protein determination were removed from freshly thawed aliquots of lysates using the deoxycholic acid–trichloroacetic acid protein precipitation technique. The protein pellets were dissolved in 100 mM NaOH and protein content was determined using the Bradford colorimetric assay. Aliquots of lysate (40 µg proteins) were mixed with sample loading buffer (LI-COR, Lincoln, NE), as per the manufacturer's instructions, and analyzed by SDS-polyacrylamide gel electrophoresis using precast mini-format Tris-glycine gradient (4–15%) gels (Bio-Rad; Hercules, CA). Commercial HeLa cell lysates from untreated and $CoCl_2$-treated cells (Novus Biologicals, Centennial, CO) were used as negative (data not shown) and positive HIF-1α controls, respectively, and a prestained (visible and near-infrared) protein ladder (LI-COR) was used. Following electrophoresis, the gels were truncated above the 260 kDa molecular weight mark to avoid gel compression artifacts during electrotransfer. For western blotting, the proteins were electrotransferred onto a 0.45-µm pore size fluorescent-grade polyvinylidene fluoride membrane (Immobilon-FL; Millipore Sigma, Burlington, MA). The membrane was air-dried, reversibly stained for total protein with acid blue (REVERT™ Total Protein Stain; LI-COR) as per the manufacturer's instructions, and imaged at 700 nm using a near-infrared fluorescence imaging system (Odyssey Fc; LI-COR). The stained membrane was then blocked/destained in commercial blocking buffer (Odyssey Blocking Buffer [PBS]; LICOR) for 1h at room temperature. Immunodetection was performed using a rabbit anti-HIF-1α antibody (Novus Biologicals, catalog no. NB100-449; diluted 1:2000 in the blocking buffer supplemented with 0.1% [v/v] polysorbate 20 [Fisher Scientific]; overnight incubation at 4°C) as the primary antibody, and a goat anti-rabbit IgG (H+L) fluorescently-labeled secondary antibody (LICOR,

catalog no. 926-32211; diluted 1:15,000 in PBS blocking buffer containing 0.1% (v/v) polysorbate 20 and 0.01% SDS; 1-h incubation at room temperature). The membrane was washed in DPBS without Ca^{2+} and Mg^{2+} (Sigma–Aldrich) and air-dried (in the dark) prior to imaging at 800 nm using the near-infrared fluorescence imaging system. Fluorescence intensity was normalized to protein content determined by acid-blue staining. Both acid-blue staining and immunostaining were quantified by densitometric analysis using Image Studio™ software v2.0 (LI-COR).

4.4.7 Statistical analysis

Outliers were identified using the Tietjen-Moore test. Statistical analysis, implemented in R v3.5.2, was performed using a linear mixed model followed by Tukey post hoc tests. The data were assumed to be normally distributed and to meet the assumption of homogeneity of variance. $p<0.05$ was considered significant. Effect sizes are presented as Cohen's *d* with 95% confidence intervals (CI). Unless otherwise specified, data are presented as means ± standard error of the mean (SEM).

4.5 Results

4.5.1 Effects of Co^{2+} and Cr^{3+} on extracellular acidification rates (ECAR)

All three glycolytic parameters increased after macrophage exposure to all Co^{2+} concentrations tested. Glycolysis increased by up to 150% with 6 ppm (d=2.7, 95% CI [2.1, 3.3]), glycolytic capacity by up to 72% with 6 ppm (d=1.8, 95% CI [1.3, 2.3]), and maximal glycolytic capacity by up to 67.5% with 24 ppm (d=1.7, 95% CI [1.2, 2.2]) ($p<0.001$ in all cases; Fig. 1A). Basal acidification also increased by 57 to 71% (d=1.5 – 3.4, 95% CI [1.0, 2.0] – [2.7, 4.0]).

Similarly, all three glycolytic parameters increased after macrophage exposure to all Cr^{3+} concentrations tested, except the highest concentration (250 ppm) where glycolytic capacity and maximal glycolytic capacity did not differ significantly from the negative control (cells unexposed

to metal ions), likely due to an increase in cytotoxicity. Glycolysis increased by up to 110% with 100 ppm (d=4.6, 95% CI [3.8, 5.5]), glycolytic capacity by up to 67% with 50 ppm (d=4, 95% CI [3.3, 4.8]), and maximal glycolytic capacity by up to 67% with 50 ppm (d=2.6, 95% CI [2, 3.2]) (p<0.001 in all cases; Fig. 1B). Basal acidification increased by 55 to 86% (d=1.5 – 4.1, 95% CI [1.0, 2.0] – [3.3, 4.8]).

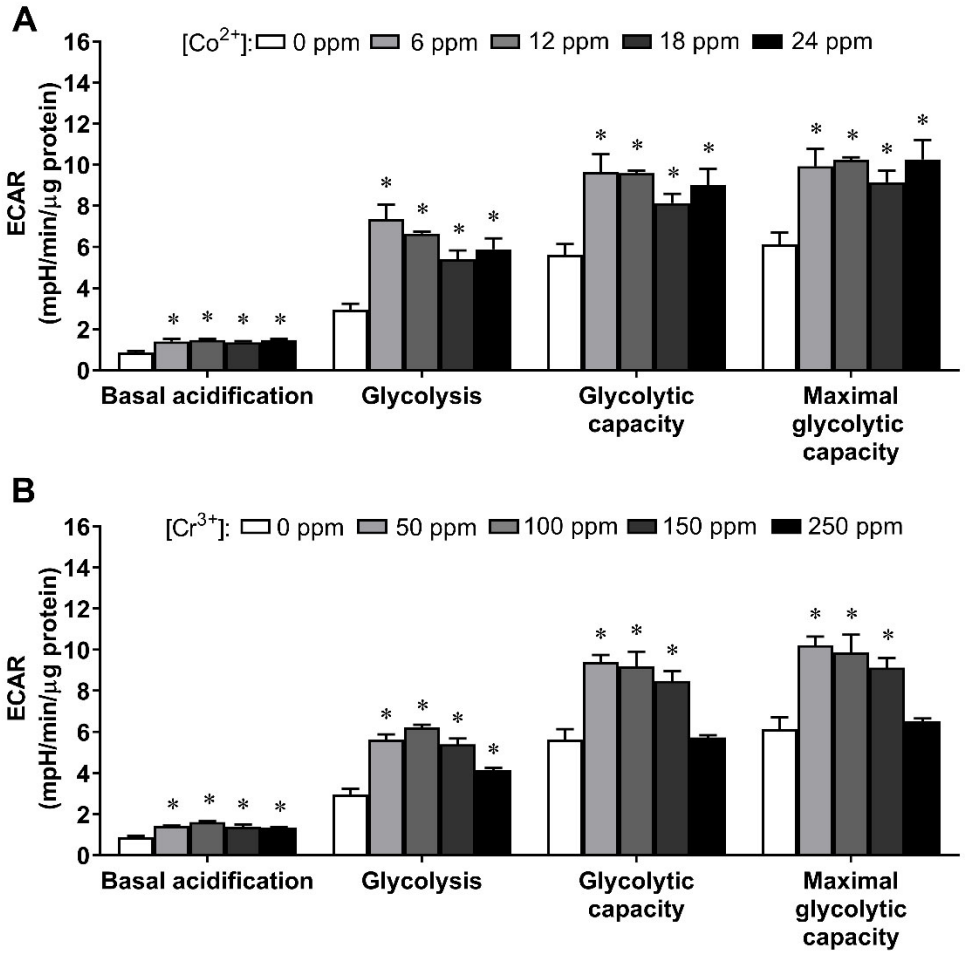

Figure 4.1: Effects of Co^{2+} (A) and Cr^{3+} (B) exposure (6h) on glycolytic flux parameters (and basal acidification) of RAW 264.7 macrophages. Extracellular acidification rates (ECAR; measured using an extracellular flux analyzer) were normalized to protein content (determined using a colorimetric assay). Data are presented as means ± SEM of 4-5 independent experiments, each performed with 5–8 replicate samples per condition. An asterisk (*) indicates a significant difference (p<0.001) between a given condition and the negative control (cells unexposed to Co^{2+} or Cr^{3+}). Statistical analysis was performed using a linear mixed model followed by Tukey post hoc tests. p<0.05 was considered significant.

4.5.2 Effects of Co^{2+} and Cr^{3+} proton efflux rates (PER) from macrophages

Glycolytic and mitochondrial contributions to total PER from the macrophages during glycolysis (see Materials and Methods for PER calculations) are presented in Figure 2. Glycolytic PER (i.e., PER attributed to glycolysis) increased after macrophage exposure to all concentrations (by up to 176% with 6 ppm Co^{2+}; d=2.8, 95% CI [2.2, 3.4]) (p<0.001 in all cases; Fig. 2A). In contrast, exposure to Co^{2+} increased mitochondrial PER (i.e., PER attributed to mitochondrial CO_2 production and the subsequent release of protons upon CO_2 hydration) by only 20% with 6 ppm (d=0.5, 95% CI [0.1, 1]; p<0.001; Fig. 2A inserts). Exposure to Cr^{3+}, like exposure to Co^{2+}, increased glycolytic PER at all concentrations (by up to 110% with 100 ppm Cr^{3+}, d=2.7, 95% CI [2.1, 3.3]) (p<0.001 in all cases; Fig. 2B). In contrast to Co^{2+}, exposure to Cr^{3+} increased mitochondrial PER at all concentrations except 250 ppm (up to 41% with 50 ppm Cr^{3+}, d=1.9, 95% CI [1.4, 2.4]) (p<0.001 in all cases; Fig. 2B inserts).

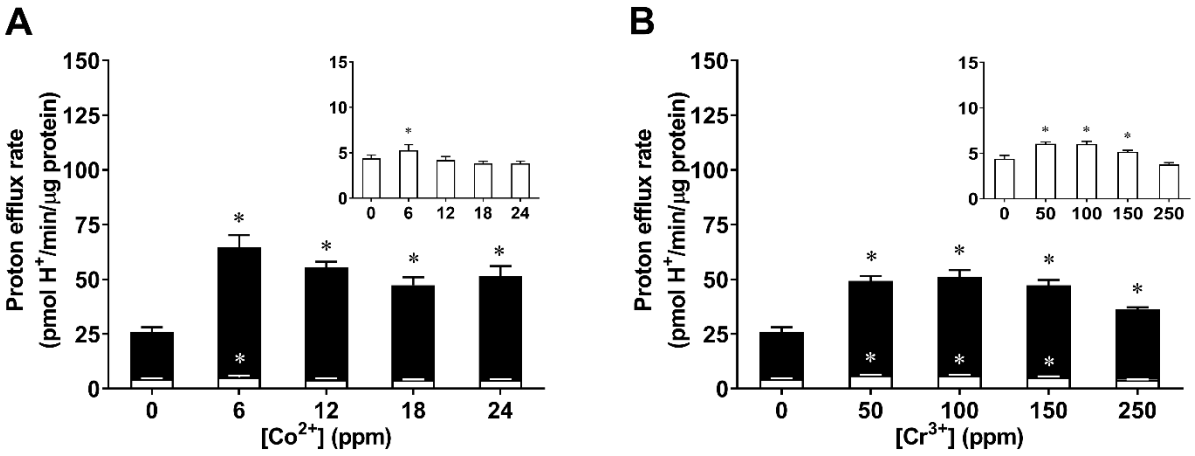

Figure 4.2: Effects of Co^{2+} (A) and Cr^{3+} (B) exposure (6h) on the proton efflux rates (PER) from RAW 264.7 macrophages incubated with glucose. Glycolytic (dark grey) and mitochondrial (white) PER, normalized to protein concentration, are presented. Inserts show mitochondrial PER at a different scale. PER were calculated as described in Materials and Methods. Statistics as in Figure 1.

4.5.3 Effects of Co^{2+} and Cr^{3+} on lactate production by macrophages

Co^{2+} increased lactate production rate after macrophage exposure to all concentrations (up to 97% with 12 ppm Co^{2+}; d=2.8, 95% CI [1.7, 3.8]) (p<0.001 in all cases; Fig. 3A). Exposure to Cr^{3+} also increased the lactate production rate, but only with 100 ppm (44%; d=1.4, 95% CI [0.6, 2.2]) and 150 ppm Cr^{3+} (39%; d=1.6, 95% CI [0.8, 2.5]; p<0.001; Fig. 3B).

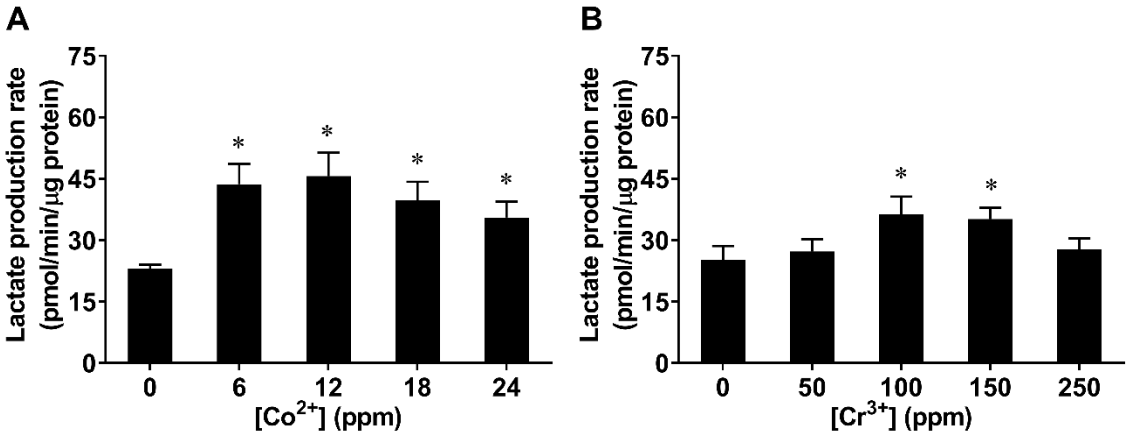

Figure 4.3: Effects of Co^{2+} (A) and Cr^{3+} (B) exposure (6h) on the average lactate production rates in RAW 264.7 macrophages during a 30-min incubation with glucose. Lactate production rates, normalized to protein content, were measured enzymatically. Data are presented as means ± SEM of 4 independent experiments, each performed with 3-4 replicate samples per condition. Statistics as in Figure 1.

4.5.4 Effects of Co^{2+} and Cr^{3+} on HIF-1α accumulation in macrophages

Co^{2+} increased the cellular accumulation of HIF-1α after macrophage exposure to all concentrations (up to 48% with 6 ppm Co^{2+}; d=18, 95% CI [7.7, 28.3]) relative to the negative control (cells unexposed to metal ions) (p<0.001 in all cases; Fig. 4A,B). In contrast, exposure to Cr^{3+} at any concentration did not induce any significant changes in the cellular level of HIF-1α (Fig. 4C,D).

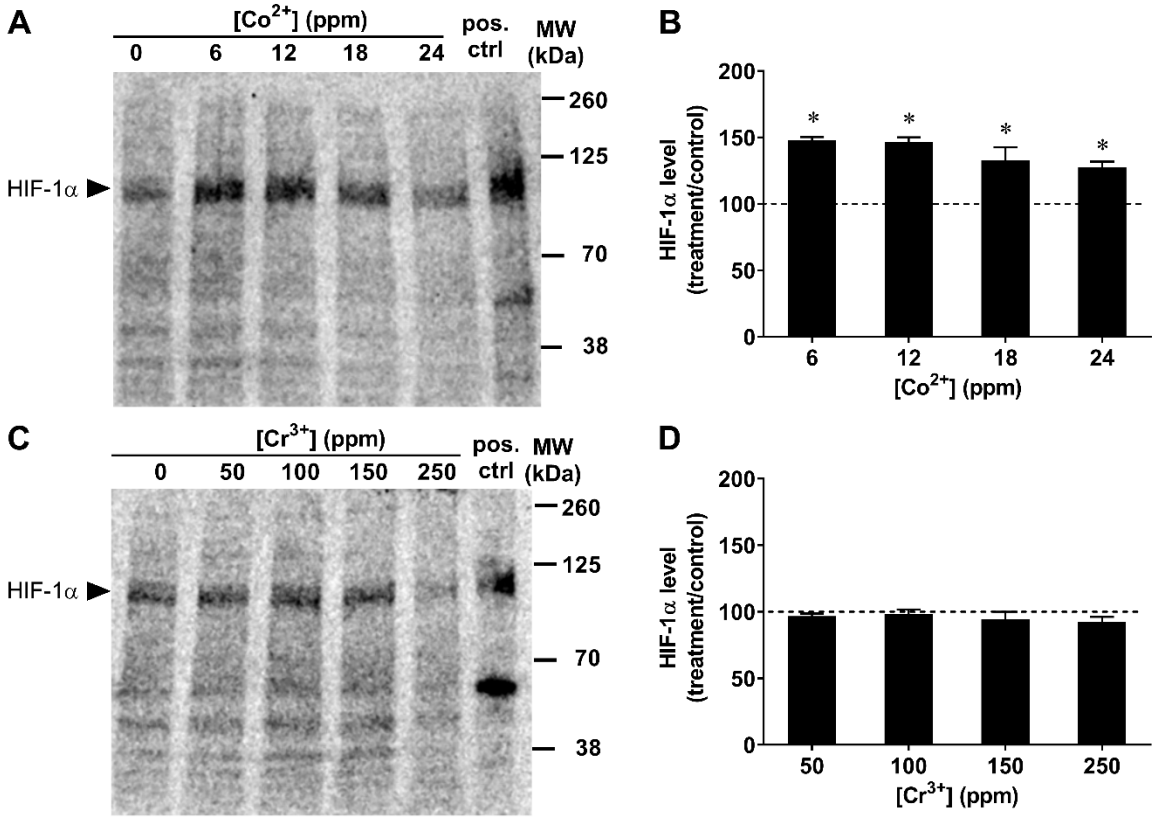

Figure 4.4: Effects of Co^{2+} (A,B) and Cr^{3+} (C,D) exposure (6h) on the level of hypoxia inducible factor-1alpha (HIF-1α) in RAW 264.7 macrophages. (A) and (C): Representative western blots of HIF-1α. (B) and (D): HIF-1α level, determined by densitometric analysis of the western blots, normalized to protein content determined by acid-blue staining of the blots, and expressed relative to the negative control (cells unexposed to metal ions) represented by a dashed line. MW (kDa): pre-stained protein molecular weight standards. Data in panels (B) and (D) are presented as means ± SEM of 3 independent experiments. Statistics as in Figure 1. [1]pos. ctrl: commercial positive control, i.e., HIF-1α in whole-cell extracts of HeLa cells exposed to 6 ppm Co^{2+} for 4h (note: the predicted MW of human HIF-1α is 120 kDa vs 94 kDa for the murine protein and HIF-1α from both species is subject to post-translational modifications).

4.6 Discussion

The present study analyzed the effects of Co^{2+} and Cr^{3+} on glycolytic flux and HIF-1α stabilization in macrophages, the predominant immune cells in periprosthetic tissues.[100,219] Overall, results showed that the exposure of RAW 264.7 macrophages to both metal ions increased glycolytic flux, albeit to a lower extent with Cr^{3+}, as determined by extracellular flux analysis and lactate assays. In contrast, only Co^{2+} stabilized HIF-1α, suggesting that the HIF-1 transcription

factor is involved in the Co^{2+}-induced, but not in the more modest Cr^{3+}-induced, increase in glycolytic flux.

ECAR measurements showed that both Co^{2+} and Cr^{3+} increased all glycolytic flux parameters, as well as basal acidification. Since ECAR are dependent on the buffering capacity of the measurement system, total PER were calculated along with the relative contributions of glycolysis and mitochondria to total PER, to quantify glycolytic flux. The calculations indicated that under glycolytic conditions (i.e., in the presence of 10 mM glucose), the increase in PER observed in the presence of Co^{2+} or Cr^{3+} was almost exclusively due to an increase in aerobic glycolysis. Interestingly, although marginal, the mitochondrial contribution to the increase in total PER was significant at the lowest Co^{2+} concentration tested and at all Cr^{3+} concentrations (except at the highest and most toxic). Since PER are indirect measurements of glycolytic flux, lactate production rates were measured to validate the extracellular flux analysis. The measured lactate production rates were in general agreement with the calculated PER, although the former showed that both Co^{2+} and Cr^{3+} had a lower, but significant, effect on glycolytic flux. The quantitative discrepancy between PER and lactate production rates may be the result of underlying assumptions and uncertainties (e.g., lack of precision of CCF measurements) in the PER calculations, or it may reflect differences between the two methodologies used. (e.g., overestimation of the PER by the extracellular flux analyzer, or a non 1:1 stoichiometry between protons released from cells and lactate molecules produced). Notwithstanding, the observed discrepancy does not affect the general interpretation of the glycolytic flux data.

Overall, the glycolytic flux analysis indicates that Co^{2+}, and to a lesser extent Cr^{3+}, can increase glycolytic flux in RAW 264.7 macrophages. This is in general agreement with previous studies on other cell types.[176,246] For example, the 97% increase in lactate production observed

with 12 ppm Co^{2+} is similar in relative magnitude to the 100% increase previously reported in chondrocytes exposed to 4.4 ppm Co^{2+}.[246] Moreover, the activation of RAW 264.7 macrophages by LPS in combination with interferon-gamma has been reported to increase lactate production by up to ca. 175% .[176] The magnitude of the relative increase of glycolytic flux induced by exposure to Co^{2+} (12 ppm) is therefore comparable to that associated with the activation of the macrophages by pro-inflammatory stimuli. As discussed below, this may reflect shared mechanisms.

Although the effect of Cr^{3+} on glycolytic flux was more modest than that of Co^{2+}, it increased the lactate production rate by as much as 44%. Surprisingly, very little is known about the effect of Cr^{3+} on glycolysis. Exposure to low doses (< 1 ppm) of chromium(III) picolinate has been reported to increase translocation of glucose transporter 4 (GLUT4) to the membrane in murine 3T3-L1 preadipocytes,[52] but not in rat L6 myotubes.[247] Moreover, chromium(III) picolinate did not increase glucose uptake in either cell types (unless insulin was present). Interestingly, we recently observed that the exposure of murine bone marrow-derived macrophages (BMDM) to Cr^{3+} did not increase glycolytic flux, and even decreased it at concentrations ≥ 100 ppm (unpublished data). The different response of RAW 264.7 macrophages and BMDM may reflect metabolic differences between transformed and primary cells.

The exposure of RAW 264.7 macrophages to Co^{2+} induced the stabilization of HIF-1α, in agreement with previous studies using various cell types.[200,250,259] For example, results show that the maximum Co^{2+}-induced accumulation of HIF-1α (ca. 48%) is comparable to that reported in THP-1 human macrophages and human primary macrophages (ca. 40%).[259] Co^{2+} has been shown to stabilize HIF-1α by oxidizing intracellular ascorbate, either directly, catalytically, or indirectly through oxidative stress.[200,250] Ascorbate is a cofactor of the PHD proteins that hydroxylate HIF-1α, enabling binding of the von Hippel-Lindau tumor suppressor (the recognition subunit of an E3

ubiquitin ligase that ubiquitylates HIF-1α), thereby targeting HIF1-α for proteasomal degradation.[248] Alternatively, Co^{2+} has also been shown to stabilize HIF-1α by binding directly to the transactivation domain of the protein.[251]

HIF-1α transcriptionally downregulates OXPHOS and upregulates glycolysis through multiple mechanisms, including: 1) the induction of glucose transporters and glycolytic enzymes[260]; 2) the induction of (PDK-1), which phosphorylates (PDH), thereby inhibiting this enzyme and redirecting pyruvate away from the mitochondria towards glycolysis[204]; 3) the induction of microRNA-210, which blocks the expression of iron-sulfur cluster assembly scaffold proteins IscU1 and IscU2 that facilitate the assembly of iron-sulfur clusters required for the function of the TCA cycle enzyme aconitase and ETC complex I; and 4) the negative regulation of mitochondrial biogenesis and O_2 consumption,[261] and the promotion of mitochondrial-selective autophagy.[205] The resulting HIF-1-induced metabolic shift from OXPHOS to aerobic glycolysis has been shown to play a central role in the polarization of macrophages towards a pro-inflammatory phenotype.[177] This metabolic shift allows mitochondrial repurposing from ATP synthesis to reactive oxygen species (ROS) production to support pro-inflammatory functions, including the secretion of interleukin-1ß.[262] Interestingly, recent findings suggest that a shift in energy metabolism, by itself, may be sufficient to impart an M1-like (i.e., pro-inflammatory)[253] or an M2-like (i.e., anti-inflammatory) phenotype in macrophages.[254] For example, overexpression of GLUT1 in RAW 264.7 macrophages has been shown to upregulate glycolysis and blunt oxidative metabolism.[253] Metabolomic analysis further demonstrated activation of the pentose phosphate pathway (PPP), which utilizes glucose to generate NADPH for use in biosynthetic pathways and ROS production.[253] This activation of the PPP was accompanied by an increase in

the oxidized/reduced glutathione (GSSG/GSH) ratio, which is consistent with an increase in ROS burden and intracellular stress.[253]

The results of the present study show that exposure to Co^{2+} induced HIF-1α stabilization and increased glycolytic flux in RAW 264.7 macrophages. These results, together with our previous results, showing that Co^{2+} can increase oxidative stress and decrease OXPHOS in RAW 264.7 macrophages,[245] indicate that Co^{2+} can induce a metabolic shift from OXPHOS to aerobic glycolysis. This metabolic shift, presumably involving HIF-1α, is similar to that associated with the polarization of macrophages towards a pro-inflammatory phenotype. Moreover, this shift in energy metabolism may play a central and potentially determinant role in the proinflammatory response induced by Co^{2+} in the periprosthetic environment. In this context, it is interesting to note that HIF-1α accumulation has been reported to be significantly higher in the periprosthetic tissues of patients with a metal-on-metal hip implant than in patients with a metal-on-polyethylene hip implant.[259]

Cr^{3+}, unlike Co^{2+}, did not induce stabilization of HIF-1α in RAW 264.7 macrophages. This is in agreement with the report that Cr^{6+} stabilized HIF-1α in 1HAEo human airway epithelial cells, but only until it was reduced to Cr^{3+}.[249] The lack of Cr^{3+}-induced HIF-1α stabilization may explain why the exposure of RAW 264.7 macrophages to Cr^{3+} induced a more modest increase in glycolytic flux than that observed after exposure to Co^{2+}. However, the mechanisms involved in the Cr^{3+}-induced increase in glycolytic flux remain unclear. Since Cr^{3+} ions tend to inhibit enzymes,[44,263] they would not be expected to activate glycolytic enzymes directly. The Cr^{3+}-induced increase in glycolytic flux, like that of Co^{2+}, may instead be due to indirect upregulation through the activation of regulatory mechanism(s). Alternatively, exposure to Cr^{3+} may create a demand for certain carbon compounds, thereby leading to an upregulation of glycolysis through

homeostatic control mechanisms. Notwithstanding, the present study rules out the involvement of HIF-1α-dependent mechanisms while our previous study, showing that Cr^{3+} neither induced ROS production nor affected mitochondrial function,[245] further rules out the involvement of ROS, and of a compensatory increase in glycolytic flux in response to a decrease in mitochondrial ATP production

4.7 Conclusion

The present study showed that the exposure of macrophages to Co^{2+} or Cr^{3+} can increase glycolytic flux, albeit to a lower extent with Cr^{3+}. In contrast, only exposure to Co^{2+} stabilized HIF-1α, suggesting that the HIF-1 transcription factor is involved in the Co^{2+}-, but not in the Cr^{3+}-, induced increase in glycolytic flux. These results, together with our previous results showing that Co^{2+}, but not Cr^{3+}, can increase oxidative stress and decrease OXPHOS in RAW 264.7 macrophages,[245] indicate that the exposure of macrophages to Co^{2+} (but not Cr^{3+}) can induce a metabolic shift from OXPHOS to aerobic glycolysis. This metabolic shift, presumably involving HIF-1α, is similar to that associated with the polarization of macrophages towards a pro-inflammatory phenotype. Given the central and potentially determinant role of energy metabolism in macrophage effector function, our results suggest that Co^{2+}-induced metabolic reprogramming may play a central role in the proinflammatory response induced by Co^{2+} in the periprosthetic environment.

4.8 Acknowledgements

The authors thank Drs. Natalia Romero and Brian Dranka in the Cell Analysis Division of Agilent Technologies for expert technical advice on extracellular flux analysis. This work was supported by the Canadian Institutes of Health Research (CIHR Operating Grant MOP-133712) (IC), the Canada Research Chairs (CRC) Program (IC), the Ontario Ministry of Research and Innovation

(MRI; Early Researcher Award ER10-07-112) (IC), and the Natural Sciences and Engineering Research Council of Canada (NSERC; Discovery Grant RGPIN 04973) (M-EH).

5. EFFECTS OF COBALT AND CHROMIUM IONS ON NITRIC OXIDE PRODUCTION AND LIPID PEROXIDATION

In the course of this project, other assays, including NO production and lipid peroxidation, were considered to evaluate metal ion-induced oxidative stress. These assays were however not included in Manuscript 1 (Chapter 3) partly because of concerns regarding potential interference of metal ions (NO assay) and because of assay limitations (TBARS assay), as detailed below. Results of these additional assays are presented in this chapter.

5.1 Effects of Co^{2+} and Cr^{3+} on nitric oxide (NO) production in macrophages

Previous histological studies showed expression of inducible nitric oxide synthase (iNOS), the enzyme catalyzing NO production, in periprosthetic tissues from patients with failed MM hip implants.[264] *In vitro* studies showed that Ni^{2+} and Co^{2+} concentrations (10 μM; i.e., 0.6 ppm) can induce significant NO production in murine peritoneal and splenic macrophages only in the presence of cytokines.[265] However, Hassoun et al.[241] showed that exposure of J774A.1 to Cr^{3+} (50-80 μM; i.e., 2.6-4.2 ppm) induced a 2-fold increase in NO production after 48h incubation, in the absence of cytokines. In addition, Petit et al.[266] reported the presence of nitrated proteins in U937 monocytes exposed to 10 ppm Co^{2+} or 150 ppm Cr^{3+} after prolonged exposure (48-72h incubation). The nitrated proteins were exclusively present in the cytoplasmic fraction.[266]

To investigate the effects of Co^{2+} and Cr^{3+} on NO production in our system, we performed a non-enzymatic colorimetric assay, adapted from an established colorimetric NO assay kit (Oxford Biomedical Research; Rochester Hills, MI). Macrophages exposed to LPS, which is a known inducer of NO production as previously reported,[267,268] served as a positive control. Cadmium beads were used to reduce nitrate to nitrites. The NO equivalents (nitrate + nitrite)

produced were quantified spectrophotometrically. Experiments were performed with both RAW 264.7 and J774.A1 macrophages.

Results with RAW 264.7 macrophages revealed no significant increase in NO production after a 24-h incubation with either Co^{2+} (Figure 5.1A) or Cr^{3+} (Figure 5.1B), relative to the negative control. Increasing the incubation time to 48h did not lead to a significant increase in NO production with neither Co^{2+} or Cr^{3+} (data not shown). On the other hand, exposure to LPS led to a 4- to 5-fold increase in NO production after a 24-h incubation (p<0.001; see Figure A6 in Appendix). Similarly to the RAW 264.7 cells, results with J774A.1 cells also showed no significant increase in NO concentrations after 24h or 48h incubation with either Co^{2+} or Cr^{3+} (data not shown).

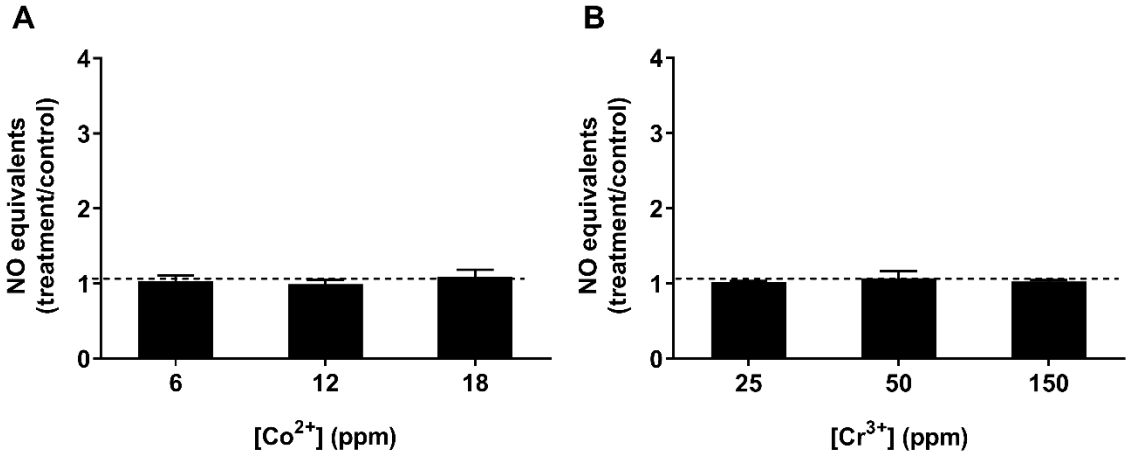

Figure 5.1: Effects of Co^{2+} (A) and Cr^{3+} (B) on nitric oxide (NO) equivalents in RAW 264.7 macrophages after a 24-h exposure. Nitrite (NO_2^-) and nitrate (NO_3^-) concentrations were measured using a non-enzymatic colorimetric assay based on the Griess reaction. Nitrate and nitrite concentrations, expressed relative to the nitrate and nitrite concentrations in the negative control (cells unexposed to Co^{2+} or Cr^{3+}; represented by a dashed line), are directly proportional to the NO equivalents. Data are presented as means ± SEM of three independent experiments, each performed with triplicate samples for each experimental condition. Statistical analysis, implemented in R v3.5.2, was performed using a linear mixed model followed by Tukey post-hoc tests. The data were assumed to be normally distributed and meet the assumption of homogeneity of variance.

Overall, these results suggest that NO is not part of the oxidative stress pathway induced by Co^{2+} and Cr^{3+} in macrophages. Interestingly, iNOS has been shown to be regulated by ferrous ions (Fe^{2+}).[269] It is therefore possible that Co^{2+} ions (cations with same valence) are inhibiting the activity of this enzyme through mismetallation, by competitively binding to the heme sites regulating the iNOS enzyme activity. Alternatively, the absence of NO production may be attributable to metal ion interference with the expression of the iNOS mRNA[270]. More importantly, it is possible that the absence of NO with Co^{2+} may have been caused by the interference of the ions with one or more of the NO assay components. For example, it was reported that other cations with the same valence (in particular Fe^{2+}) could prevent the azo dye formation (colorimetric product of the Griess reaction) by interfering with the reaction of N-(1-naphtyl) ethylenediamine (NED) with the diazo intermediate (sulfanilamide, likely interacting with the ions).[271] Co^{2+} interference with this NO assay component could explain the differences between our results and those of Petit et al.,[266] who used a different method to measure NO (immunodetection of nitrated proteins). Differences between our results and those of Hassoun et al.[241] may be explained by differences in the cell culture medium, which was supplemented with non-essential amino acids, in particular arginine, in the study by Hassoun et al. This addition may have influenced the enzymatic reaction in the cells using arginine, which is a substrate for NO production.

In summary, while some uncertainties remain regarding the potential ion interference with the NO assay components, results of the present study showed no NO production in macrophages exposed to Co^{2+} and Cr^{3+}, and suggest that NO is not part of the oxidative stress pathway induced by Co^{2+} and Cr^{3+} in RAW 264.7 macrophages.

5.2 Effects of Co^{2+} and Cr^{3+} on lipid peroxidation in macrophages

Previous studies showed no significant difference in the plasma concentration of peroxides between patients with MM bearings and patients without an implant.[272] However, malondialdehyde (MDA), a stable product of lipid peroxidation and a marker of lipid oxidative damage, was observed in periprosthetic tissues from patients with MPE implants revised for loosening or high rate of wear.[273] Lipid peroxidation is involved in the oxidative damage to cell structures and in ROS-mediated cell death.[274] Moreover, lipid peroxidation has been shown to play a key role in aseptic inflammation such as during drug-induced hepatotoxicity.[275] The thiobarbituric acid-reactive substances (TBARS) assay, which is based on the quantification of MDA, was performed in the present study to analyze the effects of Co^{2+} or Cr^{3+} on lipid peroxidation in RAW 264.7 macrophages. Diethyl maleate (DEM) was used as a positive control to validate the TBARS assay (Figure A7 in Appendix).

Results revealed a Co^{2+} concentration-dependent increase in MDA levels, up to 162% with 24 ppm Co^{2+}, after 24h incubation ($p<0.001$). Results also revealed an increase up to 21% and 45% in MDA levels with 150 ppm Cr^{3+}, relative to the negative control, after 24h and 48h incubation, respectively ($p=0.005$ and $p<0.001$, respectively) (Figure 5.2A and B).

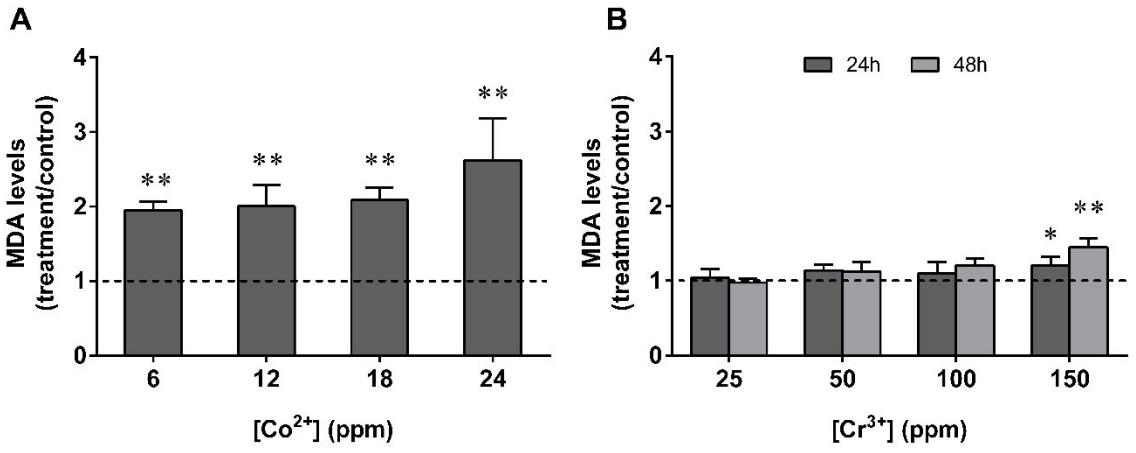

Figure 5.2: Effects of Co^{2+} (A) and Cr^{3+} (B) on lipid peroxidation in RAW 264.7 macrophages after up to a 48-h exposure. Malondialdehyde (MDA) concentrations were measured using the thiobarbituric acid reactive species (TBARS) assay. MDA concentrations, expressed relative to the MDA concentration in the negative control (cells unexposed to Co^{2+} or Cr^{3+}; represented by a dashed line), are proportional to the level of lipid peroxidation. Data are presented as means ± SEM of three independent experiments, each performed with triplicate samples per for each experimental condition. Statistical analysis, implemented in R v3.5.2, was performed using a linear mixed model followed by Tukey post-hoc tests. The data were assumed to be normally distributed and meet the assumption of homogeneity of variance. Single (*) and double asterisks (**) indicate $p<0.05$ and $p<0.001$, respectively.

These results confirmed that Co^{2+} and Cr^{3+} can induce lipid oxidative damage in RAW 264.7 macrophages, albeit to a lower extent with Cr^{3+}. Results also suggest that Co^{2+} and Cr^{3+}-induced lipid peroxidation is time- and ion concentration-dependent, most likely related to different mechanisms through which Co^{2+} and Cr^{3+} enter the cells and target different cellular components.

The increase in lipid peroxidation in macrophages exposed to Co^{2+} suggests possible "ferroptosis", a type of programmed non-apoptotic cell death characterized by the accumulation of lipid peroxides. Ferroptosis is usually triggered by the presence of free iron ions (Fe^{2+}) which starts cycles of oxidation/reduction through the Fenton reaction leading to oxidative stress.[276] It is therefore possible that through mismetallation (as described in Chapter 3 – Manuscript 1), Co^{2+}

compete with Fe^{2+} for iron binding sites, leading to Fe^{2+} release in the cytosol. This process would then start a series of Fenton reactions (catalyzed by Fe^{2+}), thereby decreasing the pool of antioxidants in the cells and favoring a state of high oxidative stress. Moreover, ferroptosis can also be triggered by blocking the glutathione peroxidase 4 (GPx4) enzyme antioxidant activity,[277] which may happen in the presence of ROS, since GSH, which is required for GPx4 function, would be depleted.[276,277] On the other hand, Cr^{3+} has been shown to lead to oxidative stress through a thiol-dependent DNA oxidative damage.[160,278] Overall, these results show that Co^{2+} and, to a lower extent, Cr^{3+} can lead to an increase of lipid peroxides, although through different mechanisms, and may ultimately induce cell death through ferroptosis.

It is important to note some limitations of the TBARS assay, and particularly the fact that thiobarbituric acid (TBA) can react with substances other than MDA.[279] Therefore, our TBARS assay results may have overestimated the level of lipid peroxidation. This limitation might explain the discrepancy between the absence of protein oxidation with Cr^{3+} (presented in Chapter 3 – Manuscript 1) and the presence of a low level of lipid peroxidation observed in macrophages exposed to Cr^{3+}. Interestingly, recent literature points to the need for more specific methods than spectrophotometry to determine MDA concentrations.[279-281] For example, MDA concentrations could be more accurately measured using high-performance liquid chromatography (HPLC) or liquid chromatography- mass spectrometry (LC-MS) detection systems since these methods allow the separation as well as the quantification of specific lipid peroxidation products based on calibrated standards.[279] Nonetheless, both lipid peroxidation assay and protein oxidation results (presented in Chapter 3) are in agreement and indicate the presence of oxidative stress with Co^{2+} at 24h. The small increase in lipid peroxidation observed with Cr^{3+}, especially after 48h, may have been caused by the assay limitations, as explained above.

Overall, the results in the sections 5.1 and 5.2 showed that neither Co^{2+} nor Cr^{3+} increased NO production in RAW 264.7 macrophages, suggesting that NO is not part of the oxidative stress pathway induced by Co^{2+} or Cr^{3+} in these cells. Moreover, the absence of NO production suggests that Co^{2+}-induced mitochondrial dysfunction is not NO-dependent. Nevertheless, some uncertainties remain, especially regarding potential ion interference with NO assay components. On the other hand, both ions induced lipid peroxidation, albeit to a lower extent and after prolonged incubation with Cr^{3+}. These results suggest that both ions can induce oxidative stress, but likely through different mechanisms.

6. THESIS DISCUSSION AND CONCLUSION

This thesis investigated the effects of metal ions released from CoCrMo-based implants on macrophage oxidative stress and energy metabolism, the latter one being currently described as the guiding force of the immune response.[105] Results presented in the first manuscript (Objective 1, Chapter 3) show the presence of oxidative stress as well as a decrease in OXPHOS suggesting mitochondrial dysfunction in RAW264.7 macrophages exposed to Co^{2+} but not Cr^{3+}. Results presented in the second manuscript (Objective 2, Chapter 4) show that Co^{2+}, and to a lower extent Cr^{3+}, increased glycolytic flux. Results also show that Co^{2+}, but not Cr^{3+}, induced HIF-1α expression, suggesting that HIF-1α may be contributing to the Co^{2+}-induced glycolytic flux and lactate production. Overall, results presented in both manuscripts indicate that the exposure of macrophages to Co^{2+} (but not Cr^{3+}) can induce a metabolic shift from OXPHOS to aerobic glycolysis. This metabolic shift, which may be involving HIF-1α, is similar to that associated with the polarization of macrophages towards a pro-inflammatory phenotype.

Additional results regarding the effects of Co^{2+} or Cr^{3+} on other oxidative markers, NO production and lipid peroxidation, are presented in Chapter 5. These results show that neither Co^{2+} nor Cr^{3+} induced NO production in RAW 264.7 macrophages at any time point tested, suggesting that NO is not part of the oxidative stress induced by Co^{2+}. Nevertheless, some uncertainties remain regarding potential ion interference with the NO assay components that may have impacted the results. In addition, results show that macrophages exposed to Co^{2+} at all concentrations analyzed, and to high Cr^{3+} concentrations for an extended incubation period (48h), exhibited lipid peroxidation, albeit to a lower extent with Cr^{3+}. There results suggest that both ions may induce oxidative stress, although through different mechanisms. Nevertheless, since lipid peroxidation

may have been overestimated when using TBARS assay (as explained in Chapter 5), the results with Cr^{3+} should be cautiously interpreted.

The present chapter will present the main contributions of this thesis, provide a discussion on some of the main technical limitations and considerations, and offer suggestions for future research.

6.1 Significant contributions of the thesis

6.1.1 Evidence of Co^{2+}-induced oxidative stress and decrease in OXPHOS in RAW 264.7 macrophages

This study analyzed the effects of Co^{2+} and Cr^{3+}, metal ions released from CoCrMo-based implants, on energy metabolism in macrophages, the predominant immune cells in periprosthetic tissues[100,219]. To the best of our knowledge, this is the first study looking into the effects of Co^{2+} and Cr^{3+} on mitochondrial respiration parameters in macrophages *in cellula*. Results showed that Co^{2+}, but not Cr^{3+}, can increase oxidative stress and decrease OXPHOS in RAW 264.7 macrophages (Manuscript 1; Chapter 3). The decrease in OXPHOS, which indicates a decrease in mitochondrial ATP production, may reflect the repurposing of the mitochondria to ROS production, potentially contributing to the macrophage pro-inflammatory response.[242]

6.1.2 Evidence of Co^{2+}- and Cr^{3+}- induced increase in glycolytic flux and of Co^{2+}- induced HIF-1α stabilization in RAW 264.7 macrophages

This study showed that the exposure of RAW 264.7 macrophages to Co^{2+} or Cr^{3+} increased glycolytic flux, albeit to a lower extent with Cr^{3+} (Manuscript 2, Chapter 4). Moreover, results showed that the increase in PER observed in the presence of Co^{2+} or Cr^{3+} was almost exclusively due to an increase in aerobic glycolysis. Finally, results showed that only Co^{2+} stabilized HIF-1α, suggesting that HIF-1α is involved in the Co^{2+}-induced increase in glycolytic flux. These results,

together with our previous results, showing that Co^{2+} can increase oxidative stress and decrease OXPHOS in RAW 264.7 macrophages (Manuscript 1, Chapter 3), indicate that Co^{2+} (but not Cr^{3+}) can induce a metabolic shift from OXPHOS to aerobic glycolysis. This metabolic shift, which may be involving HIF-1α, is similar to that associated with the polarization of macrophages towards a pro-inflammatory phenotype.

Overall, our results in macrophages showing Co^{2+}-induced glycolytic activity are in agreement with studies reporting Co^{2+} increases glucose uptake and activity of glycolytic enzymes in non-immune cells.[180] On the other hand, the Cr^{3+}-induced glycolytic activity (albeit to a lower extent than Co^{2+}) in the absence of a decrease in OXPHOS suggest that these ions may indirectly upregulate the glycolytic flux in macrophages through the activation of regulatory mechanism(s) or through homeostatic control mechanisms due to a demand for certain carbon compounds. Moreover, the exposure of macrophages to Co^{2+} stabilized HIF-1α, suggesting that the HIF-1 transcription factor is involved in the Co^{2+}-induced increase in glycolytic flux. In contrast, Cr^{3+} did not induce HIF-1α stabilization, in agreement with studies showing that Cr^{3+}, unlike Co^{2+} and Ni^{2+}, does not stabilize HIF-1α in human airway epithelial cells.[249] Given that HIF-1α accumulation has been reported to be significantly higher in the periprosthetic tissues of patients with a MM hip implant than in patients with a MPE hip implant,[259] our results suggest a key role for Co^{2+}-induced HIF-1α stabilization in regulating macrophage inflammatory response to CoCrMo-based implants.

6.1.3 Current model

The findings of this thesis on the effects of Co^{2+} on energy metabolism in macrophages are summarized in Figure 6. Overall, our results suggest a potential Co^{2+}-induced metabolic shift in macrophages that may be mediated by HIF-1α. This metabolic shift may contribute to the pro-

inflammatory response observed in periprosthetic tissues, which could also lead to lymphocyte recruitment and activation, and thereby further adverse local tissue reactions to CoCrMo-based implants.

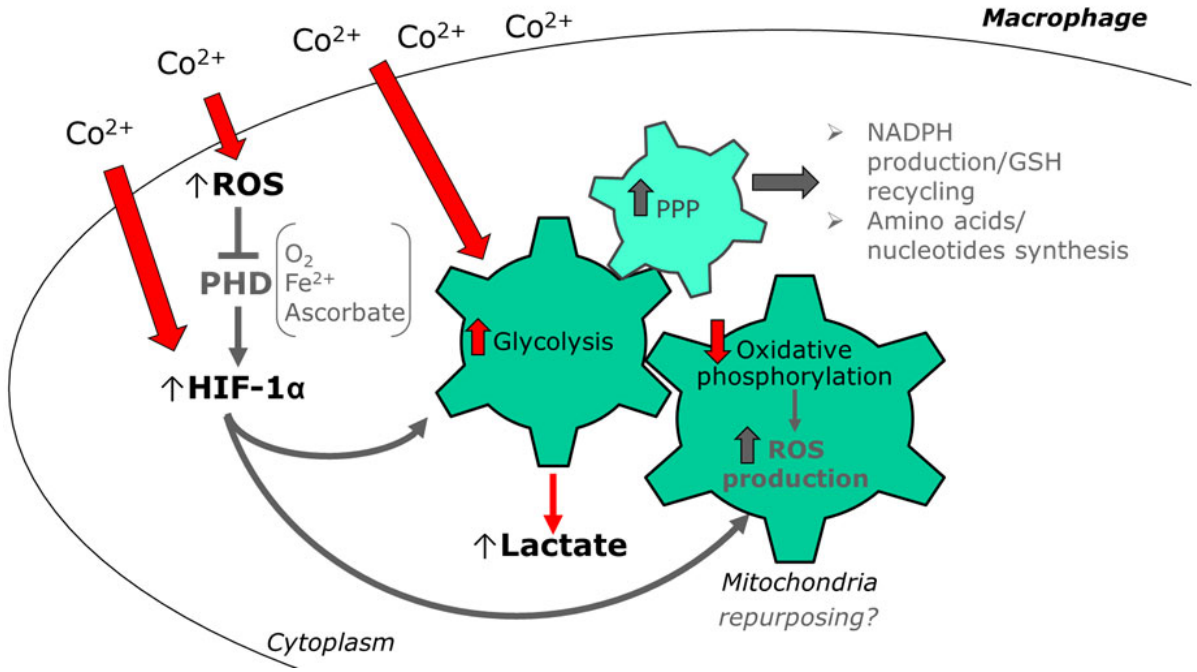

Figure 6.1: Current model on the effects of Co^{2+} on energy metabolism in macrophages. Co^{2+}-induced ROS production, mitochondrial dysfunction, glycolytic flux activation and HIF-1α stabilization are pointed out with red arrows. Other lines of investigation to pursue in future studies are marked with grey arrows/lines.

These findings bring new insights into molecular mechanisms involved in the macrophage response to metal ions. The current model points towards future studies including: 1. Determining if HIF-1α is involved in the metabolic shift, specifically in the increase of glycolytic flux; 2. Determining if members of the PHD family of enzymes are involved in ROS-mediated HIF-1α stabilization following macrophage exposure to Co^{2+}; 3. Determining if mitochondrial ROS production is increased in parallel with mitochondrial downregulation; and 4. Determining if PPP flux is increased in conjunction with the increase in glycolytic flux. These future studies, and others, will be further developed in Section 6.3.

6.2 Technical considerations and limitations

6.2.1 Use of RAW 264.7 mouse macrophage cell line

The RAW 264.7 mouse macrophage cell line was used as the experimental model. This cell line is a common model for *in vitro* studies of molecular pathways activated by implant wear particles or metal ions[114,224,225] as well as oxidative stress and mitochondrial function.[226] Limitations of the RAW 264.7 macrophage model include its murine origin,[227] as well as higher metabolic rates and OCR than primary murine macrophages.[228] However, immortalized cells, as opposed to primary cells, were selected to avoid potential inter-donor variability.

6.2.2 ROS detection

ROS levels were measured after a 6-h incubation with metal ions because the kinetics of ROS production was determined in preliminary experiments and indicated that the levels peaked around 6h of incubation with Co^{2+} (data not shown).

The fluorogenic probe DCFH-DA, which is part of the commercial ROS detection kit (OxiSelect^{TM} Intracellular ROS assay kit; Cell Biolabs, San Diego, CA) used to detect cytosolic ROS, revealed several challenges. For example, DCFH-DA and the non-fluorescent $DCFH_2$ (resulting from the intracellular esterase activity on DCFH-DA) have been shown to react with solutions containing bicarbonate, in addition to some metal ions (iron, cupper) generating the fluorescent DCF compound.[234] Moreover, DCFH-DA is prone to photo-oxidation.[234] Therefore, in order to counteract these issues and more accurately measure the background level, the probe should be prepared in a FBS-free (since FBS may contain esterase) and bicarbonate-free medium (e.g. Hank's buffered saline solution [HBSS]) (see details in Manuscript 1, Chapter 3). Our results showed an increase in DCF concentration in presence of Co^{2+}, suggesting an increase in ROS

levels, and thereby the presence of oxidative stress in response to Co^{2+}, which was confirmed by protein oxidation.

6.2.3 Protein oxidation

Protein oxidation was measured after a 24-h incubation with metal ions based on a previous study by Petit et al.[214]. Sample preparation to determine the effects of metal ions on protein oxidation revealed that macrophage exposure to high Cr^{3+} concentrations caused cell lysis resistance when using non-ionic detergents. Cell lysis required ionic detergents such as SDS at high concentrations, which resulted in the formation of a DNA hydrogel necessitating sonication. Since sonication may increase the background oxidation levels,[282] cell lysis was instead performed using a nitrogen cavitation chamber under pressurized pure-grade nitrogen (99.9%). Of note is that reducing agents should not be added at any stage during sample preparation since they have been shown to increase the protein oxidation background levels and therefore add a confounding factor that could increase the risk of false negative results.[223] Finally, it is possible that the use of a fluorescence detection system, as opposed to enhanced chemiluminescence (ECL) method, may have increased the signal to noise ratio and optimized the detection.

6.2.4 Seahorse experiments

Mitochondrial activity was measured after a 6-h incubation with metal ions based on the assumption that mitochondrial dysfunction is an important source of metal ion-induced ROS, and because ROS levels peaked after a 6-h incubation with Co^{2+}. Glycolytic flux was also measured after a 6-h incubation with metal ions to complement the mitochondrial activity measurements.

The potential of the Seahorse technology lies in monitoring, in real-time, the cell response to a pre-treatment or to a stimulant/drug injected into intact (non-permeabilized) cells. OCR reflect mitochondrial function, while ECAR are indicators of glycolytic function. Seahorse experiments

were implemented based on literature from Seahorse Bioscience (now part of Agilent Technologies) and publications from Mookerjee et al.[255,283]. Technical considerations for these experiments included: 1. The cell seeding density and HEPES (buffer) concentration in the medium for the glycolysis stress test were tested. A cell seeding density of 80,000 cells/well is recommended by the manufacturer (Seahorse Bioscience) for the RAW 264.7 macrophage cell line. However, this seeding density led to a retroinhibition of the glycolytic pathway because of high concentrations of protons (H^+) being released, likely due to the high intrinsic metabolic rate of these cells in addition to the metal ion-induced increase in glycolytic flux. The pH trace must be monitored to ensure the linearity of the pH change over time at each individual measurement during the glycolysis assay. To maintain linearity, the pH variation (ΔpH) must be ≤ ca. 0.2 pH units per minute. In order to fulfill this requirement, it was determined that a cell seeding density of 40,000 cells/well and 5 mM HEPES were optimum; 2. The drug concentrations were titrated in order to avoid any secondary side effects (common with the conventional assay); 3. Rotenone and antimycin A were injected to inhibit the ETC, thereby preventing ECAR measurements from being affected by the mitochondrial acidification; 4. The maximal glycolytic acidification was measured by maximizing the cellular ATP demand (through monensin injection) to evaluate if regulatory mechanisms are involved in the activation of the glycolytic flux. 5. The buffering factor (BF) of the glycolysis assay medium was measured by titration with cumulative HCl concentrations, as previously decribed.[256] The BF is needed for the PER calculations and should be independent of the volume of the microchamber; 6. The scaling factor (Kvol) provided by the manufacturer (Seahorse BioScience) was used for the PER calculations. The Kvol represents the geometric measurement chamber volume based on the microplates format used.[256]

6.2.5 Protocol optimization for the detection of HIF-1α protein

In HeLa and vascular smooth muscle cells, HIF-1α stabilization peaked between 4h and 8h of incubation with metal ions *in vitro*.[195,284] In RAW 264.7 macrophages, HIF-1α stabilization peaked around 6h of incubation with Co^{2+} (data not shown).

Previous studies have shown that HIF-1α can accumulate in the cytosol in response to metal ions, even under normoxic conditions, due to lack of hydroxylase, which usually targets HIF-1α for degradation.[190] It has also been suggested that the cell type, cell density, and cell culture conditions (media with or without FBS) may have a significant impact on basal HIF-1α protein levels.[285-287] Two different cell seeding densities (200,000 and 400,000 cells/cm^2) were therefore tested in the context of this thesis. Results showed that using the lower density increased the signal from 25% to almost 50% with Co^{2+}. In addition, the choice of antibody as well as the choice of detection system (ECL vs. fluorescence detection) for HIF-1α immunoblotting play a significant role in detecting the presence and the signal of HIF-1α. The expression of the full-length HIF-1α was verified using commercial HeLa cell lysates from untreated and $CoCl_2$-treated cells (negative and positive HIF-1α controls, respectively). A primary antibody targeting the C-terminus of the HIF-1α combined with a fluorescent IRDye (InfraRed Dye) secondary antibody allowed for the detection of the full-size (non-degraded) HIF-1α protein in RAW 264.7 macrophages after exposure to Co^{2+} or Cr^{3+}.

6.2.6 Other considerations

Noteworthily, additional observations from this study should be taken into account. First, the use of the bicinchoninic acid (BCA) assay for protein quantification during the lactate production measurements, likely overestimated protein concentration in presence of metal ions, especially with high Cr^{3+} concentrations. Since the assay is based on metal ion reduction (Cu^{2+})

by specific amino acid residues, it is possible that the ions remaining in the whole cell lysates interfere with the assay signal, thereby potentially overestimating protein concentration Protein quantification using the Bradford assay for protein quantification during the Seahorse experiments and HIF-1α immunoblotting, on the other hand, revealed more consistent protein concentrations between the samples analyzed with high metal ions concentration analyzed.

6.3 Future directions

6.3.1 Determining if HIF-1α is involved in the metabolic shift

To determine if HIF-1α is involved in the metabolic shift, specifically in the increase of glycolytic flux, HIF-1α expression, stabilization or activity could be targeted using pharmacological approaches. For example, the heat shock protein 90 (HSP90) inhibitor, 17-N-allylamino-17-demethoxygeldanamycin (17-AAG) has been commonly used as a HIF-1 inhibitor. This drug interferes with HIF-1 dimer interaction with HSP90, leading to the inhibition of HIF-1 nuclear translocation, therefore targeting HIF-1α for proteasomal degradation. An alternative strategy could involve the use of macrophages derived from conditional HIF-1α-knock out mice. Determining if members of the PHD family of enzymes are involved in ROS mediated HIF-1α stabilization

PHD are redox-regulated enzymes and their activity is dependent on the presence of Fe^{2+} and ascorbate, in addition to O_2. Therefore, it would be interesting to determine if members of the PHD family of enzymes are involved in ROS-mediated HIF-1α stabilization following macrophage exposure to Co^{2+} under normoxic conditions. Interestingly, Guentsch et al.[228] showed that PHD2, a member of the PHD family of enzymes, is a regulator of metabolic reprogramming in macrophages. This study also showed that regulation of PDH2 activity is critical for macrophage

immune function, which suggests a role of PHD enzymes in modulating the metal ion-induced inflammatory response in macrophages.[228]

6.3.2 Determining if mitochondrial ROS production is increased in parallel with mitochondrial downregulation

In this thesis, protein oxidative damage as well as cytosolic ROS showed that Co^{2+} but not Cr^{3+} induces oxidative stress in macrophages *in vitro*. In addition, another important finding was that Co^{2+} but not Cr^{3+} induces a decrease in OXPHOS suggesting mitochondrial repurposing from ATP production to ROS production in presence of Co^{2+}. Therefore, future studies could include the measurements of mitochondrial ROS in macrophages exposed to Co^{2+}, and determine if mitochondrial ROS production is increased as a consequence of mitochondrial downregulation.

6.3.3 Determining if PPP flux is increased in conjunction with the increase in glycolytic flux

In order to determine if PPP flux is increased in conjunction with the increase in glycolytic flux, PPP flux could be quantified by measuring the levels of PPP metabolites (such as ribose and ribulose 5-phosphate), as well as the enzymatic activity and the level of expression of rate-limiting enzymes, such as 6- phosphogluconate dehydrogenase (6-PGDH).

6.3.4 Modulating the inflammatory response *in vitro*

This thesis looked at the effects of metal ions, specifically Co^{2+} and Cr^{3+}, on oxidative stress and the energy metabolism in macrophages. Strategies to mitigate the effects of wear and corrosion products on macrophage inflammatory response could include decreasing metal ion-induced oxidative stress by using antioxidants, and inhibiting HIF-1α expression, stabilization or activity, as explained below.

6.3.4.1 Decreasing metal ion-induced oxidative stress

To modulate metal ion-induced oxidative stress, non-enzymatic antioxidants have been used to reduce ROS production and thereby decrease the inflammatory response. For example, a recent study from our lab recently showed that ascorbic acid (a ROS scavenger) can prevent caspase-1 activation and IL-1β release in macrophages exposed to Cr^{3+}.[288] However, pharmacologic ascorbate has been shown to lead to preferential formation of ascorbate radicals and hydrogen peroxide in the presence of protein-bound metal ions in the extracellular space *in vivo*.[222] Therefore, ascorbic acid should be used with caution for the potential treatment of metal ion-induced oxidative stress. Another strategy could be to target oxidative stress by using an antioxidant that would also serve as a metal ion chelator, such as N-acetyl-cysteine (NAC).[289] Interestingly, NAC has recently been reported to decrease Co and Cr ion levels in two patients with MM hip implants after oral administration.[290]

6.3.4.2 Inhibiting HIF-1α expression, stabilization or activity

HIF-1α has been shown to be essential for myeloid cell-mediated inflammation.[192] To modulate the inflammatory response of macrophages to metal ions, HIF-1α expression, stabilization or activity could be inhibited by using pharmacological approaches or genetic approaches, as described in Section 6.3.1, especially if the causal relationship between the increase in HIF-1α and glycolytic flux suggested in Manuscript 2 (chapter 4) is confirmed.

6.3.5 Analyzing the effects of additional metal ions and metal particles

The present research project focused on the effects of Co^{2+} and Cr^{3+} on pathways involved in macrophage energy metabolism. The effects of other metal ions could be considered in future studies. For example, although the amount of molybdenum and nickel ions released from CoCrMo

alloys is much lower than that of cobalt and chromium ions,[10] molybdenum and nickel ions could be considered in future studies. Of note is that Mo^{5+} and Ni^{2+} have previously been shown to induce oxidative stress in various cell types.[135,291,292] Finally, the effect of metal particles such as CoCrMo alloy particles (1-7 μm range) could also be included in future studies. Indeed, although previous studies did not report ROS production in human peripheral blood monocytes (PBMC), human MM-6 or Jurkat cell lines exposed to CoCrMo alloy particles,[293] their effects of cellular energy metabolism remain largely unknown.

6.3.6 Analyzing the effects of metal ions and particles on energy metabolism of other cell types

Previous studies showed that Co^{2+} but not Cr^{3+} induces ROS-dependent fibrotic response.[294] Other studies showed that fibroblasts contribute to the metal ion-induce inflammatory response.[80,295] However, to the best of our knowledge, the effects of metal ions on fibroblast energy metabolism remain unknown and could therefore represent a future line of investigation, since fibroblasts have been shown to play an active role in the inflammatory response in the periprosthetic tissues.[80,295]

Analyzing lymphocyte energy metabolism in the presence of metal ions could be considered in the context of hypersensitivity reactions since their energy metabolism has been shown to be a reliable indicator of their level of activation.[296] However, since lymphocytes are non-adherent cells, careful considerations would need to be taken into account when choosing the assay conditions to study these cells using Seahorse technology (designed for adherent cells). For example, poly-L-lysine, fibronectin could be used to coat the Seahorse tissue culture-treated microplates in order to enhance lymphocytes adherence during the Seahorse assays.

6.4 Conclusion of the thesis

This thesis investigated molecular pathways activated in macrophages exposed to metal ions, specifically Co^{2+} and Cr^{3+}, released from CoCrMo-based implants, and leading to an inflammatory response. This *in vitro* study confirmed the presence of oxidative stress with Co^{2+} but not Cr^{3+} in the murine RAW 264.7 macrophage cell line. This study also showed that Co^{2+} is likely inducing a metabolic shift from OXPHOS towards glycolysis which may play a critical role in Co^{2+}-induced pro-inflammatory (M1) macrophage phenotype. An efficient strategy to mitigate the effects of wear and corrosion products could be to prevent Co^{2+}-induced oxidative stress and, if the causal relationship between the increase in HIF-1α and glycolytic flux is confirmed, to inhibit Co^{2+}-induced HIF-1α stabilization. Ultimately, the goal is to modulate the chronic inflammatory reaction, and re-establish immune homeostasis around the implant in order to increase metal implant longevity.

7. REFERENCES

1. Gallo J, Goodman SB, Konttinen YT, et al. 2013. Particles disease: Biologic mechanisms of periprosthetic osteolysis in total hip arthroplasty. Innate Immun 19:213-224.

2. Evans JT, Walker RW, Evans JP, et al. 2019. How long does a knee replacement last? A systematic review and meta-analysis of case series and national registry reports with more than 15 years of follow-up. The Lancet 393:655-663.

3. Learmonth ID, Young C, Rorabeck C. 2007. The operation of the century: total hip replacement. The Lancet 370:1508-1519.

4. Canadian Institute for Health Information (CIHI). 2016-2017. Hip and knee replacements in Canada - annual report. Canada joint replacement registry (CJRR):1-51.

5. Karachalios T, Komnos G, Koutalos A. 2018. Total hip arthroplasty: Survival and modes of failure. EFORT Open Rev 3:232-239.

6. Fisher J, Dowson D. 1991. Tribology of total artificial joints. Proc Inst Mech Eng H 205:73-79.

7. Ingham E, Fisher J. 2000. Biological reactions to wear debris in total joint replacement. Proc Inst Mech Eng H 214:21-37.

8. Zhu YH, Chiu KY, Tang WM. 2001. Polyethylene wear and osteolysis in total hip arthroplasty. J Orthop Surg (Hong Kong) 9:91-99.

9. Zahiri CA, Schmalzried TP, Ebramzadeh E, et al. 1999. Lessons learned from loosening of the McKee-Farrar metal-on-metal total hip replacement. J Arthroplasty 14:326-332.

10. Nevelos J, Shelton JC, Fisher J. 2004. Metallurgical considerations in the wear of metal-on-metal bearings. Hip Int 14:1-10.

11. McKellop H, Shen FW, DiMaio W, et al. 1999. Wear of gamma-crosslinked polyethylene acetabular cups against roughened femoral balls. Clin Orthop Relat Res:73-82.

12. Muratoglu OK. 2001. The comparison of the wear behavior of four different types of crosslinked acetabular components. J Orthop Res 19:1210.

13. Jacobs CA, Christensen CP, Greenwald AS, et al. 2007. Clinical performance of highly cross-linked polyethylenes in total hip arthroplasty. J Bone Joint Surg Am 89:2779-2786.

14. Laurent MP, Yao JQ, Bhambri SK, et al. 2000. High cycle wear of highly cross-linked UHMWPE acetabular liners evaluated in hip simulator. Transactions of the 26th Annual Meeting of the Society of Biomaterials:0567.

15. Mall NA, Nunley RM, Zhu JJ, et al. 2011. The incidence of acetabular osteolysis in young patients with conventional versus highly crosslinked polyethylene. Clin Orthop Relat Res 469:372-381.

16. Bradford L, Baker DA, Graham J, et al. 2004. Wear and surface cracking in early retrieved highly crosslinked polyethylene acetabular liners. J Bone Joint Surg Am 86:1271-1282.

17. Ries MD SM, Jani S. 2001. Relationship between gravimetric wear and particle generation in hip simulators: conventional compared with cross-linked polyethylene. J Bone Joint Surg Am 2001;83-A Suppl 2 Pt 2:116-22 83-A suppl 2:116-122.

18. Purdue PE, Koulouvaris P, Potter HG, et al. 2007. The cellular and molecular biology of periprosthetic osteolysis. Clin Orthop Relat Res 454:251-261.

19. Green TR, Fisher J, Stone M, et al. 1998. Polyethylene particles of a 'critical size' are necessary for the induction of cytokines by macrophages in vitro. Biomaterials 19:2297-2302.

20. Kobayashi A, Bonfield W, Kadoya Y, et al. 1997. The size and shape of particulate polyethylene wear debris in total joint replacements. Proc Inst Mech Eng H 211:11-15.

21. Milošev I. 2012. CoCrMo Alloy for Biomedical Applications. In: Djokić SS editor. Biomedical Applications, Modern Aspects of Electrochemistry. Boston, MA: Springer; pp. 1-72.

22. Sansone V, Pagani D, Melato M. 2013. The effects on bone cells of metal ions released from orthopaedic implants. A review. Clin Cases Miner Bone Metab 10:34-40.

23. Sieber HP, Rieker CB, Köttig P. 1999. Analysis of 118 second-generation metal-on-metal retrieved hip implants. J Bone Joint Surg 81:46-50.

24. Weber BG, Rieker BC. 2002. The history of Metasul. Acta Chirurgiae Orthopaedicae et Traumatologiae Cechoslovaca 69:277-284.

25. Firkins PJ, Tipper JL, Saadatzadeh MR, et al. 2001. Quantitative analysis of wear and wear debris from metal-on-metal hip prostheses tested in a physiological hip joint simulator. Bio-medical materials and engineering 11:143-157.

26. Anissian HL, Stark A, Gustafson A, et al. 1999. Metal-on-metal bearing in hip prosthesis generates 100-fold less wear debris than metal-on-polyethylene. Acta Orthop Scand 70:578-582.

27. Australian Orthopaedic Association (AOA). 2010. Hip and Knee Arthroplasty annual report. AOA National joint replacement registry:1-179.

28. National Joint Registry (NJR). 2012. National joint Registry for England and Wales | 9th annual report. National joint registry for England and Wales:1-210.

29. Catelas I, Huk OL, Petit A, et al. 1998. Flow cytometric analysis of macrophage response to ceramic and polyethylene particles: effects of size, concentration, and composition. J Biomed Mater Res 1998 Sep 15;41(4):600-7 41:600-607.

30. Matthews JB, Besong AA, Green TR, et al. 2000. Evaluation of the response of primary human peripheral blood mononuclear phagocytes to challenge with *in vitro* generated clinically relevant UHMWPE particles of known size and dose. Biomaterials 21:2033-2044.

31. Sieving A, Wu B, Mayton L, et al. 2003. Morphological characteristics of total joint arthroplasty-derived ultra-high molecular weight polyethylene (UHMWPE) wear debris that provoke inflammation in a murine model of inflammation. J Biomed Mater Res A 64:457-464.

32. Catelas I, Jacobs JJ. 2010. Biologic activity of wear particles. Instr Course Lect 59:3-16.

33. Doorn PF, Mirra JM, Campbell PA, et al. 1996. Tissue reaction to metal on metal total hip prostheses. Clin Orthop Relat Res:S187-205.

34. Catelas I, Medley JB, Campbell PA, et al. 2004. Comparison of *in vitro* with *in vivo* characteristics of wear particles from metal-metal hip implants. J Biomed Mater Res B Appl Biomater 70:167-178.

35. Lerouge S, Huk O, Yahia L' H, et al. 1997. Ceramic-ceramic and metal-polyethylene total hip replacements - comparison of pseudo membranes after loosening J Bone Joint Surg Br 79:135-139.

36. Hattona A, Nevelosb JE, Nevelos AA, et al. 2002. Alumina–alumina artificial hip joints. Part I: a histological analysis and characterisation of wear debris by laser capture microdissection of tissues retrieved at revision. Biomaterials 23:3429-3440.

37. Tipper JL, Hatton A, Nevelos JE, et al. 2002. Alumina-alumina artificial hip joints: Part II. Characterization of the wear debris from in vitro hip joint simulations. Biomaterials 23:3441-3448.

38. Mu Y, Kobayashi T, Sumita M, et al. 2000. Metal ion release from titanium with active oxygen species generated by rat macrophages in vitro. J Biomed Mater Res 49:238-243.

39. Gibon E, Amanatullah DF, Loi F, et al. 2017. The biological response to orthopaedic implants for joint replacement: Part I: Metals. J Biomed Mater Res B Appl Biomater 105:2162-2173.

40. Baskey SJ, Lehoux EA, Catelas I. 2016. Migration of lymphocytes in response to cobalt and chromium ions. J Orthop Res 35:916-924.

41. Czarnek K, Terpilowska S, Siwicki AK. 2015. Selected aspects of the action of cobalt ions in the human body. Centr Eur J Immunol 40:236-242.

42. Devitt BM, Queally JM, Vioreanu M, et al. 2010. Cobalt ions induce chemokine secretion in a variety of systemic cell lines. Acta Orthop 81:756-764.

43. Catelas I, Petit A, Zukor DJ, et al. 2003. TNF-α secretion and macrophage mortality induced by cobalt and chromium ions in vitro-Qualitative analysis of apoptosis. Biomaterials 24:383-391.

44. Scharf B, Clement CC, Zolla V, et al. 2014. Molecular analysis of chromium and cobalt-related toxicity. Sci Rep 4:5729.

45. Cobb AG, Schmalzreid TP. 2006. The clinical significance of metal ion release from cobalt–chromium metal-on-metal hip joint arthroplasty. Proc IMechE J Engineering in Medicine 220:385-398.

46. Schmidt M, Raghavan B, Müller V, et al. 2010. Crucial role for human Toll-like receptor 4 in the development of contact allergy to nickel. Nat Immunol 11:814-819.

47. Raghavan B, Martin SF, Esser PR, et al. 2012. Metal allergens nickel and cobalt facilitate TLR4 homodimerization independently of MD2. EMBO Rep 13:1109-1115.

48. Díaz D, Bartolo R, Delgadillo DM, et al. 2005. Contrasting effects of Cd^{2+} and Co^{2+} on the blocking/unblocking of human Cav3 channels. J Membr Biol 207:91-105.

49. Gunter TE, Yule DI, Gunter KK, et al. 2004. Calcium and mitochondria. FEBS Letter 567:96-102.

50. Vincent JB. 2000. The biochemistry of chromium. J Nutr 130:715-718.

51. Tkaczyk C, Huk OL, Mwale F, et al. 2010. Investigation of the binding of Cr(III) complexes to bovine and human serum proteins: a proteomic approach. J Biomedical Mater Res A 94:214-222.

52. Chen G, Liu P, Pattar GR, et al. 2006. Chromium activates glucose transporter 4 trafficking and enhances insulin-stimulated glucose transport in 3T3-L1 adipocytes via a cholesterol-dependent mechanism. Mol Endocrinol 20:857-870.

53. Novotnik B, Ščančar J, Milačič R, et al. 2016. Cytotoxic and genotoxic potential of Cr(VI), Cr(III)-nitrate and Cr(III)-EDTA complex in human hepatoma (HepG2) cells. Chemosphere 154:124-131.

54. Lehtovirta L, Reito A, Lainiala O, et al. 2017. Analysis of bearing wear, whole blood and synovial fluid metal ion concentrations and histopathological findings in patients with failed ASR hip resurfacings. BMC Musculoskelet 18:1-11.

55. Matharu GS, Berryman F, Judge A, et al. 2017. Blood metal ion thresholds to identify patients with metal-on-metal hip implants at risk of adverse reactions to metal debris: an external multicenter validation study of Birmingham hip resurfacing and Corail-Pinnacle implants. J Bone Joint Surg Am 99:1532-1539.

56. Choi HJ, Lim SJ, Park YS, et al. 2015. Simple and robust ICP-MS method for simultaneous determination of serum Co and Cr in routine clinical practice. Clin Chim Acta 439:91-96.

57. Mayo Clinic. 2012. Evaluation of metal-on-metal wear of orthopaedic implants – the role of serum chromium and cobalt analysis. Mayo Med Lab: Communique 37:1-8.

58. Medicines and Healthcare Products Regulatory Agency. 2012. Medical device alert (MDA/2012/ 036): all metal-on-metal (MoM) hip replacements.

59. Hartmann A, Hannemann F, Lützner J, et al. 2013. Metal ion concentrations in body fluids after implantation of hip replacements with metal-on-metal bearing – Systematic review of clinical and epidemiological studies. PLoS one 8:e70359.

60. Houdek MT, Wyles C, Jannetto PJ, et al. 2018. Synovial fluid metal levels are superior to whole blood and serum metal ions levels in predicting local tissue destruction in failed hip artroplasty constructs. Orthopaedic proceedings 100-B Supp1.

61. Lehtovirta L, Reito A, Lainiala O, et al. 2019. Host-specific factors affect the pathogenesis of adverse reaction to metal debris. BMC Musculoskelet 20:1-10.

62. Gallo J, Konttinen YT, Goodman SB, et al. 2012. Aseptic loosening of total hip arthroplasty as a result of local failure of tissue homeostasis. In: Fokter DS editor. Recent Advances in Arthroplasty: Intechopen; pp. 319-362.

63. Willert HG, M. S. 1977. Reactions of the articular capsule to wear products of artificial joint prostheses. J Biomed Mater Res 11:157-164.

64. MacInnes SJ, Gordon A, Wilkinson JM. 2012. Risk factors for aseptic loosening after total hip arthroplasty. In: Fokter DS editor. Recent advances in Arthroplasty: Intechopen; pp. 275-294.

65. Gu Q, Shi Q, Yang H. 2012. The role of TLR and chemokine in wear particle-induced aseptic loosening. J Biomed Biotechnol 2012:596870.

66. Lacey DL, Timms E, Tan HL, et al. 1998. Osteoprotegerin ligand is a cytokine that regulates osteoclast differentiation and activation. Cell 93:165-176.

67. Wooley PH, EM. S. 2004. Aseptic loosening. Nature Reviews 11:402-407.

68. Fahlgren A, Bostrom MP, Yang X, et al. 2010. Fluid pressure and flow as a cause of bone resorption. Acta Orthop 81:508-516.

69. Anderson JM, Rodriguez Analiz, Chang DT. 2008. Foreign body reaction to biomaterials. Semin Immunol 20:86-100.

70. McKee AS, Fontenol AP. 2016. Interplay of innate and adaptive immunity in metal-induced hypersensitivity. Curr Opin Immunol 42:25-30.

71. Gallo J, Raska M, Kriegova E, et al. 2017. Inflammation and its resolution and the musculoskeletal system. J Orthop Translat 10:52-67.

72. Garrigues GE, Cho DR, Rubash HE, et al. 2005. Gene expression clustering using self-organizing maps: analysis of the macrophage response to particulate biomaterials. Biomaterials 26:2933-2945.

73. Haynes DR. 2004. Bone lysis and inflammation. Inflamm Res 53:596-600.

74. Nakashima Y, Sun DH, Trindade MC, et al. 1999. Induction of macrophage C-C chemokine expression by titanium alloy and bone cement particles. J Bone Joint Surg Br 81:155-162.

75. Hallab NJ, JJ. J. 2017. Chemokines associated with pathologic responses to orthopedic implant debris. Front Endocrinol (Lausanne) 8:1-10.

76. Amstutz HC, Campbell P, Kossovsky N, et al. 1992. Mechanism and clinical significance of wear debris-induced osteolysis. Clin Orthop Relat Res:7-12.

77. Crottia TN, Smith MD, Findlayc DM, et al. 2004. Factors regulating osteoclast formation in human tissues adjacent to peri-implant bone loss: expression of receptor activator NFκB, RANK ligand and osteoprotegerin. Biomaterials 25:565-573.

78. Kong YY, Yoshida H, Sarosi I, et al. 1999. OPGL is a key regulator of osteoclastogenesis, lymphocyte development and lymph-node organogenesis. Nature 397:315-323.

79. Sabokbar A, Pandey R, NA. A. 2003. The effect of particle size and electrical charge on macrophage-osteoclast differentiation and bone resorption. J Mater Sci Mater Med 14:731-738.

80. Sabokbar A, Itonaga I, Sun SG, et al. 2005. Arthroplasty membrane-derived fibroblasts directly induce osteoclast formation and osteolysis in aseptic loosening. J Orthop Res 23:511-519.

81. Kudo O, Fujikawa Y, Itonaga I, et al. 2002. Proinflammatory cytokine (TNFα/IL-1α) induction of human osteoclast formation. J Pathol 198:220-227.

82. Lam J, Takeshita S, Barker JE, et al. 2000. TNF-α induces osteoclastogenesis by direct stimulation of macrophages exposed to permissive levels of RANK ligand. J Clin Invest 106:1481-1488.

83. Lee SE, Chung WJ, Kwak HB, et al. 2001. Tumor necrosis factor-α supports the survival of osteoclasts through the activation of Akt and ERK. J Biol Chem 276:49343-49349.

84. Zhang L, Jia T-H, ChongACM, et al. 2010. Cell-Based Osteoprotegrin therapy for debris-induced aseptic prosthetic loosening on a murine model. Gene Ther 17:1262-1269.

85. Nich C, Takakubo Y, Pajarinen J, et al. 2013. Macrophages – Key cells in the response to wear debris from joint replacements. J Biomed Mater Res A 101:3033-3045.

86. Al-Saffar N, Revell PA, Kobayashi A. 1997. Modulation of the phenotypic and functional properties of phagocytic macrohages by wear particles from orthopaedic implants. Journal of materials science Materials in medicine 8:641-648.

87. Brooks RA, Sharpe JR, Wimhurst JA, et al. 2000. The effects of the concentration of high-density polyethylene particles on the bone-implant interface. J Bone Joint Surg Br 82:595-600.

88. Willert HG, Buchhorn GH, Fayyazi A, et al. 2005. Metal-on-metal bearings and hypersensitivity in patients with artificial hip joints. A clinical and histomorphological study. The Journal of bone and joint surgery 87:28-36.

89. Campbell P, Ebramzadeh E, Nelson S, et al. 2010. Histological features of pseudotumor-like tissues from metal-on-metal hips. Clin Orthop Relat Res 468:2321-2327.

90. Hallab NJ, Caicedo M, Finnegan A, et al. 2008. Th1 type lymphocyte reactivity to metals in patients with total hip arthroplasty. J Orthop Surg 3:1-11.

91. Hallab NJ, Mikecz K, Vermes C, et al. 2001. Orthopaedic implant related metal toxicity in terms of human lymphocyte reactivity to metal-protein complexes produced from cobalt-base and titanium-base implant alloy degradation. In: Shi X, Castranova V, Vallyathan V, et al. editors. Molecular Mechanisms of Metal Toxicity and Carcinogenesis Developments in Molecular and Cellular Biochemistry. Boston,MA: Springer.

92. Granchi D, Savarino L, Ciapetti G, et al. 2003. Immunological changes in patients with primary osteoarthritis of the hip after total joint replacement. J Bone Joint Surg Br 85:758-764.

93. Granchi D, Ciapetti G, Stea S, et al. 1995. Evaluation of several immunological parameters in patients with aseptic loosening of hip arthroplasty. La Chirurgia Degli Organi di Movimento 80:399-408.

94. Catelas I, Lehoux EA, Hurda I, et al. 2015. Do patients with a failed metal-on-metal hip implant with a pseudotumor present differences in their peripheral blood lymphocyte subpopulations? Clin Orthop Relat Res 476:3903-3914.

95. Pandit H, Glyn-Jones S, McLardy-Smith P, et al. 2008. Pseudotumours associated with metal-on-metal hip resurfacings. J Bone Joint Surg Br 90:847-851.

96. Bosker BH, Ettema HB, Boomsma MF, et al. 2012. High incidence of pseudotumour formation after large-diameter metal-on-metal total hip replacement: a prospective cohort study. J Bone Joint Surg Br 94:755-761.

97. Murgatroyd SE. 2012. Pseudotumor presenting as a pelvic mass: a complication of eccentric wear of a metal on polyethylene hip arthroplasty. J Arthroplasty 27:820.e821-824.

98. Carli A RA, Zukor DJ, Antoniou J. 2011. Adverse soft-tissue reactions around non-metal-on-metal total hip arthroplasty: A systematic review of the literature. Bull NYU Hosp Jt Dis 69 Suppl 1:S47-51.

99. Campbell PA, Kung MS, Hsu AR, et al. 2014. Do retrieval analysis and blood metal measurements contribute to our understanding of adverse local tissue reactions? Clin Orthop Relat Res 472:3718-3727.

100. Perino G, Ricciardi BF, Jerabek SA, et al. 2014. Implant based differences in adverse local tissue reaction in failed total hip arthroplasties: a morphological and immunohistochemical study. BMC Clin Pathol 14:1-16.

101. Davies LC, Jenkins SJ, Allen JE, et al. 2013. Tissue-resident macrophages. Nat Immunol 14:986-995.

102. Mosser DM, Edwards JP. 2008. Exploring the full spectrum of macrophage activation. Nat Rev Immunol 8:958-969.

103. Sica A, Mantovani A. 2012. Macrophage plasticity and polarization: in vivo veritas. J Clin Invest 122:787-795.

104. Lichtnekert J KT, Parks WC, JS. D. 2013. Changes in macrophage phenotype as the immune response evolves. Curr Opin Pharmacol 13:555-564.

105. Jung J, Zeng H, T. H. 2019. Metabolism as a guiding force for immunity. Nat Cell Biol 21:85-93.

106. Thomsen P, Gretzer C. 2001. Macrophage interactions with modified material surfaces. Curr Opin Solid St M 5:163-176.

107. Ingham E, J. F. 2005. The role of macrophages in osteolysis of total joint replacement. Biomaterials 26:1271-1286.

108. Brown BN, Ratner BD, Goodman SB, et al. 2012. Macrophage polarization: An opportunity for improved outcomes in biomaterials and regenerative medicine. Biomaterials 33:3792-3802.

109. Konttinen YT., Pajarinen J., Takakubo Y., et al. 2014. Macrophage polarization and activation in response to implant debris: Influence by “particle disease” and “ion disease”. J Long Term Eff Med Implants 24:267-281.

110. Jämsen E, Kouri VP, Olkkonen J, et al. 2014. Characterization of macrophage polarizing cytokines in the aseptic loosening of total hip replacements. J Orthop Res 32:1241-1246.

111. Akbar M. BJ, Grant MH. 2011. Effect of chromium and cobalt ions on primary human lymphocytes *in vitro*. J Immunotoxicol 2:140-149.

112. Balamurugan K, Rajaram R, Ramasami T, et al. 2002. Chromium(III)-induced apoptosis of lymphocytes: death decision by ROS and Src-family tyrosine kinases. Free Radic Biol Med 33:1622-1640.

113. Puleo DA, Huh WW. 1995. Acute toxicity of metal ions in cultures of osteogenic cells derived from bone marrow stromal cells. J Appl Biomater 6:109-116.

114. Kwon YM, Xia Z, Glyn-Jones S, et al. 2009. Dose-dependent cytotoxicity of clinically relevant cobalt nanoparticles and ions on macrophages *in vitro*. Biomed Mater 4:025018.

115. Petit A, Mwale F, Zukor DJ, et al. 2004. Effect of cobalt and chromium ions on bcl-2, bax, caspase-3, and caspase-8 expression in human U937 macrophages. Biomaterials 25:2013-2018.

116. Luo L, Petit A, Antoniou J, et al. 2005. Effect of cobalt and chromium ions on MMP-1, TIMP-1, and TNF-α gene expression in human U937 macrophages: A role for tyrosine kinases. Biomaterials 26:5587-5593.

117. Niki Y, Matsumoto H, Suda Y, et al. 2003. Metal ions induce bone-resorbing cytokine production through the redox pathway in synoviocytes and bone marrow macrophages. Biomaterials 24:1447-1457.

118. Baskey SJ, Beaulé PE, Lehoux EA, et al. 2014. Simvastatin modulates the release of TNF-α and CC chemokines from macrophages exposed to trivalent chromium ions. J Biomater Tissue Eng 4:981-991.

119. Xu J, Yang J, Nyga A, et al. 2018. Cobalt (II) ions and nanoparticles induce macrophage retention by ROS-mediated down-regulation of RhoA expression. Acta Biomater 72:434-446.

120. Caicedo MS, Samelko L, McAllister K, et al. 2013. Increasing both CoCrMo-alloy particle size and surface irregularity induces increased macrophage inflammasome activation in vitro potentially through lysosomal destabilization mechanisms. J Orthop Res 31:1633-1642.

121. Loftus RM, Finlay DK. 2016. Immunometabolism: Cellular metabolism turns immune regulator. J Biol Chem 291:1-10.

122. Verdeguer F, Aouadi M. 2017. Macrophage heterogeneity and energy metabolism. Exp Cell Res 360:35-40.

123. Dupré-Crochet S, Erard M, Nüβe O. 2013. ROS production in phagocytes: why, when, and where? J Leukoc Biol 94:657-670.

124. Davidson T, Ke Q, Costa M. 2007. Selected molecular mechanisms of metal toxicity and carcinogenicity. In: Nordberg GF, Fowler BA, Nordberg M editors. Handbook of the toxicology of metals. Amsterdan, The Netherlands: Elsevier; pp. 79-100.

125. Sies H, Berndt C, Jones DP. 2017. Oxidative stress. Annu Rev Biochem 86:715-748.

126. Valko M, Jomova K, Rhodes CJ, et al. 2016. Redox- and non-redox-metal-induced formation of free radicals and their role in human disease. Arch Toxicol 90:1-37.

127. Brüne B, Dehne N, Grossmann N, et al. 2013. Redox control of inflammation in macrophages. Antioxid Redox Signal 19:595-637.

128. Angajala A, Lim S, Phillips JB, et al. 2018. Diverse roles of mitochondria in immune responses: Novel insights into immuno-metabolism. Front Immunol 9:1-19.

129. Holmström KM, Finkel T. 2014. Cellular mechanisms and physiological consequences of redox-dependent signalling. Nat Rev Mol Cell Biol 15:411-421.

130. Irving H, Williams RJP. 1953. The stability of transition-metal complexes. J Chem Soc 0:3192-3210.

131. Dixon SJ, Stockwell BR. 2014. The role of iron and reactive oxidative species in cell death. Nat Chem Biol 10:9-17.

132. Wardman P, Candeias LP. 1996. Fenton Chemistry: An Introduction. Radiation research 145:523-531.

133. Kakhlon O, ZI. C. 2002. The labile iron pool: characterization, measurement, and participation in cellular processes. Free Radic Biol Med 33:1037-1046.

134. Valko M, Rhodes CJ, Moncol J, et al. 2006. Free radicals, metals and antioxidants in oxidative stress-induced cancer. Chem Biol Interact 160:1-40.

135. Terpilowska S, Siwicki AK. 2019. Cell cycle and transmembrane mitochondrial potential analysis after treatment with chromium(III), iron(III), molybdenum(III) or nickel(II) and their mixtures. Toxicol Res 8:188-195.

136. Raghunathan VK, Devey M, Hawkins S, et al. 2013. Influence of particle size and reactive oxygen species on cobalt chrome nanoparticle-mediated genotoxicity. Biomaterials 34:3559-3570.

137. Wang X, Son Y-K, Chang Q, et al. 2011. NADPH oxidase activation is required in reactive oxygen species generation and cell transformation induced by hexavalent chromium. Toxicol Sci 123:399-410.

138. Murphy MP. 2009. How mitochondria produce reactive oxygen species. Biochem J 417:1-13.

139. Jastroch M, Divakaruni AS, Mookerjee S, et al. 2010. Mitochondrial proton and electron leaks. Essays Biochem 47:53-67.

140. Valko M., Leibfritz D, Moncol J, et al. 2007. Free radicals and antioxidants in normal physiological functions and human disease. Int J Biochem Cell Biol 39:44-84.

141. Brand MD. 2010. The sites and topology of mitochondrial superoxide production. Exp Gerontol 45:466-472.

142. Mailloux RJ, Harper M-E. 2011. Uncoupling proteins and the control of reactive oxygen species production. Free Radic Biol Med 51:1106-1115.

143. West AP, Brodsky IE, Rahner C, et al. 2011. TLR signalling augments macrophage bactericidal activity through mitochondrial ROS. Nature Letters 472:476-480.

144. Blaser H, Dostert C, Mak TW, et al. 2016. TNF and ROS Crosstalk in Inflammation. Trends Cell Biol 26:249-261.

145. Naik E, Dixit VM. 2011. Mitochondrial reactive oxygen species drive proinflammatory cytokine production. J Exp Med 208:417-420.

146. Srinivasan S, Koenigstein A, Joseph J, et al. 2010. Role of mitochondrial reactive oxygen species in osteoclast differentiation. Ann N Y Acad Sci 1192:245-252.

147. Hayashi G, Cortopassi G. 2015. Oxidative Stress in Inherited Mitochondrial Diseases. Free Radic Biol Med 88:10-17.

148. Rachek LI, Grishko VI, Ledoux SP, et al. 2006. Role of nitric oxide-induced mtDNA damage in mitochondrial dysfunction and apoptosis. Free Radic Biol Med 40:754-762.

149. Wang Y, Fang J, Leonard SS, et al. 2004. Cadmium inhibits the electron transfer chain and induces reactive oxygen species. Free Radic Biol Med 36:1434-1443.

150. Zhou R, Yazdi AS, Menu P, et al. 2011. A role for mitochondria in NLRP3 inflammasome activation. Nature 469:221-225.

151. Chen H, Costa M. 2006. Effect of soluble nickel on cellular energy metabolism in A549 cells. Exp Biol Med 231:1474-1480.

152. Li X, Zhong F. 2014. Nickel induced Interleukin-1ß secretion via the NLRP3-ASC-Caspase 1 pathway. Inflammation 37:457-466.

153. Foster AW, Osman D, Robinson NJ. 2014. Metal preferences and metallation. J Biol Chem 289:28095-28103.

154. Myers CR, Antholine WE, JM. M. 2010. The pro-oxidant chromium(VI) inhibits mitochondrial complex I, complex II, and aconitase in the bronchial epithelium: EPR markers for Fe-S proteins. Free Radic Biol Med 49:1903-1915.

155. Frohnert B, Bernlohr DA. 2013. Protein carbonylation, mitochondrial dysfunction, and insulin resistance. Adv Nutr 4:157-163.

156. Christova TY, Gorneva GA, Taxirov SI, et al. 2003. Effect of cisplatin and cobalt chloride on antioxidant enzymes in the livers of Lewis lung carcinoma-bearing mice: protective role of heme oxygenase. Toxicol Lett 138:235-242.

157. Fleury C, Petit A, Mwale F, et al. 2006. Effect of cobalt and chromium ions on human MG-63 osteoblasts in vitro: Morphology, cytotoxicity, and oxidative stress. Biomaterials 27:3351-3360.

158. Tkaczyk C, Huk OL, Mwale F, et al. 2010. Effect of chromium and cobalt ions on the expression of antioxidant enzymes in human U937 macrophage-like cells. J Biomed Mater Res A 94A:419-425.

159. Permenter MG, Dennis WE, Sutto TE, et al. 2013. Exposure to cobalt causes transcriptomic and proteomic changes in two rat liver-derived cell lines. PLoS ONE 8:e83751.

160. Voitkun V, Zhitkovich A, M. C. 1998. Cr(III)-mediated crosslinks of glutathione or amino acids to the DNA phosphate backbone are mutagenic in human cells. Nucleic Acids Res 26:2024-2030.

161. Zhou R, Tardivel A, Thorens B, et al. 2009. Thioredoxin-interacting protein links oxidative stress to inflammasome activation. Nat Immunol 11:136-140.

162. West AP. 2017. Mitochondrial dysfunction as a trigger of innate immune responses and inflammation. Toxicology 391:54-63.

163. Kelly B, O'Neill LAJ. 2015. Metabolic reprogramming in macrophages and dendritic cells in innate immunity. Cell Res 25:771-784.

164. Brown GC. 1995. Nitric oxide regulates mitochondrial respiration and cell functions by inhibiting cytochrome oxidase. FEBS Letter 369:136-139.

165. López-Armada MJ, Riveiro-Naveira RR, Vaamonde-García C, et al. 2013. Mitochondrial dysfunction and the inflammatory response. Mitochondrion 13:106-118.

166. Kabe Y, Ando K, Hirao S, et al. 2005. Redox regulation of NF-kB activation: Distinct redox regulation between the cytoplasm and the nucleus. Antioxid Redox Signal 7:395-403.

167. Semenza GL. 2007. Hypoxia-Inducible Factor 1 (HIF-1) Pathway. Science 2007:1-4.

168. Eguchi Y, Shimizu S, Y. T. 1999. Intracellular ATP levels determine cell death fate by apoptosis or necrosis. Cancer Res 57:1835-1840.

169. Sandhir R, Halder A, Sunkaria A. 2017. Mitochondria as a centrally positioned hub in the innate immune response. Biochim Biophys Acta (BBA)- Molecular basis of disease 1863:1090-1097.

170. Santos JH, Hunakova L, Chen Y, et al. 2003. Cell sorting experiments link persistent mitochondrial DNA damage with loss of mitochondrial membrane potential and apoptotic cell death. JBC 278:1728-1734.

171. Battaglia V, Compagnone A, Bandino A, et al. 2009. Cobalt induces oxidative stress in isolated liver mitochondria responsible for permeability transition and intrinsic apoptosis in hepatocyte primary cultures. Int J Biochem Cell Biol 41:586-594.

172. Knull H, AP. M. 1996. Structure within eukaryotic cytoplasm and its relationship to glycolytic metabolism. Cell Biochem Funct 14:237-248.

173. Berg JM, Tymoczko JL, L. S. 2002. Glycolysis Is an Energy-Conversion Pathway in Many Organisms. In: Freeman WH editor. Biochemistry. New York: NCBI.

174. Berg JM, Tymoczko JL, L. S. 2002. The Pentose Phosphate Pathway Generates NADPH and Synthesizes Five-Carbon Sugars. In: WH F editor. Biochemistry. New York: NCBI.

175. Mullarky E, Cantley LC. 2015. Diverting glycolysis to combat oxidative stress. In: Nakao K, Minato N, Uemoto S editors. Innovative Medicine Basic Research and Development. Tokyo: Springer; pp. 3-23.

176. Rodriguez-Prados J-C, Traves PG, Cuenca J, et al. 2010. Substrate fate in activated macrophages: a comparison between innate, classic, and alternative activation. J Immunol 185:605-614.

177. Nagy C, Haschemi A. 2015. Time and demand are two critical dimensions of immunometabolism: the process of macrophage activation and the pentose phosphate pathway. Front Immunol 6:1-8.

178. Ganeshan K, Chawla A. 2014. Metabolic Regulation of Immune Responses. Annu Rev Immunol 32:609-634.

179. Robergs RA., McNulty CR., Minett GM., et al. 2018. Lactate, not lactic acid, is produced by cellular cytosolic energy catabolism. Physiology 33:10-12.

180. Hwang D-Y, Ismail-Beigi F. 2002. Glucose uptake and lactate production in cells exposed to $CoCl_2$ and in cells overexpressing the Glut-1 glucose transporter. Arch Biochem Biophys 399:206-211.

181. Skreb Y, AB. F. 1984. Toxicity of nickel for mammalian cells in culture. Toxicol Environ Chem 178:432-445.

182. Denton RM, Randle PJ, Bridges BJ, et al. 1975. Regulation of mammalian pyruvate dehydrogenase. Mol Cell Biol 9:27-53.

183. Scheiber IF, Dringen R. 2011. Copper accelerates glycolytic flux in cultured astrocytes. Neurochem Res 36:894-903.

184. Miranda ER., Dey CS. 2004. Effect of chromium and sinc on insulin signaling in skeletal muscle cells. Biological Trace Element Research 101:19-36.

185. Lipko M. DB. 2018. Mechanism of insulin-like effect of chromium(III) ions on glucose uptake in C2C12 mouse myotubes involves ROS formation. Journal of Trace Elements in Medicine and Biology 45:171-175.

186. Madathil BK. LQ, Hew CL., Mohanty M. 2010. Hypoxia-like effect of cobalt chromium alloy micro particles on fibroblasts in vitro. J Orthop Res 28:1360-1367.

187. Corcoran SE, LA. ON. 2016. HIF1α and metabolic reprogramming in inflammation. J Clin Invest 126:3699-3707.

188. Wang GL., Jiang BH., Rue EA., et al. 1995. Hypoxia-inducible factor 1 is a basic-helix-loop-helix-PAS heterodimer regulated by cellular O2 tension. Proc Natl Acad Sci U S A 92:5510-5514.

189. Krzywinska E, C. S. 2018. Hypoxia, Metabolism and Immune Cell Function. Biomedicines 6:56.

190. Maxwell P., Salnikow K. 2004. HIF-1: an oxygen and metal responsive transcription factor. Cancer Biology and Therapy 3:29-35.

191. Ke Q., Costa M. 2006. Hypoxia-Inducible Factor-1 (HIF-1). Mol Pharmacol 70:1469-1480.

192. Cramer T, Yamanishi Y, Clausen BE, et al. 2003. HIF-1α is essential for myeloid cell-mediated inflammation. Cell 112:645-657.

193. Peyssonnaux C, Datta V, Cramer T, et al. 2005. HIF-1α expression regulates the bactericidal capacity of phagocytes. J Clin Invest 115:1806-1815.

194. Westra J. BE, van Roosmalen AM I., Doornbos-van der Meer B., van Leeuwen MA., Posthumus MD., Kallenberg GM C. 2010. Expression and regulation of HIF-1alpha in macrophages under inflammatory conditions; significant reduction of VEGF by CaMKII inhibitor. BMC musculoskeletal disorders 11:1-11.

195. Triantafyllou A, Liakos P, Tsakalof A, et al. 2006. Cobalt induces hypoxia-inducible factor-1α (HIF-1α) in HeLa cells by an iron-independent, but ROS-, PI-3K- and MAPK-dependent mechanism. Informa Health care 40:847–856.

196. BelAiba RS, Djordjevic T, Bonello S, et al. 2004. Redox-sensitive regulation of the HIF pathway under non-hypoxic conditions in pulmonary artery smooth muscle cells. Biol Chem 385:249-257.

197. Pagé EL., Chan DA., Giaccia AJ., et al. 2008. Hypoxia-inducible factor-1 stabilization in nonhypoxic conditions: Role of oxidation and intracellular ascorbate depletion. MBoC 19:86-94.

198. Semenza GL., Roth PH., Fang H-M., et al. 1994. Transcriptional regulation of genes encoding glycolytic enzymes by hypoxia inducible factor 1. J Biol Chem 269:23757-23763.

199. Semenza GL. 2002. Signal transduction to hypoxia-inducible factor 1. Biochem Pharmacol 64:993-998.

200. Salnikow K, Donald SP, Bruick RK, et al. 2004 Depletion of intracellular ascorbate by the carcinogenic metals nickel and cobalt results in the induction of hypoxic stress. J Biol Chem 279:40337-40344.

201. Permenter MG, Lewis JA, Jackson DA. 2011. Exposure to nickel, chromium, or cadmium causes distinct changes in the gene expression patterns of a rat liver-derived cell line. PLoS ONE 6:e27730.

202. Semenza GL. 2011. Hypoxia-inducible factor 1: regulator of mitochondrial metabolism and mediator of ischemic preconditioning. Biochim Biophys Acta 1813:1263-1268.

203. Fukuda R, Zhang H, Kim JW, et al. 2007. HIF-1 regulates cytochrome oxidase subunits to optimize efficiency of respiration in hypoxic cells. Cell 129:111-122.

204. Papandreou I, Cairns RA, Fontana L, et al. 2006. HIF-1 mediates adaptation to hypoxia by actively downregulating mitochondrial oxygen consumption. Cell Metab 3:187-197.

205. Zhang H, Bosch-Marce M, Shimoda LA, et al. 2008. Mitochondrial autophagy is an HIF-1-dependent adaptive metabolic response to hypoxia. J Biol Chem 283:10892-10903.

206. Chan SY, Zhang YY, Hemann C, et al. 2009. MicroRNA-210 controls mitochondrial metabolism during hypoxia by repressing the iron-sulfur cluster assembly proteins ISCU1/2. Cell Metab 10:273-284.

207. Palsson-McDermott EM, Curtis AM, Goel G, et al. 2015. Pyruvate kinase M2 regulates Hif-1α activity and IL-1β induction and is a critical determinant of the warburg effect in LPS-activated macrophages. Cell Metab 21:65-80.

208. Wang T, Liu H, Lian G, et al. 2017. HIF1α-Induced glycolysis metabolism is essential to the activation of inflammatory macrophages. Mediators Inflamm 2017.

209. Case CP, Langkamer VG, James C, et al. 1994. Widespread dissemination of metal debris from implants. J Bone Joint Surg Br 76-B:701-712.

210. Goodman SB, Ma T. 2010. Cellular chemotaxis induced by wear particles from joint replacements. Biomaterials 31:5045-5050.

211. Langton DJ, Jameson SS, Joyce TJ, et al. 2011. Accelerating failure rate of the ASR total hip replacement. J Bone Joint Surg Br 93:1011-1016.

212. Cooper HJ, Della Valle CJ, Berger RA, et al. 2012. Corrosion at the head-neck taper as a cause for adverse local tissue reactions after total hip arthroplasty. J Bone Joint Surg Am 94:1655-1661.

213. Cooper HJ, Urban RM, Wixson RL, et al. 2013. Adverse local tissue reaction arising from corrosion at the femoral neck-body junction in a dual-taper stem with a cobalt-chromium modular neck. J Bone Joint Surg Am 95:865-873.

214. Petit A, Mwale F, Tkaczyk C, et al. 2005. Induction of protein oxidation by cobalt and chromium ions in human U937 macrophages. Biomaterials 26:4416-4422.

215. Luo S, Wehr NB. 2009. Protein carbonylation: avoiding pitfalls in the 2,4-dinitrophenylhydrazine assay. Redox report 14:159-166.

216. Sies H. 2015. Oxidative stress: a concept in redox biology and medicine. Redox Biology 4:180-183.

217. Mailloux RJ, McBride SL, Harper M-E. 2013. Unearthing the secrets of mitochondrial ROS and glutathione in bioenergetics. Trends Biochem Sci 38:592-602.

218. Fisher-Wellman H, Lin C-T, Ryan TE, et al. 2015. Pyruvate dehydrogenase complex and nicotinamide nucleotide transhydrogenase constitute an energy-consuming redox circuit. Biochem J 467:271-280.

219. Landgraeber S, Jäger M, Jacobs J, et al. 2014. The pathology of orthopedic implant failure is mediated by innate immune system cytokines. Mediators Inflamm 2014:1-9.

220. Wehr NB, Levine RL. 2013. Quantification of protein carbonylation. Methods Mol Biol 965:265-281.

221. Shacter E, Williams JA, Lim M, et al. 1994. Differential susceptibility of plasma proteins to oxidative modification: examination by western blot immunoassay. Free Radic Biol Med 17:429-437.

222. Chen Q, Espey MG, Sun AY, et al. 2007. Ascorbate in pharmacologic concentrations selectively generates ascorbate radical and hydrogen peroxide in extracellular fluid *in vivo*. PNAS 104:8749-8754.

223. Wang P, Powell SR. 2010. Decreased sensitivity associated with an altered formulation of a commercially available kit for detection of protein carbonyls. Free Radic Biol Med 49:119-121.

224. Beidelschies MA, Huang H, McMullen MR, et al. 2008. Stimulation of macrophage TNFα production by orthopaedic wear particles requires activation of the ERK1/2/Egr-1 and NF-κB pathways but is independent of p38 and JNK. J Cell Physiol 217:652-666.

225. Chen W, Li Z, Guo Y, et al. 2015. Wear particles promote reactive oxygen species-mediated inflammation via the nicotinamide adenine dinucleotide phosphate oxidase pathway in macrophages surrounding loosened implants. Cell Physiol Biochem 35:1857-1866.

226. Badding MA, Fix NR, Antonini JM, et al. 2014. A comparison of cytotoxicity and oxidative stress from welding fumes generated with a new nickel-, copper- based consumable versus mild and stainless steel-based welding in RAW 264.7 mouse macrophages. PLoS ONE 9:e101310.

227. Raschke WC, Baird S, Ralph P, et al. 1978. Functional macrophage cell lines transformed by Abelson leukemia virus. Cell 15:261-267.

228. Guentsch A, Beneke A, Swain L, et al. 2016. PHD2 Is a regulator for glycolytic reprogramming in macrophages. Mol Cell Biol 37:1-16.

229. Catelas I, Petit A, Vali H, et al. 2005. Quantitative analysis of macrophage apoptosis vs. necrosis induced by cobalt and chromium ions in vitro. Biomaterials 26:2441-2453.

230. Wang JY, Wicklund BH, Gustilo RB, et al. 1996. Titanium, chromium and cobalt ions modulate the release of bone- associated cytokines by human monocytes/macrophages *in vitro*. Biomaterials 17:2233-2240.

231. Catelas I, Petit A, Zukor DJ, et al. 2001. Cytotoxic and apoptotic effects of cobalt and chromium ions on J774 macrophages - Implication of caspase-3 in the apoptotic pathway. J Mater Sci Mater Med 12:949-953.

232. Kirkham P. 2007. Oxidative stress and macrophage function: a failure to resolve the inflammatory response. Biochem Soc Trans 35:284-287.

233. Gieche J, Mehlhase J, Licht A, et al. 2001. Protein oxidation and proteolysis in RAW264.7 macrophages: effects of PMA activation. Biochim Biophys Acta 1538:321-328.

234. Chen X, Zhong Z, Xu Z, et al. 2010. 2',7'-Dichlorodihydrofluorescein as a fluorescent probe for reactive oxygen species measurement: Forty years of application and controversy. Free Radic Res 44:587-604.

235. Birben E, Sahiner UM, Sackesen C, et al. 2012. Oxidative stress and antioxidant defense. World Allergy Organ J 5:9-19.

236. Van den Bossche J, Baardman J, Otto NA, et al. 2016. Mitochondrial dysfunction prevents repolarization of inflammatory macrophages. Cell Rep 17:684-696.

237. Lemire JA, Harrison JJ, Turner AJ. 2013. Antimicrobial activity of metals: mechanisms, molecular targets and applications. Nat Rev Microbiol 11:371-384.

238. Brand MD, Nicholls DG. 2011. Assessing mitochondrial dysfunction in cells. Biochem J 435:297-312.

239. Choksia KB, Boylstona WH, Rabeka JP, et al. 2004. Oxidatively damaged proteins of heart mitochondrial electron transport complexes. Biochim Biophys Acta 1688:95-101.

240. Morel F, Doussiere J, Vignais PV. 1991. The superoxide-generating oxidase of phagocytic cells. Physiological, molecular and pathological aspects. Eur J Biochem 201:523-546.

241. Hassoun EA, Stohs DJ. 1995. Chromium-induced production of reactive oxygen species, DNA single-strand breaks, nitric oxide production, and lactate dehydrogenase leakage in J774A.1 cell cultures. J Biochem Toxicol 10:315-321.

242. Van den Bossche J, O'Neill LA, Menon D. 2017. Macrophage immunometabolism: where are we (going)? Trends Immunol 38:395-406.

243. Ricciardi BF, Nocon AA, Jerabek SA, et al. 2016. Histopathological characterization of corrosion product associated adverse local tissue reaction in hip implants: a study of 285 cases. BMC Clin Pathol 16:1-17.

244. Kominsky DJ, Campbell EL, SP. C. 2011. Metabolic shifts in immunity and inflammation. J Immunol 184:4062-4068.

245. Salloum Z, Lehoux EA, Harper M-E, et al. 2018. Effects of cobalt and chromium ions on oxidative stress and energy metabolism in macrophages in vitro. J Orthop Res 36:3178-3187.

246. Mobasheri A, Platt N, Thorpe C, et al. 2006. Regulation of 2-deoxy-D-glucose transport, lactate metabolism, and MMP-2 secretion by the hypoxia mimetic cobalt chloride in articular chondrocytes. Ann NY Acad Sci 1091:83-93.

247. Hoffman NJ, Penque BA, Habegger KM, et al. 2014. Chromium enhances insulin responsiveness via AMPK. J Nutr Biochem 25:565-572.

248. Semenza GL. 2013. HIF-1 mediates metabolic responses to intratumoral hypoxia and oncogenic mutations. J Clin Invest 123:3664-3671.

249. Kaczmarek M, Timofeeva OA, Salnikow K. 2007. The role of ascorbate in the modulation of HIF-1α protein and HIF-dependent transcription by chromium(VI) and nickel(II). Free Radic Biol Med 42:1246-1257.

250. Kaczmarek M, Cachau RE, Topol IA, et al. 2009. Metal ions-stimulated iron oxidation in hydroxylases facilitates stabilization of HIF-1α protein. Toxicol Sci 107:394-403.

251. Yuan Y, Hilliard G, Ferguson T, et al. 2003. Cobalt inhibits the interaction between hypoxia-inducible factor-α and von Hippel-Lindau protein by direct binding to hypoxia-inducible factor-α. J Biol Chem 278:15911-15916.

252. Li C, Wang Y, Li Y, et al. 2018. HIF1α-dependent glycolysis promotes macrophage functional activities in protecting against bacterial and fungal infection. Sci Rep 8:3603.

253. Freemerman AJ, Johnson AR, Sacks GN, et al. 2014. Metabolic reprogramming of macrophages: glucose transporter 1 (GLUT1)-mediated glucose metabolism drives a proinflammatory phenotype. J Biol Chem 289:7884-7896.

254. Ouimet M, Ediriweera HN, Gundra UM, et al. 2015. MicroRNA-33-dependent regulation of macrophage metabolism directs immune cell polarization in atherosclerosis. J Clin Invest 125:4334-4338.

255. Mookerjee SA, Goncalves RLS, Gerencser AA, et al. 2015. The contributions of respiration and glycolysis to extracellular acid production. Biochim Biophys Acta 1847:171-181.

256. Romero N, Swain P, Neilson A, et al. 2017. White paper: Improving quantification of cellular glycolytic rate using Agilent Seahorse XF technology. http://seahorseinfo.agilent.com/acton/fs/blocks/showLandingPage/a/10967/p/p-00ca/t/page/fm/1.

257. Noll. F. 1983. L-(+)-Lactate determination with lactate dehydrogenase and NAD, Third ed: Weinhem; Deerfield Fla.: Verlag Chemie;

258. Passonneau JV. 1974. L-(+)-Lactate determination with lactate dehydrogenase and NAD - Fluorimetric method: Verlag Chemie Weinheim; 1468-1470 p.

259. Samelko L, Caicedo MS, Lim S-J, et al. 2013. Cobalt-alloy implant debris induce HIF-1α hypoxia-associated responses: a mechanism for metal-specific orthopedic implant failure. PLoS one 8:e67127.

260. Semenza GL. 2004. Hydroxylation of HIF-1: oxygen sensing at the molecular level. Physiology (Bethesda) 19:176-182.

261. Zhang H, Gao P, Fukuda R, et al. 2007. HIF-1 inhibits mitochondrial biogenesis and cellular respiration in VHL-deficient renal cell carcinoma by repression of C-MYC activity. Cancer Cell 11:407-420.

262. Mills EL, Kelly B, Logan A, et al. 2016. Repurposing mitochondria from ATP production to ROS generation drives a pro-inflammatory phenotype in macrophages that depends on succinate oxidation by complex II. Cell 167:457-470.

263. Janson CA, Cleland WW. 1974. The inhibition of acetate, pyruvate, and 3-phosphogylcerate kinases by chromium adenosine triphosphate. J Biol Chem 249:2567-2571.

264. Hukkanen M, Corbett SA, Batten J, et al. 1997. Aseptic loosening of total hip replacement: macrophage expression: of inducible nitric oxide synthase and cyclo-oxygenase, together with peroxynitrite formation, as a possible mechanism for early prosthesis failure. The Bone and Joint Journal 97-B 467-474.

265. Tian L, Lawrence DA. 1996. Metal-induced modulation of nitric oxide production *in vitro* by murine macrophages: lead, nickel, and cobalt utilize different mechanisms. Toxicol Appl Pharmacol 141:540-547.

266. Petit A, Mwale F, Tkaczyk C, et al. 2006. Cobalt and chromium ions induce nitration of proteins in human U937 macrophages *in vitro*. J Biomed Mater Res A 79:599-605.

267. Jones E, Adcock IM, Ahmed BY, et al. 2007. Modulation of LPS stimulated NF-kappaB mediated nitric oxide production by PKCε and JAK2 in RAW macrophages. J Inflamm 4:23.

268. Stuchr DJ, Marietta MA. 1987. Synthesis of nitrite and nitrate in murine macrophage cell lines. Cancer Res 47:5590-5594.

269. Li H, Poulos TL. 2005. Structure-function studies on nitric oxide synthases. J Inorg Biochem 99:293-305.

270. Cortese-Krott MM, Kulakov L, Opländer C, et al. 2014. Zinc regulates iNOS-derived nitric oxide formation in endothelial cells. Redox Biol 2:945-954.

271. Colman BP. 2010. Understanding and eliminating iron interference in colorimetric nitrate and nitrite analysis. Environ Monit Assess 165:633-641.

272. Tkaczyk C, Petit A, Antoniou J, et al. 2010. Significance of elevated blood metal ion levels in patients with metal-on-metal prostheses: An evaluation of oxidative stress markers. Open Orthop J 4:221-227.

273. Kinov P, Peter T. 2012. Evidence linking oxidative stress and aseptic loosening of hip arthroplasty. In: Fokter DS editor. Recent advances in Arthroplasty: Intech.

274. Repetto M, Semprine J, Boveris A. 2012. Lipid peroxidation: Chemical mechanism, biological implications and analytical determination. In: Catala A editor. Lipid Peroxidation: IntechOpen; pp. 3-30.

275. Xie Y, Hou W, Song X, et al. 2016. Ferroptosis: process and function. Cell Death Differ 23:369-379.

276. Cao JY, Dixon SJ. 2016. Mechanisms of ferroptosis. Cell Mol Life Sci 73:2195-2209.

277. Feng H, BR S. 2018. Unsolved mysteries: How does lipid peroxidation cause ferroptosis? PloS Biol 16:e2006203.

278. Shumilla JA, Wetterhahn KE, A. B. 1998. Inhibition of NF-kB binding to DNA by chromium, cadmium, mercury, zinc, and arsenite *in vitro*: Evidence of a thiol mechanism. Arch Biochem Biophys 349:356-362.

279. Moselhy HF, Reid RG, Yousef S, et al. 2013. A specific, accurate, and sensitive measure of total plasma malondialdehyde by HPLC. J Lipid Res 54:852-858.

280. Domijan AM, Ralić J, Radić Brkanac S, et al. 2015. Quantification of malondialdehyde by HPLC-FL - application to various biological samples. Biomed Chromatogr 29:41-46.

281. Fucile C, Marini V, Zuccoli ML, et al. 2013. HPLC determination of malondialdehyde as biomarker for oxidative stress: application in patients with alcohol dependence. Clin Lab 59:837-841.

282. Miljevic B, Hedayat F, Stevanovic S, et al. 2014. To sonicate or not to sonicate PM filters: Reactive oxygen species generation upon ultrasonic irradiation. Aerosol Sci Tech 48:1276-1284.

283. Mookerjee SA, Nicholls DG, MD. B. 2016. Determining maximum glycolytic capacity using extracellular flux measurements. Ploos One 11:e0152016.

284. Patten DA, Lafleur VN, Robitaille GA, et al. 2010. Hypoxia-inducible factor-1 activation in nonhypoxic conditions: the essential role of mitochondrial-derived reactive oxygen species. Mol Biol Cell 21:3247-3257.

285. Talks KL, Turley H, Gatter KC, et al. 2000. The expression and distribution of the hypoxia-inducible factors HIF-1alpha and HIF-2alpha in normal human tissues, cancers, and tumor-associated macrophages. Am J Pathol 157:411-421.

286. Karaczyn A, Ivanov S, Reynolds M, et al. 2006. Ascorbate depletion mediates up-regulation of hypoxia-associated proteins by cell density and nickel. J Cell Biochem 97:1025-1035.

287. Blouin CC, Pagé EL, Soucy GM, et al. 2004. Hypoxic gene activation by lipopolysaccharide in macrophages: implication of hypoxia-inducible factor 1α. Blood 103:1124-1130.

288. Ferko MA, Catelas I. 2018. Effects of metal ions on caspase-1 activation and interleukin-1β release in murine bone marrow-derived macrophages. PLoS One 13:e0199936.

289. Flora SJS. 2009. Structural, chemical and biological aspects of antioxidants for strategies against metal and metalloid exposure. Oxid Med Cell Longev 2:191-206.

290. Giampreti A, Lonati D, Ragghianti B, et al. 2016. N-Acetyl-Cysteine as effective and safe chelating agent in metal-on-metal hip-implanted patients: Two cases. Case Rep Orthop 8682737:1-7.

291. Caicedo MS, Desai R, McAllister K, et al. 2009. Soluble and particulate Co-Cr-Mo alloy implant metals activate the inflammasome danger signaling pathway in human macrophages: A novel mechanism for implant debris reactivity. J Orthop Res 27:847-854.

292. Terpilowska S, AK. S. 2018. Pro- and antioxidant activity of chromium(III), iron(III), molybdenum(III) or nickel(II) and their mixtures. Chem-Biol Interact 298:43-51.

293. Chamaon K, Schönfeld P, Awiszus F, et al. 2019. Ionic cobalt but not metal particles induces ROS generation in immune cells in vitro. J Biomed Mater Res B Appl Biomater 107:1246-1453.

294. Xu J, Nyga A, Li W, et al. 2018. Cobalt ions stimulate a fibrotic response through matrix remodelling, fibroblast contraction and release of pro-fibrotic signals from macrophages. Eur Cell Mater 36:142-155.

295. Koreny T, Tunyogi-Csapó M, Gál I, et al. 2006. The role of fibroblasts and fibroblast-derived factors in periprosthetic osteolysis. Arthritis Rheum 54:3221-3232.

296. Dumitru C, Kabat AM, KJ. M. 2018. Metabolic Adaptations of CD4+ T Cells in Inflammatory Disease. Front Immunol 9:1-17.

297. Kang KA, Lee HC, Lee JJ, et al. 2014. Effects of combined radiofrequency radiation exposure on levels of reactive oxygen species in neuronal cells. J Radiat Res 55:265-276.

298. Van den Bossche J, Baardman J, de Winther MP. 2015. Metabolic characterization of polarized M1 and M2 bone marrow-derived macrophages using real-time extracellular flux analysis. J Vis Exp 105:53424.

299. Haschemi A, Kosma P, Gille L, et al. 2012. The sedoheptulose kinase CARKL directs macrophage polarization through control of glucose metabolism. Cell Metab 15:813-826.

300. Stacey NH, Klaassen CD. 1982. Effects of phospholipase A2 inhibitors on diethyl maleate-induced lipid peroxidation and cellular injury in isolated rat hepatocytes. J Toxicol Environ Health 9:439-450.

APPENDIX

VALIDATION OF THE BIOCHEMICAL ASSAYS

Positive controls not included in the manuscripts are presented in this section.

1. H_2O_2 for the ROS detection assay

H_2O_2, a known ROS, was used as positive control to validate the cytosolic ROS detection assay. Macrophages were exposed to H_2O_2 (100 μM) for 6h (Figure A1). The magnitude of the increase observed with H_2O_2 is similar to that reported in the literature.[297]

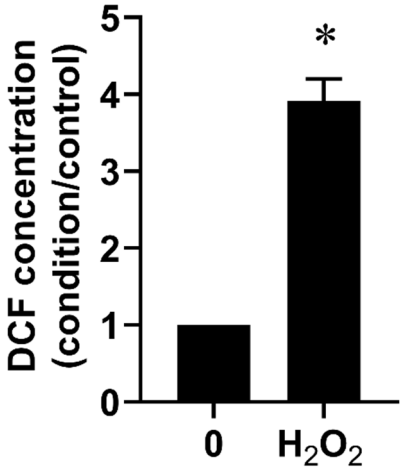

Figure A1: Effects of H_2O_2 (100 μM) on cytosolic reactive oxygen species (ROS) levels in RAW 264.7 macrophages after a 6-h incubation. ROS were assayed using the redox sensitive probe 2′,7′-dichlorodihydrofluorescein diacetate. 2′,7′-dichlorofluorescein (DCF) concentration, expressed relative to the DCF concentration in the negative control (cells unexposed to Co^{2+} or Cr^{3+}), is directly proportional to the level of cytosolic ROS. Data are presented as means ± SEM of three independent experiments, each performed with 5-6 replicate samples per condition. Statistical analysis was performed using a t-test. The data were assumed to be normally distributed and meet the assumption of homogeneity of variance. $p<0.05$ was considered significant. A single asterisk (*) indicates $p<0.001$ compared to the negative control.

2. LPS for the mitochondrial stress assay (OCR measurements)

LPS is a known pro-inflammatory stimulus inducing mitochondrial dysfunction, as previously reported.[207,236] Therefore, LPS was used as positive control to validate the mitochondrial stress assay. Macrophages were exposed to LPS (1 μg/mL) for 6h (Figure A2). Because maximal respiration is the mitochondrial parameter expected to be the most significantly inhibited by LPS,[298] LPS effects on this parameter are presented in Figure A2, along with the resting respiration. The magnitude of the decrease in maximal respiration observed with LPS is similar to that reported in the literature.[236,298]

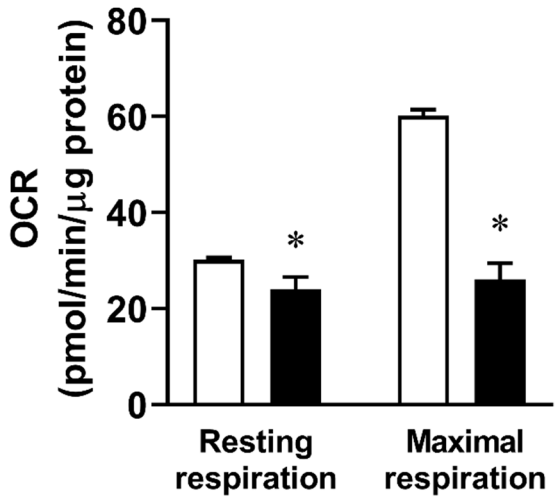

Figure A2: Effects of LPS (1 μg/mL) on resting and maximal respiration of RAW 264.7 macrophages after a 6-h incubation. OCR (measured using an extracellular flux analyzer) were normalized to protein content (determined using a colorimetric assay). Data are presented as means ± SEM of three independent experiments, each performed with 7-8 replicate samples per condition. Statistical analysis was performed using a t-test. The data were assumed to be normally distributed and meet the assumption of homogeneity of variance. $p<0.05$ was considered significant. A single asterisk (*) indicates $p<0.001$ compared to the negative control.

3. LPS for the improved glycolysis stress assay (ECAR measurements)

Since LPS is known to increase glycolytic flux,[177,299] it was used as positive control to validate the improved glycolysis stress assay. Macrophages were exposed to LPS (1 μg/mL) for 6h (Figure A3). Interestingly, the glycolytic capacity and the maximal glycolytic capacity in the presence of LPS were similar, suggesting that the macrophages had reached their maximal glycolytic activity. The magnitude of the increase observed in glycolysis with LPS is similar to that reported in the literature.[299] Notably, the increase with LPS was lower than that observed with Co^{2+} (Figure 4.1A), in agreement with the known difference in the kinetics of these two stimuli.[177]

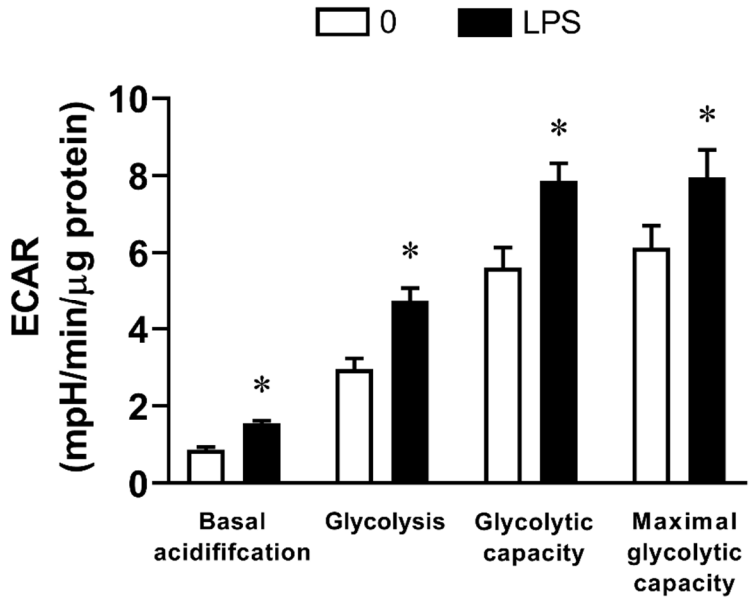

Figure A3: Effects of LPS (1 μg/mL) on glycolytic flux parameters and basal acidification of RAW 264.7 macrophages after a 6-h incubation. Extracellular acidification rates (ECAR; measured using an extracellular flux analyzer) were normalized to protein content (determined using a colorimetric assay). Data are presented as means ± SEM of 4-5 independent experiments, each performed with 5–8 replicate samples per condition. Statistical analysis was performed using a t-test, treating each parameter as a separate dataset. The data were assumed to be normally distributed and meet the assumption of homogeneity of variance. $p<0.05$ was considered significant. A single asterisk (*) indicates $p<0.001$ compared to the negative control.

PER were calculated from ECAR data to illustrate that the ECAR increases are mostly attributed to an increase in glycolysis (Figure A4).

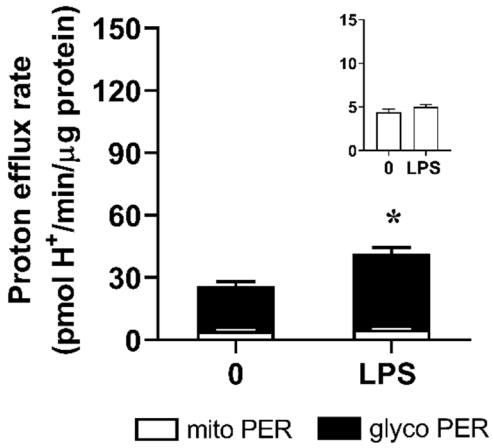

Figure A4: Effects of LPS (1 µg/mL) exposure (6h) on the proton efflux rates (PER) from RAW 264.7 macrophages incubated with glucose. Glycolytic (black) and mitochondrial (white) PER, normalized to protein concentration, are presented. Inserts show mitochondrial PER at a different scale. PER were calculated as described in Section 4.4.4) Statistical analysis was performed using a t-test. The data were assumed to be normally distributed and meet the assumption of homogeneity of variance. $p<0.05$ was considered significant. A single asterisk (*) indicates $p<0.001$ compared to the negative control.

4. LPS for the lactate production assay

Since LPS is known to increase lactate production,[176] it was used as positive control to validate the lactate production assay. Macrophages were exposed to LPS (1 µg/mL) for 6h, then cells were washed incubated again with glucose for 30 minutes to mimic the Seahorse assay setup (Figure A5). The magnitude of the increase in lactate production observed with LPS is similar to that reported in the literature for RAW 264.7 macrophages.[176]

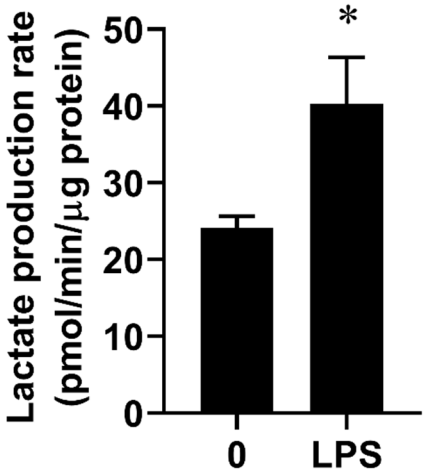

Figure A5: Effects of LPS (1 μg/mL) exposure (6h) on the average lactate production rates in RAW 264.7 macrophages during a 30-min incubation with glucose. Lactate production rates, normalized to protein content, were measured enzymatically. Data are presented as means ± SEM of 4 independent experiments, each performed with 3-4 replicate samples per condition. Statistical analysis was performed using a t-test. The data were assumed to be normally distributed and meet the assumption of homogeneity of variance. $p<0.05$ was considered significant. A single asterisk (*) indicates $p<0.001$ compared to the negative control.

5. LPS for the NO production assay

LPS is a known inducer of NO production in RAW 264.7 macrophages, as previously reported.[267,268] Therefore, LPS was used as positive control to validate the NO production assay. Macrophages were exposed to LPS (1 μg/mL) for 24h (Figure A6). The magnitude of the increase in NO production observed with LPS is similar to that reported in the literature for RAW 264.7 macrophages.[267]

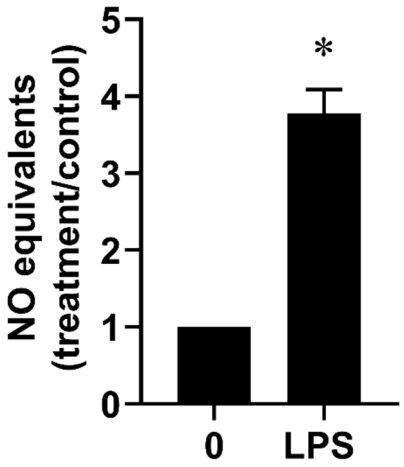

Figure A6: Effects of LPS (1 μg/mL) on nitric oxide (NO) equivalents in RAW 264.7 macrophages after a 24-h incubation. NO equivalents were measured using a non-enzymatic colorimetric assay followed by the Griess reaction. Nitrate and nitrite concentrations, expressed relative to the nitrate and nitrite concentrations in the negative control (cells unexposed to Co^{2+} or Cr^{3+}), are directly proportional to the NO equivalents. Data are presented as means ± SEM of three independent experiments, each performed with triplicate samples for each condition. Statistical analysis was performed using a t-test. The data were assumed to be normally distributed and meet the assumption of homogeneity of variance. $p<0.05$ was considered significant. A single asterisk (*) indicates $p<0.001$ compared to the negative control.

6. Diethyl maleate (DEM) for the lipid peroxidation assay (TBARS)

DEM is a known inducer of lipid peroxidation in macrophages, as previously reported.[300] Therefore, DEM was used as positive control to validate the TBARS assay. Macrophages were exposed to LPS (1 μg/mL) for 24h and 48h (Figure A7). The magnitude of the increase observed with DEM at 24h is similar to that reported in the literature.[300] The magnitude of the increase in lipid peroxidation observed at 48h was lower than that observed at 24h (likely due to cytotoxicity), but remained significant.

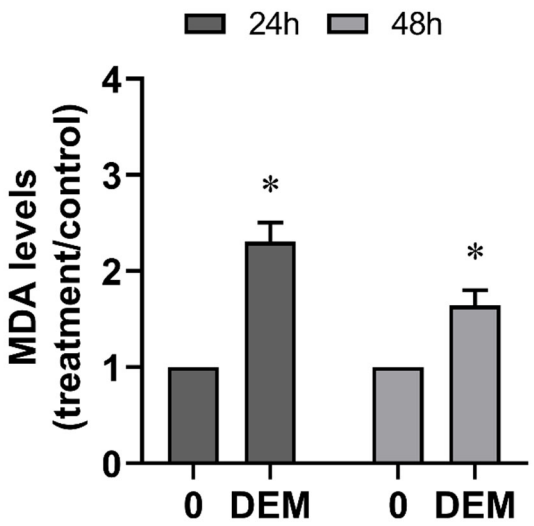

Figure A7: Effects of DEM (5 mM) on lipid peroxidation in RAW 264.7 macrophages after a 24- or 48-h incubation. Malondialdehyde (MDA) concentrations were measured using the thiobarbituric acid reactive species (TBARS) assay. MDA concentrations, expressed relative to the MDA concentration in the negative control (cells unexposed to Co^{2+} or Cr^{3+}), are proportional to the level of lipid peroxidation. Data are presented as means ± SEM of three independent experiments, each performed with triplicate samples per for each condition. Statistical analysis was performed using a t-test. The data were assumed to be normally distributed and meet the assumption of homogeneity of variance. $p<0.05$ was considered significant. A single asterisk (*) indicates $p<0.001$ compared to the negative control.